Electronic Thesis and Dissertation Repository

2-10-2011 12:00 AM

The Life Cycle of Pannexins: Trafficking, Cell Surface Dynamics, Turnover and Degradation

Ruchi Gehi, *The University of Western Ontario*

Supervisor: Dr. Dale Laird, *The University of Western Ontario*
A thesis submitted in partial fulfillment of the requirements for the Doctor of Philosophy degree in Anatomy and Cell Biology
© Ruchi Gehi 2011

The Life Cycle of Pannexins: Trafficking, Cell Surface Dynamics,
Turnover and Degradation

(Spine title: The Life Cycle of Pannexins: from Trafficking to Degradation)

(Thesis format: Integrated Article)

by

Ruchi <u>Gehi</u>

Graduate Program in Anatomy and Cell Biology

A thesis submitted in partial fulfillment
of the requirements for the degree of
Doctor of Philosophy

The School of Graduate and Postdoctoral Studies
The University of Western Ontario
London, Ontario, Canada

CERTIFICATE OF EXAMINATION

Supervisor

_____

Dr. Dale Laird

Supervisory Committee

_____

Dr. Daniel Belliveau

_____

Dr. Lique Coolen

_____

Dr. John Di Guglielmo

Examiners

_____

Dr. Martin Sandig

_____

Dr. Peter Merrifield

_____

Dr. Moshmi Bhattacharya

_____

Dr. Paul Lampe

The thesis by

Ruchi Gehi

entitled:

The Life Cycle of Pannexins: Trafficking, Cell Surface Dynamics, Turnover and Degradation

is accepted in partial fulfillment of the
requirements for the degree of
Doctor of Philosophy

_____   _____
Date   Chair of the Thesis Examination Board

ABSTRACT

Pannexins (Panxs) are a recently identified family of channel-forming glycoproteins, comprised of three members: Panx1, Panx2 and Panx3. Panxs were classified as gap junction (GJ) proteins based on their shared sequence homology to the invertebrate GJ protein, innexins. While no sequence homology exist between Panxs and the GJ proteins, connexins (Cxs), they share similar topology with four transmembrane domains, two extracellular loops, an intracellular loop and cytoplasmic exposed amino and carboxy terminal tails. In this study, we investigated if Panx1 and Panx3 exhibit unique or shared properties of cell surface delivery, mobility, cytoskeletal dependency, internalization and degradation, to the well characterized Cx43 GJ protein. Over-expression of a dominant-negative Sar1 mutant revealed that, like Cx43, Panx1 and Panx3 followed the classical secretory pathway en route to the cell surface. At the plasma membrane, Panx1 and Panx3 distributed in a relatively uniform pattern independent of the presence of an adjoining cell, a feature distinct from the punctate localization of Cx43 at cell-cell apposition. Rapid time-lapse imaging and photo-bleaching revealed high mobility of Panx1 and Panx3 at the cell surface, unlike Cx43-GJs. Using pharmacological inhibitors of microtubule and microfilament polymerization, Panx1 and Panx3 were identified to rely primarily on actin filaments for their overall cell surface stability. Interestingly, co-sedimentation and co-immunoprecipitation assays revealed that actin bound directly to the C-terminal tail of Panx1. Truncation of the Panx1 C-terminal tail at residue 307 (Panx1^{T307}) inhibited its trafficking to the cell surface causing it to be retained within the endoplasmic reticulum. Co-expression of full length Panx1 could not rescue the

delivery of Panx1^{T307} to the cell surface but exhibited limited co-interaction. Blocking of protein synthesis and secretion revealed a prolonged half-life of Panx1 in comparison to Cx43. Rapid time-lapse imaging of cells expressing Panx1-GFP uncovered a unique pattern of Panx1 internalization through dynamic tubular-like extensions. Chloroquine-induced inhibition of lysosomal function revealed that Panx1 is degraded by lysosomes. Collectively, our studies show that Panx1 and Panx3 exhibit many properties that are distinct from Cx43, further supporting that pannexins forms a unique class of channel proteins that should be considered separate from connexin-based GJ channels.

Keywords

CO-AUTHORSHIP STATEMENT

All the experimental work was performed by Ruchi Gehi except for the following:

Chapter 2

Dr. Qing Shao engineered the retroviral constructs of Panx1 and Panx3

Dr. Silvia Penuela generated the expression constructs of Panx1 and Panx3, characterized the custom designed pannexin antibodies and conducted the actin co-sedimentation assay

Jared Churko engineered and purified the carboxy tail of Panx1

Chapter 3

The RFP tagged expression constructs of Panx1^{T307} and Panx1 were designed in collaboration with Dr. Qing Shao

DEDICATION

To G-unit and my entire family.

ACKNOWLEDGEMENTS

TABLE of CONTENTS

LIST of FIGURES

Chapter 4: Panx1 Exhibits a Distinct Internalization Pattern from the Connexin Family of Gap Junction Proteins

LIST of APPENDICES

LIST of ABBREVIATIONS

AP2	adapter protein 2
BFA	brefeldin A
BICR-M1R$_k$	rat mammary tumor cells
BSA	bovine serum albumin
Ca^{2+}	calcium
cAMP	cyclic adenosine monophosphate
Cav	caveolin
cDNA	complementary deoxyribonucleic acid
CHX	cycloheximide
COPII	coat protein II
CREB	cAMP response element-binding
Cx	connexin
Cx43	connexin43
DMEM	Dulbecco's Modified Essential Medium
DynII	dynamin II
ER	endoplasmic reticulum
ERAD	ER-associated degradation
F-actin	filamentous actin
FRAP	fluorescence recovery after photobleaching
GAPDH	glyceraldehydes 3-phosphate dehydrogenase
GJ	gap junctions
HEK-293T	human embryonic kidney 293 cells
5-HT	5-hydroxytryptamine receptor
Inx	innexin
K$^+$	potassium
kDa	kilodalton
MDCK	Madin-Darby canine kidney cells
OPUS	ogre, Passover, unc-7 and shaking-B (acronym for the founding members of the innexin family of gap junction proteins)
Panx	pannexin
Panx1	pannexin1
Panx1-GFP	pannexin1-green fluorescent protein
Panx1-RFP	pannexin1-red fluorescent protein
Panx1^{T307}-RFP	pannexin1-truncated-red fluorescent protein
Panx3	pannexin3
Panx3-GFP	pannexin3-green fluorescent protein
PDI	protein disulfide isomerise
pS	picosiemens
REK	rat epidermal keratinocytes
Sar1	secretion-associated and Ras-related

CHAPTER 1

1 INTRODUCTION

1.1 Evolutionary aspect of innexins, connexins and pannexins

A family of channel forming proteins, termed pannexins (Panxs), was first identified in the year 2000 by Panchin and colleagues [1]. Pannexins were discovered as the vertebrate homologs of invertebrate gap junction proteins, innexins (Inxs) [1, 2], and were therefore proposed to share functional features similar to gap junctions.

Gap junctions (GJs) are tightly packed intercellular channels that are assembled from two halves or hemi-channels composed of GJ proteins [3, 4]. GJ channels connect the cytoplasm of two apposing cells for bi-directional passage of ions, small metabolites and messenger molecules less than 1 kDa in size [4, 5]. The intercellular communication mediated by GJ channels regulates physiological processes related to development, synchronization, differentiation and proliferation [6-8].

In the 1980s, the pioneer work done on characterizing GJs led to the identification of a multigene family of vertebrate proteins, connexins (Cxs) [9, 10], and the nomenclature of Cxs was based according to their predicted molecular mass [9, 10]. Ever since the cloning of the first connexin, Cx32, from rat and human liver [11, 12], 20 murine and 21 human connexin family members have been identified [13]. Based on the cDNA and genomic sequences, Cxs were also evident in animals of chordate branch: tunicates, ascidians and appendicularians (GenBank accession numbers AY380580, AY386312, AY386311) [14]. Despite

being a large family, several initiatives could not identify connexin homologs in the genomes of *Caenorhabditis elegans* (nematode) or *Drosophila melanogaster* (arthropod), thereby suggesting an existence of a distinct family of proteins for the formation of GJs in invertebrates [15]. A second GJ protein, unrelated to Cxs, was then found in several bilaterian protostome phylas including Platyhelminthes, Nematoda, Annelida, Molluscs and Arthropoda (Figure 1.1). This family of proteins was originally designated as OPUS, derived from the founding members: ogre, Passover, unc-7 and shaking-B, but were later renamed innexins (invertebrate analog of connexin) based on their shared ability to form intercellular channels, like connexins [16-20].

With the renaming of invertebrate GJs to innexins, the genomic sequence of mollusk and flatworm were aligned and compared against the human genome using a PSI-BLAST (Position Specific Iterative-Basic Local Alignment Search Tool) approach [21]. The BLAST search identified two mRNA sequences with no previously assigned functions that encoded MRS1 (GenBank accession number AF093239) and MRS1-related proteins (GenBank accession number AL022328). Interestingly, sequence searches based on the MRS1 protein retrieved the invertebrate gap junction protein, Unc-7 from *C. elegans*, thus expanding the innexin homolog family into the chordata phyla [21]. Due to the apparent ubiquitous presence of this family of proteins in the metazoan animal kingdom, and their putative role as GJs, they were termed 'pannexins' (from the Latin Pan-all, throughout and nexus- connection) [1, 21]. As a result, the human MRS1 protein was denoted as PANX1, and its related form as PANX2. In addition, a

protein sequence query (TBLASTN) applied against the human genome detected a final member of this family, PANX3 [21].

From an evolutionary perspective, it appeared that innexins emerged to provide gap junctional intercellular communication in animals of Cnidarian lineage, which was later inherited by protostomes and deuterostomes (Figure 1.1). In comparison, Cxs emerged in deuterostomes as a second class of GJ proteins, presumably by a gene duplication in the early protochordate lineage [22]. This divergence led innexins to be found in a subfamily within deuterostomes- as pannexins [23].

Connexins were originally identified to be chordate-specific, however, additional genomic sequence analysis from other organisms have shown some exception to this criteria, as animals (e.g. lancelets) within one of the branches of the chordata phylum (cephalochordate) are devoid of connexins, but have pannexins [24] (Figure 1.1).

From the functional point of view, pannexins might have emerged to provide compensatory, overlapping or unique physiological roles compared to that of connexins. The assessment of the phylogenetic relationship between different members of this superfamily has been an ongoing effort in the gap junction research community. Being a vertebrate homolog of innexins, it therefore became logical to determine if pannexins exhibited similar characteristics to the well studied gap junction proteins of vertebrates, connexins.
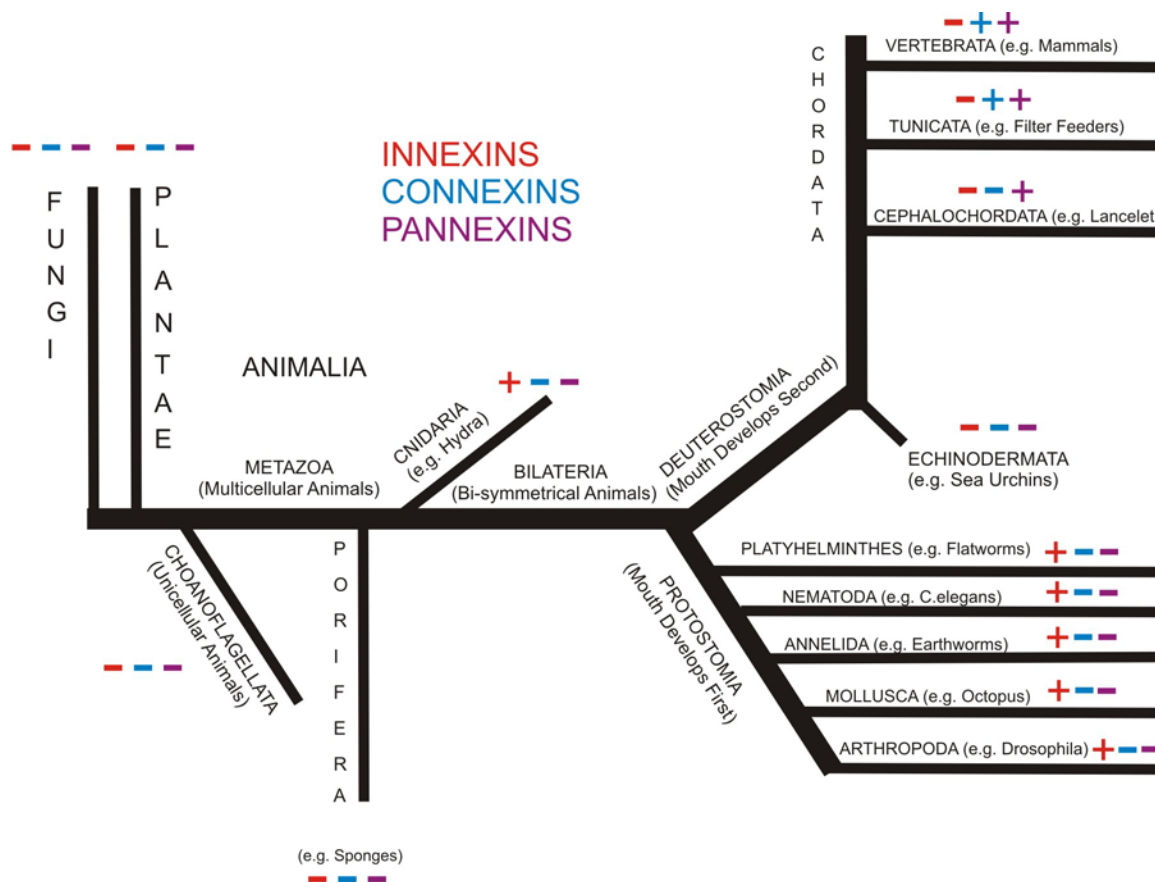
Figure 1.1 Evolutionary aspect of innexins, connexins and pannexins

Schematic representation of presence (+) and absence (-) of innexins, connexins and pannexins in various taxonomic groups. Adapted from Shestopalov and Panchin (2008).

1.2   Human and murine pannexin genes

Amino acid sequence alignment of the three human pannexins members: PANX1, PANX2 and PANX3, revealed 49-94% similarity with murine pannexins [2]. While human pannexins are written in uppercase, murine pannexins are represented by the Panx1, Panx2 and Panx3 nomenclature.

PANX1 located on human chromosome 11q14.3, contains five exons and four introns and encodes a 426 amino acid protein (Accession number NP_056183) with an expected molecular mass of 47.6 kDa [21]. On the other hand, murine *Panx1* is located on chromosome 9, and similar to human *PANX1* encodes five exons and four introns [21], generating a product of 426 amino acids (Accession number NP_062355) with a molecular weight of ~45 kDa [25].

PANX2 located on human chromosome 22q13.31-13.33, contains 4 exons and has two protein isoforms [21]. PANX2 isoform 1 contains 677 amino acids (Accession number NP_443071), and isoform 2 contains 643 amino acids (Accession number NP_001153772), with a predicted molecular mass of ~70 kDa [21]. The murine *Panx2* is located on chromosome 15 and similar to the human *PANX2*, contains 4 exons and encodes a protein product of 677 amino acids (Accession number NP_001002005) with a molecular weight of ~80 kDa [21]. Finally, the human *PANX3* is similar to the murine *Panx3*, as they both contain 4 exons and encodes a 392 amino acids long protein with a molecular weight of ~44.7 kDa and ~43 kDa, respectively (human: Accession number NP_443191; murine: Accession number NP_766042) [21]. While human *PANX3* is located on 11q24.2, murine *Panx3* is located on chromosome 9 [21].

Interestingly, both the human and murine pannexin genes for Panx2 and Panx3 are located on shorter chromosome segments (less than 6 kb from first to last exon) than Panx1 (more than 40 kb from first to last exon) [21]. Moreover, Panx1 and Panx3 are located on the same chromosomes in human and mouse, with a separation of 30 Mb and 22 Mb, respectively, and share 41% identity and 59% conservation at the primary structure level [21]. Given the overall similarity in the exon-intron organization, chromosomal location, and the shared conservation at the amino acid level, it is postulated that the close relationship of Panx1 and Panx3 may have arisen from chromosomal duplication [21]. Furthermore, the phylogenetic mapping of vertebrate pannexins revealed more divergence of Panx1 from Panx2, suggesting unique roles for these family members [21]. Given that Panx1 and Panx3 are more closely related to each other, this thesis will predominantly focus on these two members of the pannexin family.

1.3   Diversity of pannexin expression

In addition to the human and mouse genomes, the expression of all three pannexin members have now been identified in at least 5 more species including: *Rattus norvegicus* (rat), *Canis familaris* (dog), *Bos Taurus* (cow), *Danio rerio* (zebrafish) and *Tetraodon nogrovirdis* (puffer fish) [2]. Despite the vast inter-species distribution, pannexins are most well characterized in human and rodent tissues, with Panx1 being the most studied member. The first studies relied on detecting pannexins at only the transcript level due to the unavailability of high-quality, custom-designed antibodies.

1.3.1 Pannexin1

Northern blot analysis of human tissues revealed Panx1 expression in brain, heart, skeletal muscle, skin, testis, ovary, placenta, thymus, prostate, lung, liver, small intestine, pancreas, spleen, colon, blood endothelium and erythrocytes [21]. In the central nervous system (CNS), Panx1 transcripts were detected in cerebellum, cortex, lens (fiber cells), retina (retinal ganglion, amacrine and horizontal cells), pyramidal cells, interneurons of the neocortex and hippocampus, amygdale, substantia nigra, olfactory bulb, neurons and glial cells [21, 24, 26-35]. Developmentally, a gradient of Panx1 expression was found in mouse brain, such that higher levels were expressed during the embryonic (E13.5-18) and postnatal stages with lower levels in the adult brain [30, 32]. Notably, our tissue survey using custom-designed affinity purified anti-Panx1 antibodies demonstrated a robust expression of Panx1 in the brain, with variable levels of Panx1 in the lung, kidney, spleen, heart ventricle, skin and sources of cartilage from ear and tail of a 3-week old mice [25]. More recently, Panx1 protein expression was also detected in the rodent cochlea, specifically in supporting cells of the Organ of Corti, spiral limbus, cochlear lateral wall and strial blood vessels [36].

1.3.2 Pannexin2

In comparison to Panx1, Panx2 mRNA was restricted to several areas of the human adult brain including: cerebellum, cerebral cortex, medulla, occipital pole frontal lobe, temporal lobe and putamen [21]. While Northern blot analysis revealed higher levels of Panx2 transcript in the rodent brain, spinal cord and

eyes, other tissues such as thyroid, kidney and liver also revealed some level of Panx2 expression [26-28]. Interestingly, in-situ hybridization revealed co-expression of Panx2 with Panx1 in various regions of adult rat brain, such as hippocampus, olfactory bulb, pyramidal cells, dentate gyrus, Purkinje cells of the cerebellum, pyramidal cells and interneurons of the hippocampus and neocortex [32]. Unlike Panx1, Panx2 transcript expression was low during prenatal development of rat brain, and substantially increased in postnatal brains [32]. Recently, Panx2 protein expression was identified in the basal cells of the stria vascularis and spiral ganglion neurons of the rat cochlear system [36].

1.3.3 Pannexin3

Based on expressed sequence tags, Panx3 was predicted to be present in osteoblasts, synovial fibroblasts, whole joints of mouse paws, and cartilage from the inner ear [21]. In addition, Panx3 transcript expression, albeit low, was also detected in human hippocampus extracts [21]. Recently, Panx3 protein expression was reported in murine cochlear bone [36], while *in-situ* hybridization of embryonic day 16.5 mice strongly revealed *Panx3* expression in prehypertrophic chondrocytes, perichondrium and osteoblasts [37]. Furthermore, we demonstrated that while Panx3 protein exhibits two forms at ~43 kDa and ~70 kDa, when expressed in skin, cartilage, and ventricle, only the ~70 kDa species is detected in lung, liver, kidney, thymus and spleen of a 3 week old mice [25]. It is however yet to be determined if the occurrence of ~70 kDa species is due to a splice variant or Panx3 dimerization.

1.4 Pannexin family members share similar topology to connexins

The discovery of pannexins led to further analysis of the protein topology using multiple sequence alignment systems [2]. Connexins, innexins and pannexins all share the same topology with four alpha-helical transmembrane (TM) domains, two extracellular loops (EL), one intracellular loop (IL) and intracellular amino (NT) and carboxy (CT) termini [1, 2, 21] (Figure 1.2). While primary sequence homology does not exist between Panxs and Cxs, various motifs of Panxs and Inxs share significant sequence homology [2]. Both Inxs and Panxs share two cysteine residues in each of their EL domains (Figure 1.2), with the exception of *Drosophila* Inx4 that has 3 pairs of cysteines [2, 38].

The two cysteine residues within the 1st EL are fully conserved between Panxs and Inxs, with 37% identity and 58% amino acid similarity when flanked by 24 additional amino acids. However, only 1 of the 2 cysteine residues is conserved in the 2nd EL of Panxs and Inxs [2]. Comparatively, the well characterized Cx family member, Cx43, has 3 cysteine residues in each of its ELs [39] (Figure 1.2) which is the same for all characterized connexins with the exception of Cx23, which harbors 2 pairs of cysteines [40]. In the case of Cx43, and likely all other family members, these cysteine residues are critical for forming intramolecular disulfide linkages between ELs, such that when docked at the apposing plasma membrane, each half of the GJ channel is stabilized by intermolecular hydrogen bonds [41].
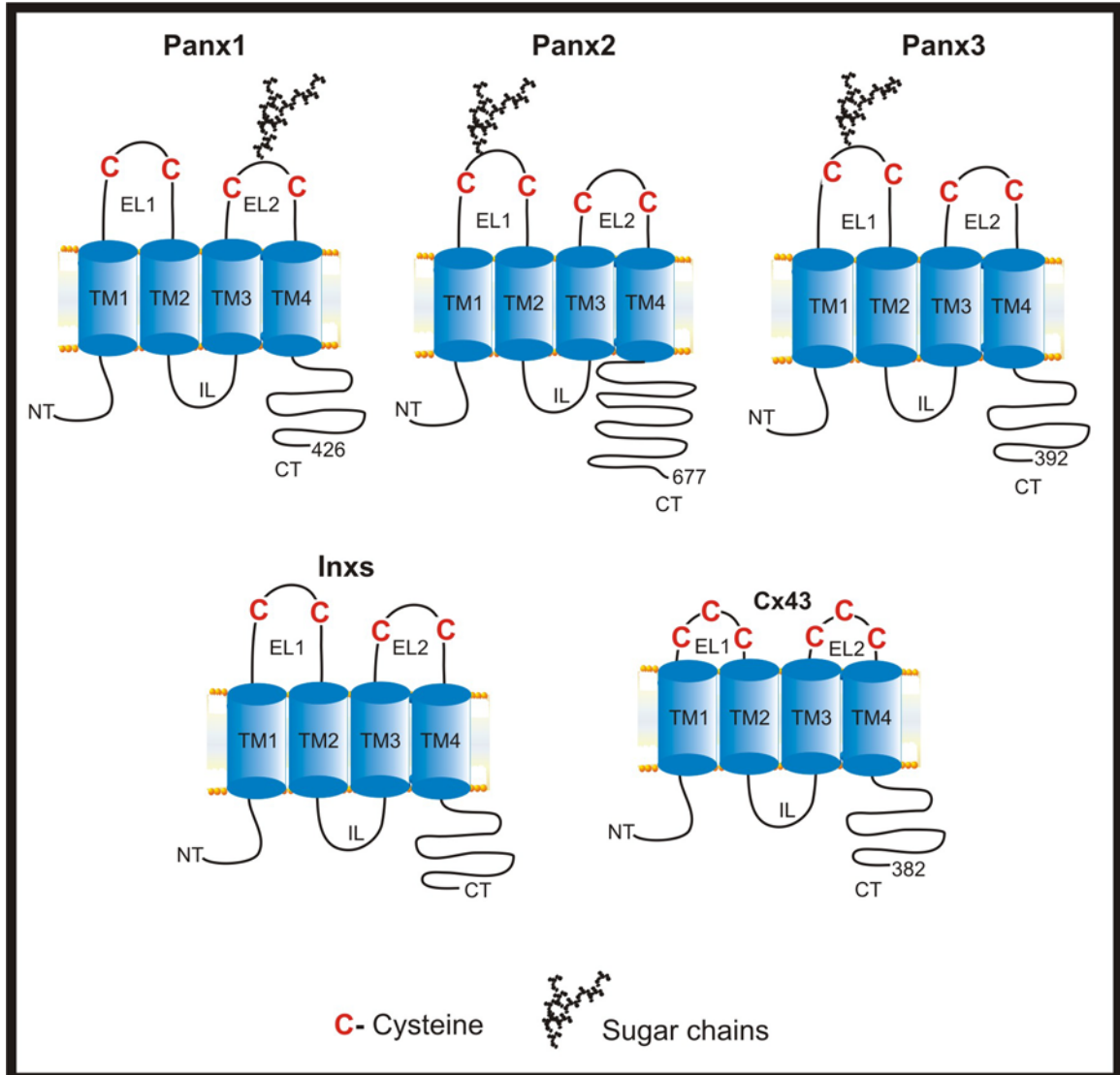
Figure 1.2 Topology of innexins, connexins and pannexins

Panx1, Panx2 and Panx3 share similar topology of four transmembrane domains (TM), two extracellular loops (EL), one intracellular loop (IL) and intracellular amino (NT) and carboxy (CT) groups with innexins and Cx43. Pannexins and innexins also share two cysteine residues in each of their ELs, while Cx43 has three cysteine residues. Panx1 is glycosylated on the second EL, whereas Panx2 and Panx3 are glycosylated on the first EL.

Interestingly, a signature sequence of all Inxs (YYQWV) is not conserved in Panxs. However, this motif along with a 23 amino acid flanking region in Inxs exhibits 39% identity and 61% similarity in TM2 of Panxs [2]. Additionaly, a proline motif (correlated with conformation changes associated with channel-gating in Cxs) is conserved in TM2 of Inxs and Panxs, and is found in relatively the same position in Cxs [42].

While Inxs and Panxs contain two fully conserved cysteine residues in their CT region, it is the NT domains that are better conserved [2]. All connexin members posses almost the same length of intracellular NT domain with major differences found in the length of the CT domain [43]. In contrast to Panx1 and Panx3, Panx2 exhibits a very large CT domain (Figure 1.2) which is speculated to convey unique functions to Panx2 regulation, targeting or macromolecular interactions [2]. The regulatory role of the Cx43 CT domain is multifaceted. This includes many interactions with scaffolding and cytoskeletal proteins [44] that contribute to the overall size and number of gap junction plaques at the cell surface [45] and the channel gating properties [46]. However, the role of the CT domain in Panxs has yet to be investigated.

1.5   Pannexins and connexins form multimeric channels

Initial characterization of Panx1 oligomerization revealed that 6 subunits were required for a channel formation [47]. The monomers of Panx1 resolved at ~43-49 kDa, whereas the dimeric and hexameric configuration was detected at ~98 kDa and ~290 kDa, respectively [47]. While Panx1 and Cx43 channels share a

hexameric configuration, this is quite different from the heptamers or octomers reported for Panx2 [48]. On the other hand, the state of oligomerization for Panx3 is currently unknown. Distinct from Cx43, Panx1 forms a wider pore channel [49] likely due to relatively longer ELs (~50-60 amino acids) than seen in Cxs (~30 amino acids) [24] (Figure 1.2). Pannexin hexamers are termed pannexons [47], following the nomenclature devised for connexins (as connexin hexamers are termed connexons) [3, 4]. While 'connexons' are also referred as 'hemi-channels' (i.e. a structure constituting half of the channel), the term 'pannexons' primarily reflects the single-membrane channel. It is well established that connexons from adjacent cells dock at the plasma membrane to form intercellular channels, however, an ongoing effort continues in the field to deduce if single membrane channels of pannexins also possess the capability to form intercellular junctions [50].

1.6 Pannexins do not readily form intercellular channels

Currently, there are conflicting reports in the literature as to whether pannexins are involved in direct intercellular communication. It was initially reported that over-expression of Panx1 mRNA, but not Panx2 or Panx3, formed intercellular channels, albeit, 24-48 hours after pairing Xenopus oocytes [26, 51, 52]. In a parallel study, Boassa et al., [47] reported that while Panx1 intercellular channels did not form resulting in a significant junctional conductance within 6 hours of oocytes pairing, the Cx46 formed robust intercellular channels within 1 hour [47]. Additional evidence of intercellular channel formation by Panx1 was

derived from two independent studies using C6 glioma cells [53] and LNCaP prostate cancer epithelial cells [54]. While these studies revealed the passing of sulfurodamine 101 dye in C6 gliomas [53] and Ca^{2+} permeability in LNCaP neighboring cells [54], they were performed under highly artificial conditions of either bathing or perfusing the cells with chemical agents, thus questioning the ability of pannexins to readily or efficiently form intercellular channels. A scrape loading assay (a commonly used technique to detect intercellular communication) conducted by Boassa et al., [47] further revealed the inability of Panx1 to pass Lucifer yellow dye in communication-deficient Madin-Darby Canine Kidney cells. This study was in line with our findings that revealed no electrical coupling conductance in gap junction-deficient neuro-2A (N2A) cells expressing either Panx1 or Panx3 [25]. Additional reports in erythrocytes [55] as well as neuronal and glial cells [56] have also failed to provide evidence that Panxs can in fact form gap junctions, thus providing further indication that the pannexin family of proteins does not serve a role redundant to that of connexins by readily forming intercellular channels.

1.7 Pannexins form functional non-junctional channels

It was first identified in 2003, that Panx1, but not Panx2, possesses the ability to form non-junctional membrane channels, in single *Xenopus* oocytes [26]. The unitary conductance of Panx1 single-membrane channels was determined to be 550 pS [57], which was approximately 200 pS larger than that of any of the connexins [58]. Co-injections of Panx1 and Panx2 transcripts, revealed a ~15%

reduction in the conductance of heterotypic channels (comprised of different subunits), thus reflecting a dominant negative effect of Panx2 on Panx1 channel function [26]. Since then, we have reported that all family members: Panx1, Panx2 and Panx3 can form variable levels of single-membrane channels, capable of dye uptake [59]. However, intermixing of Panx1 with Panx2, but not Panx3, attenuated the channel function by lowering the incidence of dye uptake [59]. While Panx1 channels can be activated by mechanical stimulation, cytoplasmic Ca^{2+}, membrane depolarization and extracellular ATP [49, 57, 60-62]; its conductance is abolished by CO_2-mediated cytoplasmic acidification [60], negative feedback from ATP release [63], mimetic peptides [64] and channel blockers such as carbenoxolone, probenecid and fluefenamic acid [65, Barbe, 2006 #3]. It is now well established that the activation of pannexin single-membrane channels allows for cellular communication with the extracellular environment to fulfill a diverse range of functions [50, 56, 60, 66, 67].

1.8 Physiological roles of pannexin single-membrane channels

1.8.1 Paracrine signaling mediated by Panx1

Indirect communication between cells is typically mediated through activation of single-membrane channels and releasing molecules such as ATP [68] into the extracellular space.

Calcium waves: Ca^{2+} is a versatile, ubiquitously expressed second messenger that can regulate several cellular responses [69]. Initiation of Ca^{2+} waves is

mediated by the activation of ATP-sensitive purinergic receptors, P2Y and P2X [70]. Binding of ATP to the membrane receptor increases inositol 1, 4, 5-triphosphate, which in turn, releases Ca^{2+} from the ER stores. Once released, Ca^{2+} activates single-membrane channels, leading to further release of ATP, and propagation of signal to the neighboring cells [71]. Essential to this notion is the fact that Panx1 has been shown to be a part of the $P2X_7$ receptor complex, necessary for ATP release [55, 72]. Furthermore, ATP-induced ATP release was also reported when Panx1 channels were activated through P2Y receptors and cytoplasmic Ca^{2+} [60], thus supporting the role of Panx1 in the initiation and propagation of regenerative Ca^{2+} signaling.

Vasodilation: Release of ATP from erythrocytes occurs during stress and hypoxic conditions [73]. It was recently discovered that erythrocytes endogenously express Panx1, and mechano-sensitive activation of Panx1 channels regulate ATP release [55]. It is hypothesized that under conditions of stress, activation of Panx1 channels control blood flow, by releasing ATP from red blood cells, and initiating Ca^{2+} wave propagation through stimulation of purinergic receptors on the endothelial cells [55]. Elevation of Ca^{2+} subsequently releases NO onto the smooth muscle, leading to vasodilation [55].

Taste sensation: Taste buds are comprised of two distinct population of cells, some that express taste receptors (receptor cells), and others that contain synapses (presynaptic cells) [74]. It has been reported that Panx1 is expressed in the receptor cells, and upon taste stimulation, ATP is released through Panx1 single-membrane channels [65, 74]. Once released in the extracellular medium,

ATP stimulates P2 receptors of the presynaptic cells to release serotonin (5-HT) [65, 74], thereby providing a mechanism for cell-cell signaling and information processing within taste bud.

Airway defense: Airway epithelium provides a defense mechanism by controlling mucociliary clearance, which depends on maintaining adequate airway surface liquid volume and ciliary activity [75].   In the differentiated human airway epithelium cells, expression of Panx1 single-membrane channels in the apical region has been linked to ATP release under hypotonic stress [75].   Panx1-evoked ATP release is proposed to be crucial for regulating the ciliary beat frequency and surface liquid volume for mucous clearance [75].

1.8.2 Intracellular responses mediated by Panx1

Immune response: Interaction of Panx1 with $P2X_7$ receptors elicits an immune response by releasing the pro-inflammatory cytokine interleukin (IL)-1 β, in response to receptor stimulation by ATP followed by a subsequent activation of caspase-1 [49]. Panx1 is also reported to trigger the Toll-like receptor-independent inflammasome (comprising cryopyrin), based on recognition of bacterial molecules passing from endosomes to cytosol [76]. Furthermore, $P2X_7$-mediated activation of Panx1 channel is potentiated by high extracellular K^+ levels in neuronal/astrocytic inflammasomes [77].

Tumorigenesis: Exogenous expression of Panx1 has been linked to tumor-suppressive properties in C6 gliomas [53]. In the presence of Panx1, C6 gliomas exhibit a flattened morphology and a reduction in proliferation, motility,

anchorage-independent growth [53]. In addition, injection of Panx1 expressing cells in nude mice reduced the *in vivo* tumor growth [53]. Taken together, it is suggested that Panx1 plays a role as a tumor suppressor.

Ischemic cell death and Epileptic seizure: The rapid decrease of O_2 and glucose in mouse hippocampal pyramidal neurons has been associated with the opening of Panx1 single-membrane channels that leads to conductance of large currents [78]. This, in turn, causes a profound ionic dysregulation, thereby leading to neuronal death [78]. In addition, the N-methyl-$_D$-aspartate receptor-based opening of Panx1 channels leads to epileptiform seizure activities in pyramidal neurons [66], further supporting the importance of precise regulation of Panx1 channel openings.

Apoptosis: Panx1 forms the pore unit of the $P2X_7$ death complex [72]. The co-expression of Panx1 with $P2X_7$ receptor revealed ATP-induced zeiosis in *Xenopus* oocytes, which was not observed upon the injection of Panx1 transcript alone or together with P2Y receptor [60, 72]. These results suggest that although activation of purinergic P2Y receptor can mediate Panx1 currents, the specific cell death signaling is through interaction with ionotropic $P2X_7$ receptor. Quite recently, Panx1 channels have been documented to mediate the release of nucleotide signals from apoptotic cells for the recruitment of activated monocytes [79]. In this situation, Panx1 channels gets activated by caspases which cleave Panx1 and opens the channel for ATP and UTP release as a "find me" signal to attract phagocytes [79].

Keratinocyte differentiation: We have previously shown that ectopically expressed Panx1 reduces the proliferation rate of rat epidermal keratinocytes (REKs), however, it does not significantly alter their migratory properties [67]. Furthermore, over-expression of Panx1 in organotypic cultures (generated from monolayer REKs) disrupts the overall architecture of the epidermis, reduces the thickness of vital layer (likely stratum spinosum and granulosum) and re-localizes the basal cell marker, cytokeratin 14, throughout the vital layer [67], thus, arguing for an adequate expression of Panx1 in maintaining keratinocyte differentiation.

1.8.3 Intracellular responses mediated by Panx3

Keratinocyte and Chondrocyte differentiation: In contrast to Panx1, much less is known about the channel capabilities of Panx3. We have shown that, similar to Panx1, Panx3 also reduces the proliferation of REKs without altering its migration rates [67]. However, unlike Panx1, Panx3 maintains the integrity of the organotypic epidermis and keratinocyte differentiation upon its over-expression [67]. In addition, Panx3 expression in cartilage has recently been associated with chondrocyte differentiation [37]. Specifically, Panx3 promotes ATP release into the extracellular medium (likely by the action of Panx3 single membrane channels), and reduces the parathyroid hormone-mediated proliferation of chondrocytes by decreasing cAMP levels and inhibiting phosphorylation of CREB [37]. Thus, these results support a role for Panx3 in switching the fate of chondrocytes from proliferation to differentiation.

1.9 Distinct from Cx43, Panx1 and Panx3 are glycosylated

Consensus site analysis of Panx1 and Panx3 polypeptide sequences followed by experimental investigation revealed that glycosylation occurs at asparagine 254 in the second extracellular loop of Panx1 (Figure1.2), and at asparagine 71 in the first extracellular loop of Panx3 [25]. Treatment with N-glycosidase F, revealed the glycosylation status of Panx1 [25, 47, 59] and Panx3 [25, 59]. Three distinct glycosylation species of Panx1 and Panx3 were revealed: the non glycosylated form that constitutes the core protein- Gly0 (resolves at ~37 kD for Panx1 and ~30 kD for Panx3), the predominant ER resident high mannose form- Gly1 (resolves at ~42-43 kD for Panx1 and ~43 kD for Panx3) and the complex glycosylated form that is fully processed- Gly2 (resolves at ~48 kD for Panx1 and at ~44-45 kD for Panx3). Glycosylation of pannexins is a post-translational modification that is not found on any connexin, including Cx43. Instead, the multiple banding profile of Cx43 detected by immunoblotting is due to differential states of phosphorylation [80]. Although both Panx1 and Panx3 encode several consensus sites for phosphorylation [25], alkaline phosphatase treatment did not change the protein banding pattern for either Panx1 or Panx3, unlike Cx43 [25]. Nevertheless it remains possible that Panxs could serve as a substrate for phosphorylation events without causing any shift in the banding profile.

The extended carbohydrate modifications on the ELs of pannexins have been reported to prevent the close docking of single-membrane channels at cell-cell appositions, in contrast to the connexons which are never glycosylated. Electron micrographs of Panx1 in the areas of apposing cells revealed intercellular

spacing of 20-50 nm, which is quite distinct from the 2-4 nm spacing seen in Cx43-based gap junctions [47]. The glycosylation status of Panxs has also been proposed to be mechanistically inhibitory to gap junction formation. This notion is based on the report where removal of all cell surface glycan chains from rat Panx1 as well as all other cell surface glycoproteins increased the junctional conductance in *Xenopus* oocytes [81]. Interestingly, the GJ coupling did not occur until 6 hours post pairing, which is greatly delayed from paired Oocytes that express connexins [47, 81].

Glycosylation of Panx1 and Panx3 is important for proper trafficking to the cell surface. This conclusion is based on reduced [25] or absent cell surface localization [47] of the glycosylation-deficient mutants Panx1^{N254Q} or Panx3^{N71Q}. Our recent data has shown that a subpopulation of both the N-glycosylation deficient mutants of Panx1 and Panx3 that do reach the cell surface are capable of forming functional single membrane channels [59], thus suggesting that glycosylation of pannexins mediates their cell surface trafficking, without impairing the ability to assemble into functional channels. Overall, the distinct post-translational modification of Panx1 and Panx3 in comparison to Cx43 separates the pannexin family from the better understood connexin family of proteins. While the life cycle aspects of Cx43 are well characterized, our knowledge of trafficking events regulating the Panx1 and Panx3 function remains poor.

1.10 The life cycle of Cx43-from biogenesis to degradation

1.10.1 Biogenesis of Cx43

Cx43 has a relatively short half life of approximately 1-3 hours [82]. As a result, gap junction channels composed of Cx43 are continually being transported to and removed from the plasma membrane. Being an integral membrane protein, Cx43 becomes co-translationally inserted into the ER membrane prior to oligomerization into connexons [13, 83]. Although several connexins have been reported to oligomerize in the ER [84-86], this is not the case for Cx43. Instead, Cx43 exist in a monomeric form after exiting the ER, and undergoes oligomerization in the *trans*-Golgi network prior to the cell surface trafficking [87].

1.10.2 Transport of Cx43 to the plasma membrane

Time-lapse imaging of the GFP-tagged Cx43 has revealed its delivery to the plasma membrane in pleiomorphic vesicles and tubular extensions, originating from the distal end of the Golgi apparatus [88]. Transport of Cx43 is also facilitated in part by microtubules. This understanding is based on the fact that Cx43 gap junction plaques failed to readily regenerate in the presence of nocodazole-induced depolymerized microtubules [88]. Interestingly, other reports suggest that neither microfilaments nor microtubules are an absolute requirement for the assembly of gap junctions; however, intact microtubules are necessary for the enhanced growth of gap junctions and Cx43 transport to the plasma membrane [89]. The targeting of Cx43 to specific cell surface micro-domains, however, remains relatively unclear with some evidence supporting a role for adherens-based junctions in the formation of gap junctions [90, 91].

Once at the cell surface, connexons were originally proposed to exist in a gated-closed state to avoid unwanted exchange of small molecules with the extracellular environment [13]. However, this notion is currently evolving as several lines of evidence supports the role of unpaired connexons, otherwise called hemichannels, in non-junctional plasma membranes for the intercellular communication through paracrine signaling [92, 93].

1.10.3 Assembly of Cx43 gap junctions at the cell surface

At the cell surface, connexons from two adjacent cells dock to form gap junction channels that tightly cluster into gap junction plaques [13]. Studies using tetracysteine and GFP-tagged Cx43 supported a model in which new gap junctions formed at the outer edge of the plaques, with mature channels coalescing at the center of the plaques [94, 95]. Cx43 was documented to cluster into gap junction plaques through lateral movements [88]. Fluorescence recovery after photobleaching (FRAP) revealed two states of Cx43 lateral mobility, high and low [96]. The differential rates of Cx43 mobility was proposed to be either due to scaffolding with binding partners, and/or acquiring different states of channel packing-ranging from loose (new) to crystalline (mature) structures [96]. Electron microscopy images of Cx43 containing fragments budding from the inner segment of gap junction plaques further support the mature aspects of the gap junction being destined for internalization and degradation [94].

1.10.4 Internalization and degradation of Cx43

Several electron microscopic studies have reported the internalization of connexons into one of the two neighboring cells in the forms of double-membrane structures [97-100], recently coined connexosomes [13]. Micro-injection studies with anti-Cx43 antibody, together with rapid time-lapse imaging revealed connexosomes to originate from pre-existing gap junction plaques and internalize in one of the two adjacent cells [101]. Furthermore, a close association of Cx43 double-membrane structures to clathrin-coated pits and actin cytoskeleton [102-104] suggests additional mechanisms may be involved in Cx43- gap junction internalization.

Once internalized, degradation of Cx43 is mediated by both lysosomes and proteasomes [105, 106]. Evidence suggests that mono-ubiquitination of Cx43 serves as an internalization cue, whereas poly-ubiquitination directs it to the lysosomes [107]. Alternatively, it is hypothesized that proteasomal-mediated degradation of Cx43 might be correlated with ER-associated degradation (ERAD) of mis-folded proteins, while lysosomes function to degrade Cx43 removed from the plasma membrane [13].

Although Cx43 is well characterized from biogenesis to degradation, an in-depth knowledge of the life cycle of pannexins remains obscure.

1.11 Rationale, Hypothesis and Objectives of the Thesis

1.11.1 Rationale

Ever since the discovery of pannexins, considerable focus has been given towards understanding the function of these channels and their physiological roles; however, trafficking events that regulate the overall function of pannexins are not fully understood. Although pannexins and connexins were reported to share structural similarities [1, 108], it was not clear if pannexins exhibit characteristics similar to connexins in terms of their plasma membrane delivery and localization, cell surface mobility dynamics, interplay with the cytoskeletal network and pathways governing their turnover and degradation. Therefore, we paralleled our study to the well-characterized life cycle of Cx43. For our studies we mainly utilized Cx43 positive BICR-M1R$_k$, (rat mammary tumor) cell line as these cells are devoid of Panx1 and Panx3 expression, and have previously proven to be an excellent reference model for characterizing the trafficking, assembly and turnover of Cx43 [96, 109]. BICR-M1R$_k$ cells can also be readily engineered to express either Panx1 or Panx3.

1.11.2 Hypothesis

I hypothesize that in comparison to Cx43, Panx1 and Panx3 exhibit distinct subcellular distributions, cell surface motilities and cytoskeletal dependencies; while Panx1 is further governed by unique turnover dynamics and mechanistic pathways that lead to its internalization and degradation.

1.11.3 Objectives (Figure 1.3)

Objective 1 (Chapter 2)   To characterize the subcellular distribution of Panx1 and Panx3, to identify the secretory pathway involved in Panx1 and Panx3 cell surface trafficking, to analyze the mobility dynamics of GFP-tagged Panx1 and Panx3 at the cell surface and to assess the role of the cytoskeleton in Panx1 trafficking and cell surface dynamics.

Objective 2 (Chapter 3)   To identify the role of the carboxyl terminal tail in Panx1 trafficking and homomeric interactions.

Objective 3 (Chapter 4)   To explore the pathways for Panx1 internalization and degradation
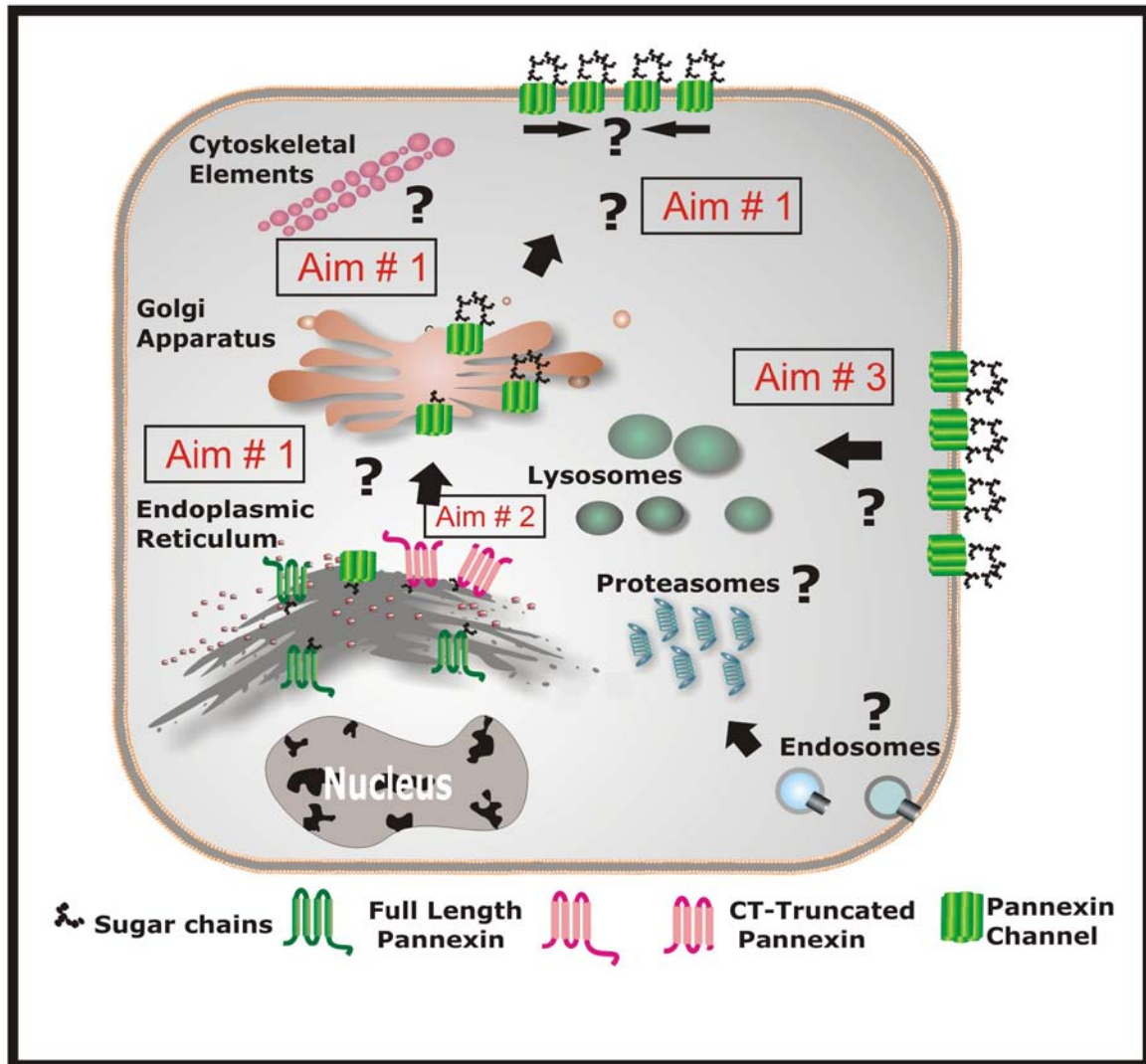
Figure 1.3 Schematic representation of the aims addressed in the study

<u>Aim#1:</u> To characterize the subcellular distribution profile of Panx1 and Panx3, to identify the secretory pathway involved in Panx1 and Panx3 cell surface trafficking, to analyze the mobility dynamics of GFP-tagged Panx1 and Panx3 at the cell surface to assess the role of the cytoskeleton in Panx1 trafficking and cell surface dynamics. **<u>Aim #2:</u>** To identify the role of carboxyl terminal tail in Panx1 trafficking and homomeric interactions. **<u>Aim #3:</u>** To explore pathways for Panx1 internalization and degradation.

CHAPTER 2: Pannexin1 and Pannexin3 Delivery, Cell Surface Dynamics, and Cytoskeletal Interactions

2.0 OVERVIEW

This study was designed to determine if Panx1 and Panx3 exhibit unique characteristics (trafficking, cell surface dynamics and interplay with the cytoskeletal network) or are similar to the well studied gap junction protein, Cx43.

2.1   INTRODUCTION

The pannexin family is a new class of integral membrane glycoproteins that have been identified to share sequence homology to the invertebrate gap junction proteins, innexins [1]. Unlike the connexin family that is comprised of 21 members [110], both the human and mouse genomes contain only three pannexin-encoding genes (*Panx1, Panx2 and Panx3*) [1]. Although connexins and pannexins exhibit no sequence homology, pannexins are predicted to share similar topology to connexins which includes four transmembrane domains, two extracellular loops, a cytoplasmic loop and intracellular amino and carboxy terminals [21, 25, 47]. Our previous study has shown that ectopically expressed Panx1 and Panx3 are capable of trafficking to normal rat kidney (NRK) cell surfaces; however, their distribution profile at cell-cell interfaces is not typically clustered or punctate as seen for Cx43 [25]. Consistently, electron micrographs of Panx1 over-expressing Madin-Darby Canine Kidney cells also revealed dispersed Panx1 localization at the plasma membrane with no evidence of gap junction plaques [47].

Cx43 has a relatively short half-life of approximately 1-3 hours [82]. As a result, Cx43 subunits assembled into connexons within the *trans* Golgi network [87] are constantly being transported to and removed from the plasma membrane [88]. Recent reports provide evidence that although Panx1 appears to form similar hexameric channel units defined as pannexons [47], they exhibit slower turnover dynamics in comparison to Cx43, as assessed by the use of pharmacological blockers of protein synthesis and protein trafficking [25, 47]. Functionally, most

studies support the premise that pannexins, in particular Panx1, form single membrane channels [25, 47, 50, 71, 111, 112], while far less evidence supports the notion that they also can form intercellular channels [26, 53].

The delivery of Cx43 for the assembly of functional channels at the cell surface has been extensively studied using fluorescent protein and epitope tags [94, 96]. Cx43-GFP has been shown to exhibit similar distribution and functional characteristics as its untagged counterpart, when assessed by dye permeability and electrical conductance [88, 113]. Likewise, GFP tagging of the carboxyl terminal tail of Panx1 did not significantly alter the localization profile of Panx1 in NRK cells [25]. However, a recent electrical conductance assessment provided evidence that mouse Panx1-GFP exhibits reduced channel function when expressed in human embryonic cells (HEK) 293 cells [114], suggesting that its functional state is somewhat impaired but not completely eliminated by the GFP tag. In other studies, untagged and tetracysteine-tagged Panx1 exhibited comparable capabilities in rescuing the trafficking of the glycosylation-defective mutant of Panx1 in Madine-Darby canine kidney cells [81]. Collectively, these studies would suggest that the trafficking and life cycle properties of Panx1 can be assessed by GFP tagging approaches in conjunction with real-time dynamic imaging.

It has been previously established through a number of studies using both untagged and GFP-tagged Cx43 that the delivery and regeneration of Cx43 gap junction plaques is facilitated by microtubules and requires a fully functional secretory pathway [88, 89, 95]. Other studies using rapid time-lapse imaging of

GFP and tetracysteine tagged Cx43 have shown that Cx43 is delivered in 100-150 nanometer vesicles that coalesce laterally into the pre-existing gap junction plaques [94, 115]. However, the delivery of pannexins to the cell surface, their dynamic organization at specific cell surface micro-domains, and their dependency on an intact cytoskeletal network, have yet to be investigated.

The life-cycle of Cx43 is governed, in part, by many direct and indirect binding partners [13, 44, 116], while pannexin binding partners are only beginning to be identified with some evidence to support Panx1 interaction with a protein subunit of the voltage-dependent potassium channel [117] and regulatory cross-talk with P2X7 receptors [49, 111]. In the present study we further expand on a very limited number of pannexin binding proteins by identifying actin as a specific Panx1 binding protein.

2.2 EXPERIMENTAL PROCEDURES

2.2.1 Cell Culture and Reagents

BICR-M1R$_k$ cells originally derived from a rat mammary tumor, HEK-293T, NRK and REK (rat keratinocytes) cells were cultured in high glucose DMEM (Invitrogen, Burlington, ON, Canada), supplemented with 10% fetal bovine serum, 100 units/ml penicillin, 100 μg/ml streptomycin, and 2 mM L-glutamine (all from Invitrogen, Burlington, ON, Canada). B16-BL6 murine melanoma cells were kindly provided by Dr. Moulay A. Alaoui-Jamali-(Department of Medicine and Oncology, McGill University; Montreal, Canada) and cultured as previously described [118]. Trypsin (0.25%, 1mM EDTA), Opti-MEM1 media and Lipofectamine 2000 were purchased from Invitrogen. Brefeldin-A (BFA), nocodazole and cytochalasin B were purchased from Sigma-Aldrich (Oakville, ON, Canada).

2.2.2 Expression Constructs of Mouse Panx1, Panx2, and Panx3 and Engineering of the GST-Panx1 Carboxyl domain

Untagged and GFP-tagged expression constructs encoding full length mouse Panx1 and Panx3 were previously described [25], and correspond to current NCBI reference sequence encoding 426 amino acids for Panx1 (NP_062355) and 392 amino acids for Panx3 (NP_766042).

As previously described, Panx2 was originally cloned from mouse brain and the purified PCR product was inserted into the *EcoR*1-*Sal*1 site of pEGFP-N1 vector (Clonetech, CA) to generate the untagged Panx2 [59]. The sequence was

confirmed to encode 677 amino acids according to RefSeq. Furthermore, Panx2 cDNA was amplified using forward primer: 5'- CCCAAGCTTATGCACCACCTC to create a *HindIII* site and 5'- GGCGACCGGTCCAAACTCCACA to create a *AgeI* site at the 5' and 3' ends of Panx2, respectively. PCR products and the vector pEGFP-N1 (Clonetech, Palo Alto, CA) were digested with *HindIII* and *Age1,* ligated and clones were selected. GFP was fused in frame to the carboxyl terminus of Panx 2 with the addition of a five-amino acid polylinker (GGACCGGTCGCCACC) and validated by sequencing.

Panx1 carboxy tail primers (Forward 5'- CTAGGATTCCGGCAGAAAACGGAC, Reverse 5'- CGAGTCGACTTAGCAGGACGGATT), with flanking sites for BamHI and SalI amplifying the Panx1 carboxy tail sequence (corresponding to amino acid 299-426), were created. This sequence was ligated into the pGEX-6P-3 GST vector and transformed into BL21 bacteria. Batch purification using Sepharose 4B was performed as described in GST Gene Fusion System manual with some modifications (GE Healthcare, Buckinghamshire, UK). A single BL21 clone transformed with either GST alone or GST-Panx1 carboxyl tail was grown to absorbance $_{(600nm)}$ of 1 and was induced by the addition of 0.5 mM isopropyl β-D-1-thiogalactopyranoside. A total of 500 mL of either GST or GST-Panx1 carboxy tail bacterial culture was shaken overnight at room temperature. The next day purification was performed using 400 μL of 50% sepharose slurry, washed in PBS seven times and stored at 4°C for the co-sedimentation assays.

2.2.3 Transfection and Engineering of Stable Cell Lines

DsRed tagged $Sar1^{WT}$ and $Sar1^{H79G}$ cDNA constructs were previously described [88] and used for transfection into BICR-M1R$_k$ cells engineered to express Panx1 or Panx3. Briefly, BICR-M1R$_k$ cells were grown overnight to 50-70% confluency on glass coverslips and transfected in Opti-MEM1 media containing 4 µL of Lipofectamine 2000 and 1 µg of Panx1 or 3 µg of Panx3 plasmid DNA together with 2 µg of *Sar1*^{WT} or *Sar1*^{H79G} expression constructs.

Panx1-GFP cDNA construct was previously described (5) and used to transfect BICR-M1R$_k$ cells stably expressing untagged Panx1, and B16-BL6 cells. Cells were grown overnight to 50-70% confluency on 35mm glass bottom dishes and transfected in Opti-MEM1 media containing 1.5 µL of Lipofectamine 2000 and 1.5 µg of Panx1-GFP plasmid DNA for 4 hours at 37°C.

For Panx3 and Panx3-GFP co-transfections: BICR-M1R$_k$ cells were grown overnight to 20-30% confluency on 35mm glass bottom dishes and transfected in Opti-MEM1 media containing 4 µL of Lipofectamine 2000 and 3 µg of Panx3 together with 1.5 µg of Panx3-GFP plasmid DNA. Opti-MEM1 media was replaced with complete culture media 4 hours after transfection at 37 ˚C.

For Panx2 and Panx2-GFP expression: BICR-M1R$_k$ cells grown overnight to 50-70% confluency on glass coverslips were transfected in Opti-MEM1 media containing 3 µL of Lipofectamine 2000 and 1.5 µg of Panx2 or 1.5 µg of Panx2-GFP plasmid DNA. For co-transfection of Panx2 with Panx2-GFP 0.75 µg of

each plasmid DNA was used in Opti-MEM1 media containing 3 µL of Lipofectamine 2000.

Full length constructs encoding mouse Panx1, Panx1-GFP and Panx3 were inserted into the AP-2 retroviral vector and transfected into the 293GPG packaging cell line as described earlier by Qin et al. [119]. Following transfection, replication-defective retroviral supernatants were collected and filtered through a 0.45 µm filter (Pall Gelman Laboratories, Ann Arbor, MI). BICR-M1R$_k$ cells expressing Cx43-GFP were engineered to stably express Panx1 and Panx3 by following a previously described protocol [119]. Retrovirus encoding Panx1-GFP was also used to stably express GFP-tagged Panx1 in BICR-M1R$_k$ cells.

2.2.4 Treatments with pharmacological reagents

Panx1 and Panx3 over-expressing BICR-M1R$_k$ cells were treated with 5µg/mL of BFA for 19 hours at 37°C, and cell lysates were collected and subjected to immunoblotting. For elucidating the role of cytoskeletal elements in pannexin trafficking, Panx1-GFP expressing cells were treated with 10µM nocodazole or 2.5 µg/mL cytochalasin B for 90 minutes and fixed for immunocytochemistry. For fluorescence recovery after photobleaching (FRAP) studies, Panx1-GFP expressing cells were pre-treated with cytoskeletal inhibitors for 90 minutes prior to imaging up to 3-4 hours in presence of these same inhibitors.

2.2.5 Immunocytochemistry

Cells were immunolabeled as previously described [25]. Briefly, cells grown on glass coverslips were fixed using ice-cold 80% methanol and 20% acetone for 20 minutes at 4°C. Cytochalasin B-treated cells were fixed using 3.7% formaldehyde for 30 minutes at room temperature and permeabilized for 45 minutes in a 1% blocking solution (Bovine Serum Albumin-(BSA; Sigma)) containing 0.1% Triton-X-100. Cells were incubated with a 500-fold dilution of polyclonal anti-Cx43 antibody (Sigma), a 100 fold dilution of polyclonal anti-GPP130 antibody (Convance), polyclonal anti-Panx2 antibody (Zymed Laboratories, San Francisco, CA) or monoclonal anti-tubulin antibody (Convance) for 1 hour at room temperature. Affinity-purified polyclonal Panx1 and Panx3 antibodies were used at a concentration of 2 µg/mL. F-actin was localized using a 200 fold dilution of rhodamine phalloidin (Invitrogen). Cells were incubated in goat anti-rabbit antibody conjugated to Texas Red or fluorescein isothiocyanate (FITC) (1:100, Jackson Laboratories, Westgrove, PA) or a goat anti-mouse antibody conjugated to Texas Red (1:100, Jackson Laboratory). Cells were rinsed with PBS and nuclei were stained with Hoechst 33342 and mounted. Immunolabeled cells were imaged using a 63x oil objective lens mounted on a Zeiss LSM 510 META (Zeiss, Toronto, ON) system.

2.2.6 Immunoblotting and Co-immunoprecipitation

Cell lysates from BICR-M1R$_k$ cells transiently co-transfected with Sar1 and Panx1 or Panx3 cDNA constructs, and BFA-treated cells were collected using a lysis buffer containing 1% Triton-X-100, 10 mM Tris, 150 mM NaCl, 1 mM EDTA, 1

mM EGTA, 0.5% NP-40, 100 mM sodium fluoride and 100 mM sodium orthovanadate and a protease inhibitor tablet (one tablet per 10 mL buffer; Roche, Laval, QC), pH 7.4. Protein concentrations were measured using a BCA protein determination kit (Pierce). In total, 20-30 µg of protein was resolved using 10% SDS-PAGE and transferred to nitrocellulose membrane (Pall Life Sciences, NY). Nitrocellulose membranes were blocked in Licor blocking solution (Lincoln, NE) or 3% BSA solution, and probed overnight with polyclonal affinity purified anti-Panx1 or anti-Panx3 antibodies (0.2 µg/mL) at 4C. Monoclonal anti -β-actin antibody (1:5000, Sigma) was used to assess gel loading. Detection of primary antibody binding was performed by using mouse IgG IR dye 800 (Rockland Immunochemicals, PA) and rabbit IgG Alexa 680 (Invitrogen) with Odyssey infrared imaging system (Licor).

For co-immunoprecipitation experiments, 1 mg of protein lysates from WT, Panx1 and Panx1-GFP over-expressing BICR-M1R$_k$ cells were incubated overnight at 4°C in the lysis buffer (1% Triton-X-100, 10 mM Tris, 150 mM NaCl, 1 mM EDTA, 1 mM EGTA, 0.5% NP-40, 1 mM sodium fluoride and 1mM sodium orthovanadate containing 10 µg/mL of anti-Panx1 antibody. The antibody complex was pulled down with 30 µl of pre-cleaned protein A-sepharose beads (in PBS) for 2 hours on the rocker at 4°C. The antibody-bead complex was centrifuged at 4500 RPM at 4°C for 2 minutes and supernatant was aspirated. Unbound nonspecific protein was separated from bound proteins by washing three times with 500 µL of lysis buffer, and the bound complex was detached by boiling for 5 minutes in 30 µL of 2x Laemmli loading sample buffer containing $\beta-$

mercaptoethanol. Samples were resolved by 10% SDS-PAGE and transferred to nitrocellulose membranes which were probed with anti-Panx1 and anti-β-actin antibodies.

2.2.7 FRAP analysis

To assess Panx1 or Panx3 dynamics at the cell surface, BICR-M1R$_k$ cells expressing Panx1-GFP alone or in combination with the untagged, Panx1, or Panx3-GFP together with Panx3, were cultured on 35 mm glass bottom dishes and subjected to FRAP. B16-BL6 cells expressing Panx1-GFP were also subject to FRAP analysis. Rapid time-lapse imaging was performed on a Zeiss LSM 510 META to quantify the movement of Panx1-GFP into the bleached region of interest (ROI), as previously described [96]. Briefly, glass bottom dishes were placed in an environmentally-controlled chamber and ROIs representing the various plasma membrane domains were selected and photo-bleached using scan iterations at 488 nm with 100% laser strength. Images were acquired ~2-5 seconds apart for up to 60 seconds with 0.9% laser strength, to avoid further photobleaching. Fluorescence intensities within ROIs were quantified as previously described [96]. Briefly, fluorescence recovery was recorded: before photobleaching, immediately upon completion of photobleaching (t was set to 0 seconds), and post bleaching at the following time intervals (15, 25, 50 and 60 seconds). Post-bleach intensities were corrected and normalized for any residual fluorescence, and the recoverable fraction of Panx1-GFP or Panx3-GFP was calculated using $F_{Nt} = (F_t - F_0)/(F_i - F_0)$ as previously described [120]; where F_{Nt} = normalized fluorescence at a t time point; F_t = fluorescence intensity within ROI at

t seconds post photo-bleach; F_0 = fluorescence intensity upon photo-bleaching at t = 0 and Fi = fluorescence intensity prior to photobleaching. All FRAP experiments were repeated 3 times for each experimental set, with each set containing multiple ROIs at t = 15, 25, 50 and 60 seconds. F_{Nt} values from replicates of each experimental set were combined and a non-linear regression analysis was performed to obtain a curve of best fit using GraphPad Prism software (San Diego, CA). To compare the mobility dynamics of Panx1-GFP or Panx3-GFP in various plasma membrane domains, a one-way ANOVA followed by Tukey's multiple comparison tests were performed. For comparisons between untreated versus nocodazole and cytochalasin B treated experimental sets, t tests were performed using GraphPad Prism software.

2.2.8 Vesicle Movement

Panx1-GFP containing vesicles were analyzed by measuring the total distance traveled of vesicles that remained in confocal plane of focus for the duration of the analysis. Vesicles of ~0.5-0.8 µm in diameter were monitored by 1.8 second interval image scans for a total period of 8.8 seconds. (n= 18-20, over 4 independent repeats).

2.2.9 Actin co-sedimentation assays

Muscle actin (Cytoskeleton Inc., Denver, CO) was resuspended in buffer (5 mM Tris-HCl pH 8.0, 0.2 mM $CaCl_2$) to a concentration of 1 mg/mL in 250 µl on ice for 30 min. 25 µLs of 10X actin polymerization buffer (500 mM KCl, 20 mM $MgCl_2$, 10 mM ATP, 100 mM Tris pH 7.5) was added to the monomeric actin and

incubated at room temperature for 1h (F-actin stock at 23 µM). Protein samples of BSA, GST, Panx1 C-tail and GST tagged Panx1 C-tail were centrifuged at 150,000 x g for 1 h at 4 ºC. Supernatants were collected and placed on ice. For co-sedimentation assays, a GST fusion protein containing the C-tail of mouse Panx1 was used, either as a fusion protein after elution from the sepharose beads or after cleavage of the Panx1 C-tail from the fusion protein using PreScission Protease (GE Healthcare, Buckinghamshire, UK) for 16 h at 4 ºC, as per manufacturer's instructions. Following the Cytoskeleton Inc. protocol for actin binding protein assays, 50 µL samples were prepared with either F-actin alone, GST protein with or without F-actin, BSA (negative control) plus F-actin, and Panx1 C-tail or GST fusion protein with or without F-actin. Samples were incubated at room temperature for 30 min, followed by centrifugation at 150,000 x g for 1.5 h at 24 ºC. Supernatants were carefully removed and mixed with 10 µL 4X Laemmli reducing-sample buffer. The pellets were resuspended in 30 µL of double-distilled water and mixed with 30 µL of 2X Laemmli buffer. Equal volumes of resuspended pellets and supernatants were run in duplicate on 10% SDS-PAGE. Gels containing samples were either stained overnight with Sypro-Ruby Protein gel stain (Invitrogen) or transferred onto nitrocellulose membranes using an iBlot apparatus for dry transfer (Invitrogen). Sypro-Ruby stained gels were de-stained and exposed to UV for visualization of the major bands. Nitrocellulose membranes were incubated overnight with primary anti-Panx1 antibodies, washed, and probed with Alexa-680 anti-rabbit secondary for detection of Panx1 bands with a LiCor scanner as described previously [25].

2.2.10 Biotinylation assays

BICR-M1R$_k$ cells grown on 100 mm dishes were transiently transfected with 5-10 μg of Panx3-GFP encoding cDNA constructs, and 48 hours post transfection, cells expressing Panx3-GFP were subjected to biotinylation treatment on ice as previously described [25]. Cells were incubated in PBS or with cold PBS containing EZ-link Sulfo NHS-LC-biotin (0.5 mg/mL; Pierce Biotechnology) for 20 min at 4°C. Control and biotin-treated cells were washed and incubated in 100 mM glycine buffer for 15 min at 4°C to quench the biotin. Cells were then lysed with SDS lysis buffer (1% Triton X-100 and 0.1% SDS in PBS) and protein concentrations were measured using a BCA protein determination kit (Pierce). In total, 1000 μg of protein from control and biotin-treated cell lysates were rocked overnight at 4°C in the presence of 50 μL of neutravidin-agarose beads (Pierce Biotechnology). Beads were washed three times with immunoprecipitation lysis buffer (IP) (150 mM NaCl, 10 mM Tris-HCl, pH 7.4, 1 mM EDTA, 0.5% NP-40, and 1% Triton X-100) containing 1 mM NaF and 1 mM Na$_3$VO$_4$; and once with PBS containing 1 mM NaF and 1 mM Na$_3$VO$_4$. The beads were air dried and resuspended in 50 μL of 2x Laemmli loading sample buffer containing β–mercaptoethanol before boiling for 5 minutes. As a lysate control, 40 μg of total protein from control and biotin samples was also resolved by SDS-PAGE and transferred to nitrocellulose membranes for immunoblotting with anti-Panx3 antibody.   GAPDH was used as a control to detect any unexpected biotin internalization.

2.3 RESULTS

We have previously shown that the Cx43-positive BICR-M1R$_k$ (rat mammary tumor) cell line is an excellent reference model for investigating dynamic delivery events, assembly and turnover mechanisms of Cx43 [96, 109]; therefore, we designed our experimental approach to compare Panx1 and Panx3 trafficking dynamics in Cx43-positive BICR-M1R$_k$ cells. We engineered stable cells lines to ectopically express Panx1 or Panx3. Western blots analysis revealed that wild-type BICR-M1R$_k$ cells are negative for Panx1 and Panx3 (Figure 2.1A) but when engineered to express pannexins, Panx1 resolved as multiple species ranging from ~41-48 kDa; whereas, Panx3 was detected as a doublet at ~43kDa (Figure 2.1A). These multiple pannexin species have previously been shown to be the result of glycosylation [25, 47]. Immunolabeling of both Panx1 and Panx3 revealed that both of these pannexins were capable of trafficking and localizing in a relatively uniform pattern at the apposing cell surface (Figure 2.1B). In contrast, detectable Panx2 and Panx2-GFP were mainly localized in the intracellular compartments of, not only BICR-M1R$_k$ cells, but also in HEK 293T, NRK and rat keratinocytes (Supplementary Figure 1). Not unexpected, the co-expression of Panx2 with Panx2-GFP did not alter the distribution pattern of untagged or tagged Panx2. These studies indicate that Panx2 has a unique distribution when compared to Panx1 and Panx3 even when expressed in the same reference cells.
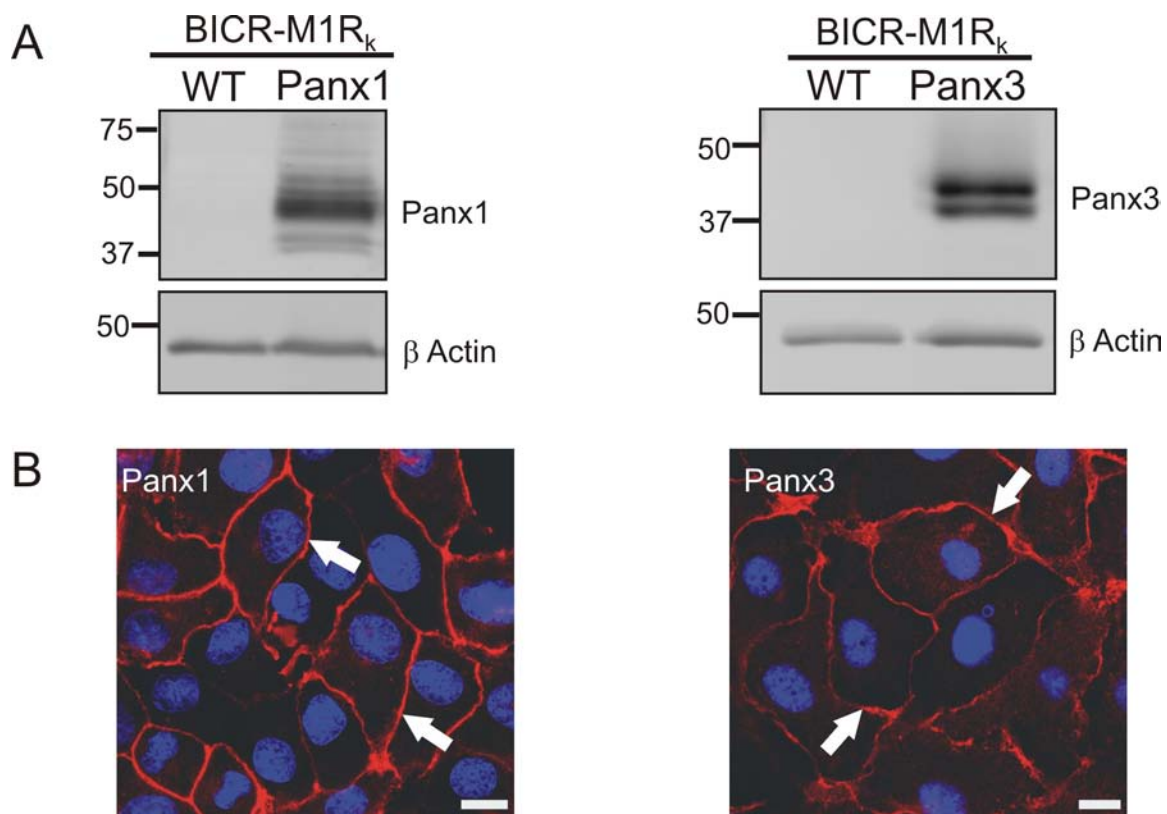
Figure 2.1 Panx1 and Panx3 are capable of trafficking to the cell surface in BICR-M1R$_k$ cells

BICR-M1R$_k$ cells were engineered to stably express Panx1 or Panx3. Immunoblotting with affinity purified antibodies (anti-Panx1 and anti-Panx3) revealed multiple banding profiles of Panx1 (~41-48 kDa) and Panx3 (~41-43 kDa) (A). β-actin was used as a protein loading control (A). Immunolabeling of Panx1 and Panx3 (B) identified that both pannexins trafficked and localized to the cell surface (arrows). Nuclei are stained with Hoechst 33342 (blue). Bars= 10 μm. Representative of three independent experiments.

2.3.1 Trafficking of Panx1 and Panx3 is mediated through Sar1-dependent COPII vesicles

It has been widely documented that Sar1 (secretion associated and Ras related) GTPase is critical for COPII (coat protein II) assembly and vesicular transport of newly synthesized proteins from the endoplasmic reticulum (ER) compartment [121, 122]. Dominant-negative GTP-bound mutant Sar1^{H79G} has previously been shown to block the ER-Golgi transport of newly synthesized Cx43 in BICR-M1R$_k$ cells [88]. In order to determine if Panx1 and Panx3 follow the classical ER-Golgi secretory pathway mediated through a COPII-dependent mechanism, we engineered BICR-M1R$_k$ cells to co-express Panx1 or Panx3 along with Sar1^{WT} or Sar1^{H79G}. Co-expression of Panx1 with Sar1^{WT} revealed a typical uniform distribution of Panx1 at the cell surface (Figure 2.2A, arrows), while Sar1^{WT} was localized to the paranuclear region in an intact Golgi-like compartment (Figure 2.2A, B). In comparison, expression of Sar1^{H79G} resulted in fragmentation of a Golgi-like compartment in the paranuclear region (Figure 2.2A, B); and retention of Panx1 and Panx3 in ER-like patterns with little evidence of cell surface localization (Figure 2.2A, B arrowheads). In the same culture environments, BICR-M1R$_k$ cells expressing Panx1 or Panx3 but not Sar1^{H79G} revealed a uniform cell surface labeling of Panx1 and Panx3 (Figure 2.2A, B inserts, arrows). Furthermore, as we previously reported [88], the distribution of Cx43 gap junction plaque-like structures was not evident in the presence of Sar1^{H79G} (not shown). Since Panx1 and Panx3 resolve as multiple bands (Figure 2.1A and 2C), we wanted to determine the effect of dominant-negative Sar1 on the different molecular species.
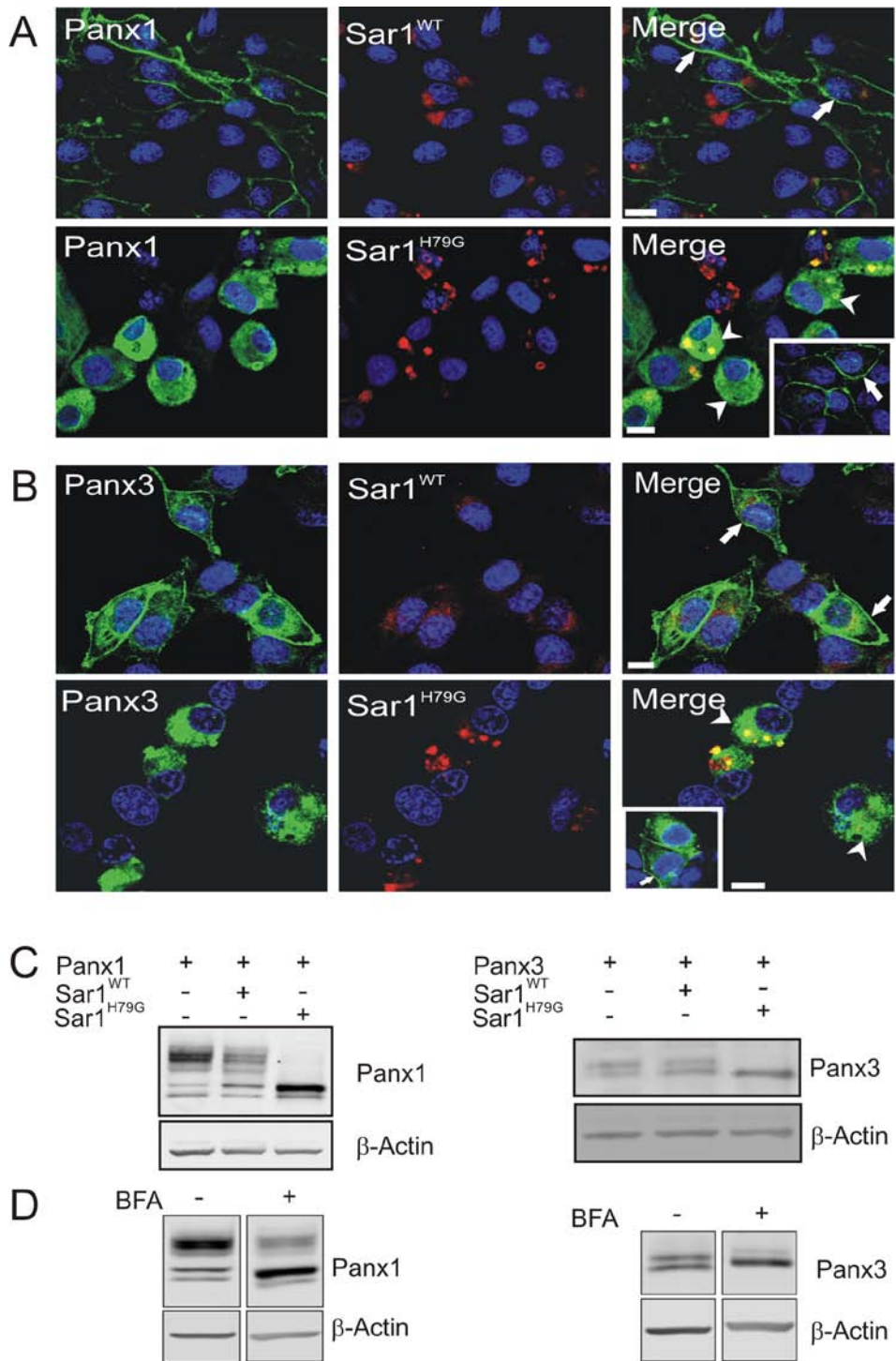
Figure 2.2 Trafficking of Panx1 and Panx3 was disrupted in the presence of a dominant-negative Sar1 mutant

BICR-M1R$_k$ cells expressing Panx1 or Panx3 together with Sar1^{WT} or Sar1^{H79G} were immunolabeled for Panx1 (A) or Panx3 (B). Both Panx1 and Panx3 were

capable of trafficking and localizing to the cell surface in the presence of Sar1^{WT} (A, B filled arrows). Expression of Sar1^{H79G} resulted in Panx1 and Panx3 being retained in an ER-like compartment (A, B arrowheads); however, when cells expressed Panx1 or Panx3 without expressing Sar1^{H79G} in the same cellular environment, both Panx1 and Panx3 trafficked to the plasma membrane (A, B, insets, arrows). Western blotting of Panx1 and Panx3 in the presence of Sar1^{H79G} (C), or after long term BFA treatment (19hr; D) revealed an accumulation of the high mannose species of Panx1 and Panx3, with a noticeable reduction in the higher molecular weight glycosylation species (C and D). Nuclei are stained with Hoechst 33342 (blue). Bars= 10 μm. Representative of three independent experiments.

When compared to Panx1 alone or with Sar1^{WT}, the presence of Sar1^{H79G} revealed an accumulation of the intermediate species (previously demonstrated to be a high mannose glycosylation species [47]), with a noticeable reduction in the most extensively glycosylated species of Panx1 (Figure 2.2C). Similarly, an accumulation of lower molecular weight species (previously reported to be a high mannose glycosylation species [59]) of the Panx3 doublet was also revealed in the presence of Sar1^{H79G} (Figure 2.2C), suggesting that the higher molecular weight species of Panx1 and Panx3 is the consequence of additional post-translational processing that occurs upon exiting the ER. Consistently, long term brefeldin A (BFA) treatment (19hr) (a pharmacological blocker known to inhibit anterograde transport of proteins between the ER and Golgi apparatus [123]) of Panx1 and Panx3 expressing BICR-M1R$_k$ cells caused a detectable increase in the high mannose species of Panx1 and Panx3, with a noticeable reduction in the higher molecular weight species of both Panx1 and Panx3 (Figure 2.2D). Collectively, these results suggests that both Panx1 and Panx3 are co-translationally inserted into the ER and transported in a COPII-dependent mechanism to the Golgi apparatus, where they are substrates for further glycosylation and processing.

2.3.2 GFP-tagged Panx1 mimics the distribution profile of untagged Panx1 and is suitable to investigate the dynamic distribution of Panx1

In order to assess the dynamic properties of Panx1, we first stably expressed Panx1-GFP in BICR-M1R$_k$ cells and evaluated its distribution profile with respect to untagged Panx1. Immunofluorescent labeling revealed that Panx1-GFP

exhibited a similar cell surface distribution pattern (Figure 2.3A, arrows) as observed for untagged Panx1 (Figure 2.3F, arrows), with a notable increase in intracellular fluorescent signal (Figure 2.3A). Clearly, the cell surface pattern for Panx1-GFP was distinct from that observed for Cx43-GFP when expressed in the same cell type (Figure 2.3A, insert). To assess the dynamic activity of Panx1 at the cell surface and within intracellular compartments we performed rapid time-lapse imaging on cells that expressed Panx1-GFP. Panx1-GFP was not only visualized in a relatively uniform pattern at the cell surface (Figure 2.3A), but also as mobile bright fluorescent clusters (Figure 2.3B and C). Rapid time-lapse imaging revealed that these clusters (suggestive of Panx1-GFP aggregates) were mobile at the plasma membrane and in regions devoid of cell-cell contacts (Figure 2.3B and C, filled arrows, see Movie 2.1). In addition, Panx1-GFP was also found in distinct intracellular vesicle-like structures that were highly mobile (Figure 2.3D, unfilled arrows, Movie 2.1). Surprisingly, and distinct from that observed for functional Cx43, Panx1-GFP was found in dynamic finger-like projections indicative of membrane protrusion (Figure 2.3E, arrowheads, Movie 2.1). This localization to membrane protrusion was also frequently evident in cells expressing untagged Panx1, suggesting that this localization profile is not a consequence of the GFP tag (Figure 2.3F, arrowheads).
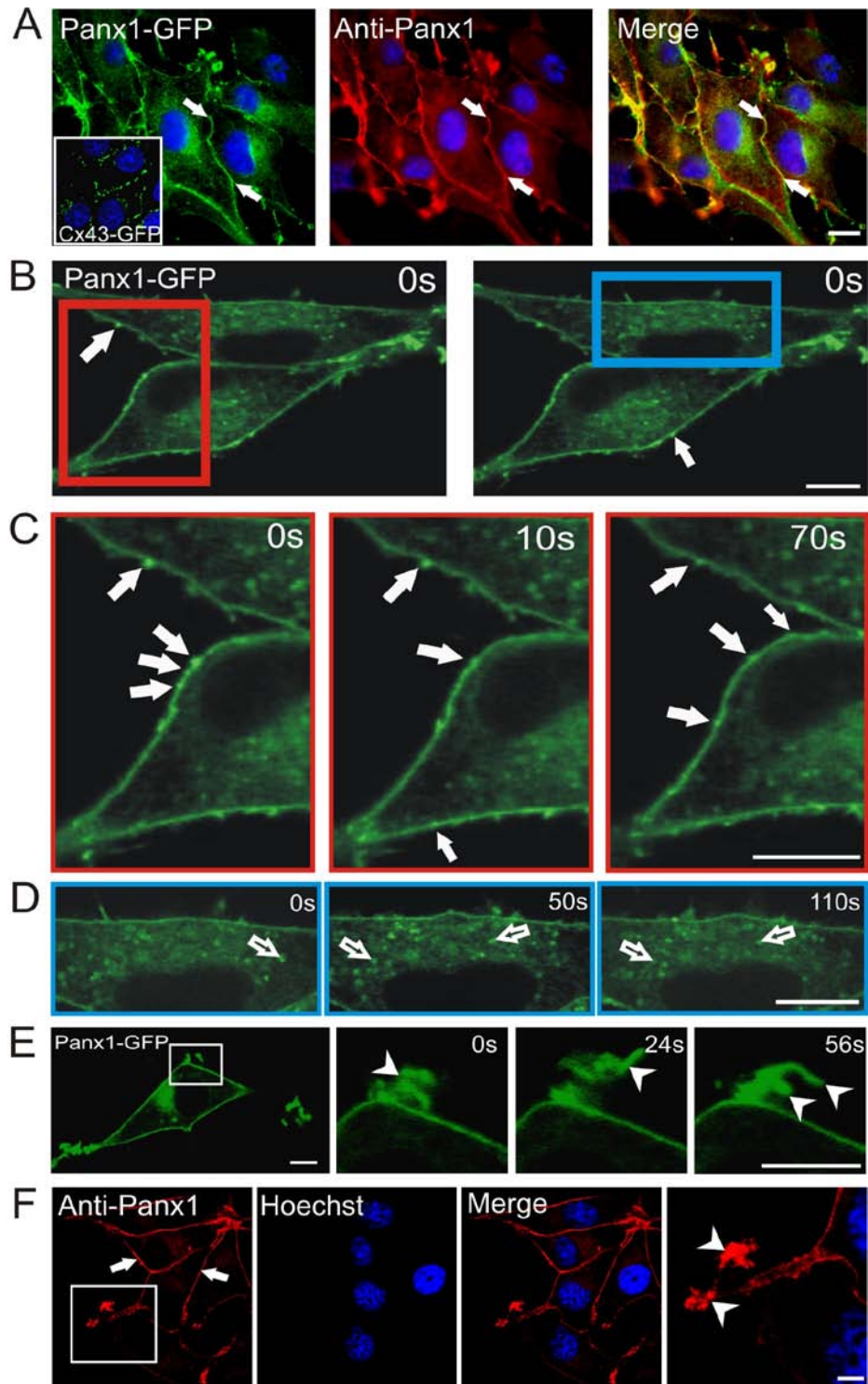
Figure 2.3 Panx1 was localized to multiple sites, compartments and microdomains

Immunolabeling of Panx1-GFP with an anti-Panx1 antibody revealed its localization at the cell surface (A, filled arrows) in a pattern that was distinct from

Cx43-GFP (A, insert). Regions of interest from live BICR-M1R$_k$ cells expressing Panx1-GFP (B, red and blue rectangles) were chosen for live imaging and imaged at t= 0, 10, 50, 70 and 110 seconds (C and D). Rapid time-lapse imaging revealed that Panx1-GFP is distributed primarily in a uniform pattern, while mobile bright fluorescent clusters could be identified at the cell surface (B and C, filled arrows) and within the cell (D, unfilled arrows). Panx1-GFP was clearly localized to dynamic plasma membrane protrusions (E, arrowheads), that were evident in BICR-M1R$_k$ cells expressing untagged Panx1 (F, arrowheads). Nuclei in A and F are stained with Hoechst 33342 (blue).   Bars= 10μm. Representative of three independent experiments. See Movie 2.1: http://www.jbc.org/

Movie 2.1 Dynamic structures carrying Panx1-GFP are distributed intracellularly and at the cell surface

Rapid time-lapse imaging was performed on Panx1-GFP expressing BICR-M1R$_k$ cells to assess the overall localization and distribution pattern of Panx1. Panx1-GFP was localized in a relatively uniform manner at the cell surface with some evidence of cell surface clusters. Intracellular vesicle-like structures carrying Panx1-GFP were evident as bright clusters. Panx1-GFP was also localized to membrane protrusions that were constantly being remodeled. The movie sequence represents 32 frames scanned every 5 seconds, with a total elapsed time of 160 seconds.

2.3.3 Panx1-GFP is highly mobile at all plasma membrane domains as revealed by FRAP analysis

To analyze the dynamic mobility characteristics of Panx1-GFP, we first assessed the ability of Panx1-GFP to traffic and localize at three distinct plasma membrane domains where there was no neighboring cell (Figure 2.4A, red arrow), the neighboring cell expressed Panx1-GFP (Figure 2.4A, blue arrow), or the neighboring cell was devoid of Panx1-GFP (Figure 2.4A, purple arrow). Once it was determined that Panx1-GFP was not differentially distributed to any of these cell surface domains (Figure 2.4A), regions of Panx1-GFP located at these distinct domains were selected and subjected to fluorescence recovery after photobleaching (FRAP) analysis (Figure 2.4B-E). After initial photobleaching, within 2 seconds there was a rapid movement of fluorescent molecules from the outer edges into the photobleached area of all bleached cell surface domains (Figure 2.4B-D, inserts). FRAP curve analysis revealed the mobile fluorescent fractions to be 45-60% at all micro-domains over a time course of only 60 seconds (Figure 2.4E). Moreover, there was no significant difference in the total recovered fraction of Panx1-GFP within any of the plasma membrane domains; an observation that was similar to when we analyzed the percentage recovery of transiently transfected Panx1-GFP (40-50%) in BICR-M1R$_K$ cells stably expressing untagged Panx1 (Supplementary Figure 2), or B16-BL6 cells, identified for the first time to express endogenous Panx1 (Supplementary Figure 3A and B).

Figure 2.4 Panx1-GFP is highly mobile at all plasma membrane locations

Panx1-GFP was localized to three distinct plasma membrane domains of BICR-

$1R_k$ cells, as depicted by the schematic diagram (A). Fluorescent images of Panx1-GFP were superimposed with DIC images to highlight the microenvironment surrounding the cell being analyzed (A-D). Selected cell regions where Panx1-GFP was localized at the three distinct plasma membrane domains were photobleached and fluorescence recovery back into the photobleached areas was assessed and normalized over 60s (B, C and D). Panx1-GFP recovery within the photo-bleached area was not significant different (P>0.05) amongst all three domains (E). Bars = 10 μm. n = 6-9 per plasma membrane domain collected from three independent experiments.

2.3.4 A sub-population of GFP-tagged Panx3 is evident at the cell surface when expressed alone or co-expressed with Panx3 and reveals dynamic localization to the membrane protrusions

We have previously reported that Panx3-GFP has a substantial trafficking defect causing it to be retained within the endoplasmic reticulum of NRK cells [25]. However, when over-expressed in BICR-M1R$_k$ cells, some evidence of Panx3-GFP localization to the cell surface was detected (Figure 2.5A, filled arrows), along with the intracellular ER-like distribution of Panx3-GFP (Figure 2.5A, unfilled arrows). To further confirm that a sub-population of Panx3-GFP can traffic and localize to the cell surface, we performed biotinylation assays in live BICR-M1R$_k$ cells transiently expressing Panx3-GFP. Incubation of Panx3-GFP expressing cells with biotin followed by pull downs with neutravidin beads revealed that the ~70 kD Panx3-GFP indeed traffics to the cell surface (Supplementary Figure 4). GAPDH was used as a negative control to confirm cell integrity and specificity (Supplementary Figure 4). It was interesting to note that when Panx3-GFP was co-expressed with Panx3 in BICR-M1R$_k$ cells, there was an apparent increase in the cell surface population of Panx3-GFP (Figure 2.5B, filled arrows), with some expected intracellular distribution (Figure 2.5B, unfilled arrows). This data suggests that Panx3-GFP may interact with Panx3 to facilitate its traffic to the plasma membrane.
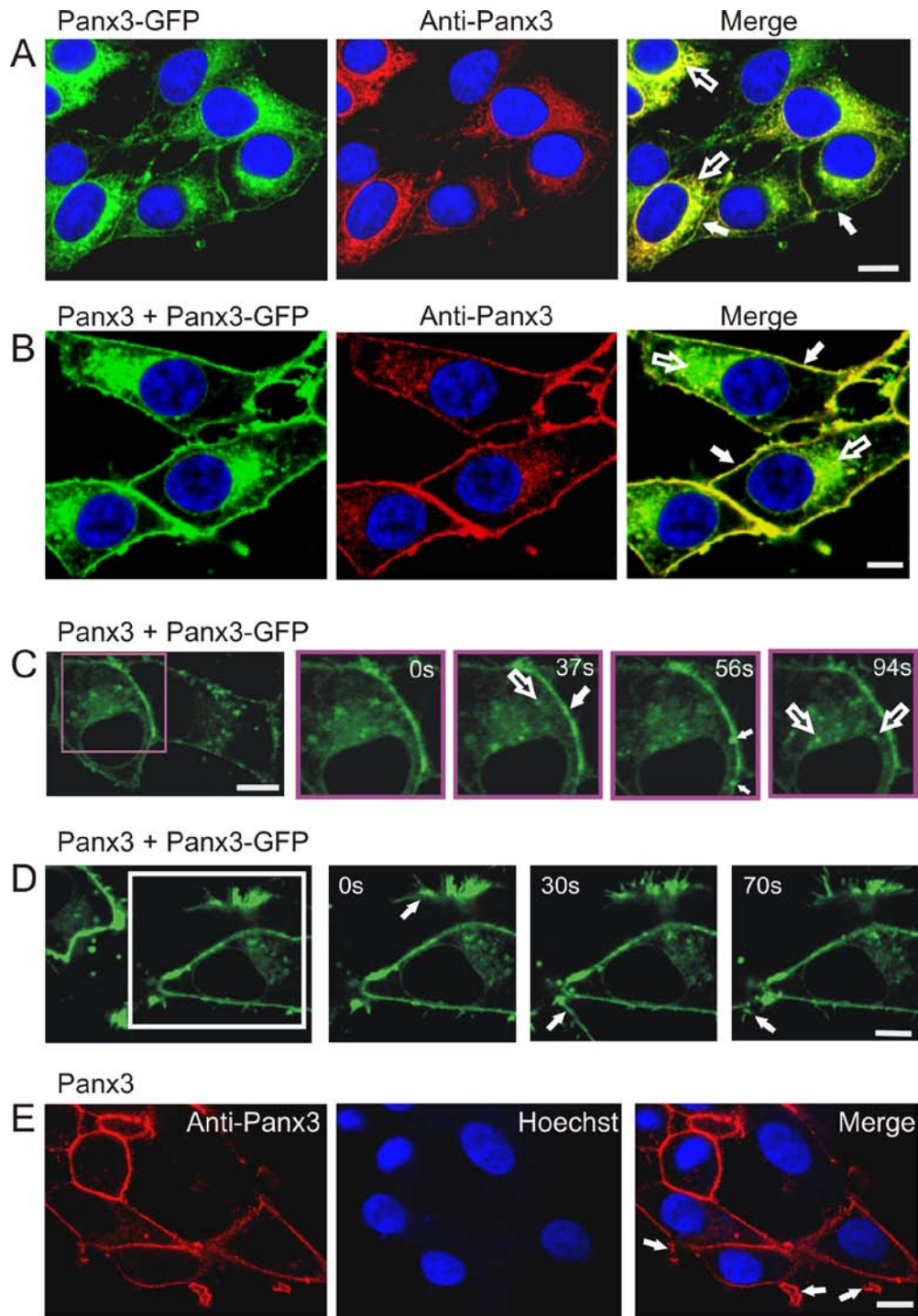
Figure 2.5 Delivery of Panx3-GFP to the cell surface

Wild-type BICR-M1R$_k$ cells engineered to express Panx3-GFP (A), or both Panx3

and Panx3-GFP (B) were immunolabeled with anti-Panx3 antibody. Panx3-GFP

was retained mainly in an ER-like pattern (A, B, unfilled arrows) with some evidence of a cell surface distribution (A, B, filled arrows), while co-expression of Panx3 appeared to increase the cell surface population of Panx3-GFP (B). Rapid time-lapse imaging of live BICR-M1R$_k$ cells co-expressing Panx3-GFP and Panx3 revealed that Panx3-GFP was distributed primarily in a uniform pattern with notable mobile fluorescent clusters at the cell surface (C, filled arrows), and within the cell (C, unfilled arrow). Localization of Panx3-GFP to plasma membrane protrusions (D, arrows) was similar to that found in cells expressing only Panx3 (E, arrows). Nuclei in A, B and E are stained with Hoechst 33342 (blue). Bars= 10 μm. Representative of three independent experiments.

To assess the dynamic activity of Panx3-GFP at the cell surface and within intracellular compartments, we performed rapid time-lapse imaging on cells co-expressing Panx3 and Panx3-GFP. Panx3-GFP was localized at the cell surface in a relatively uniform pattern and as bright clusters either approaching or at the cell surface (Figure 2.5C, filled arrows). In addition, Panx3-GFP was also visualized in distinct vesicle-like structures (Figure 2.5C, unfilled arrows); and observed in cell surface protrusions (Figure 2.5D, arrows), that were also occasionally identified in cells expressing only Panx3 (Figure 2.5E, arrows).

2.3.5 Panx3-GFP is highly dynamic at all cell surface domains

We co-expressed Panx3 with Panx3-GFP and used GFP-tagged Panx3 as a tracer to assess and quantify the mobile fraction in various plasma membrane domains where: the neighboring cell surface was devoid of Panx3-GFP (Figure 2.6A), the neighboring cell expressed Panx3-GFP (Figure 2.6B, see Movie 2.2) or there was no neighboring cell (Figure 2.6C). FRAP analysis of selected regions expressing Panx3-GFP revealed that within 60s after photobleaching, there was a rapid re-entry of GFP-tagged Panx3 molecules into the photobleached area at all micro-domains (Figure 2.6A-C, inserts), and the mobile fraction was calculated to be ~30-40%. However, no significant difference was noticed in the total recovered fraction of Panx3-GFP within any of the plasma membrane domains (Figure 2.6D).
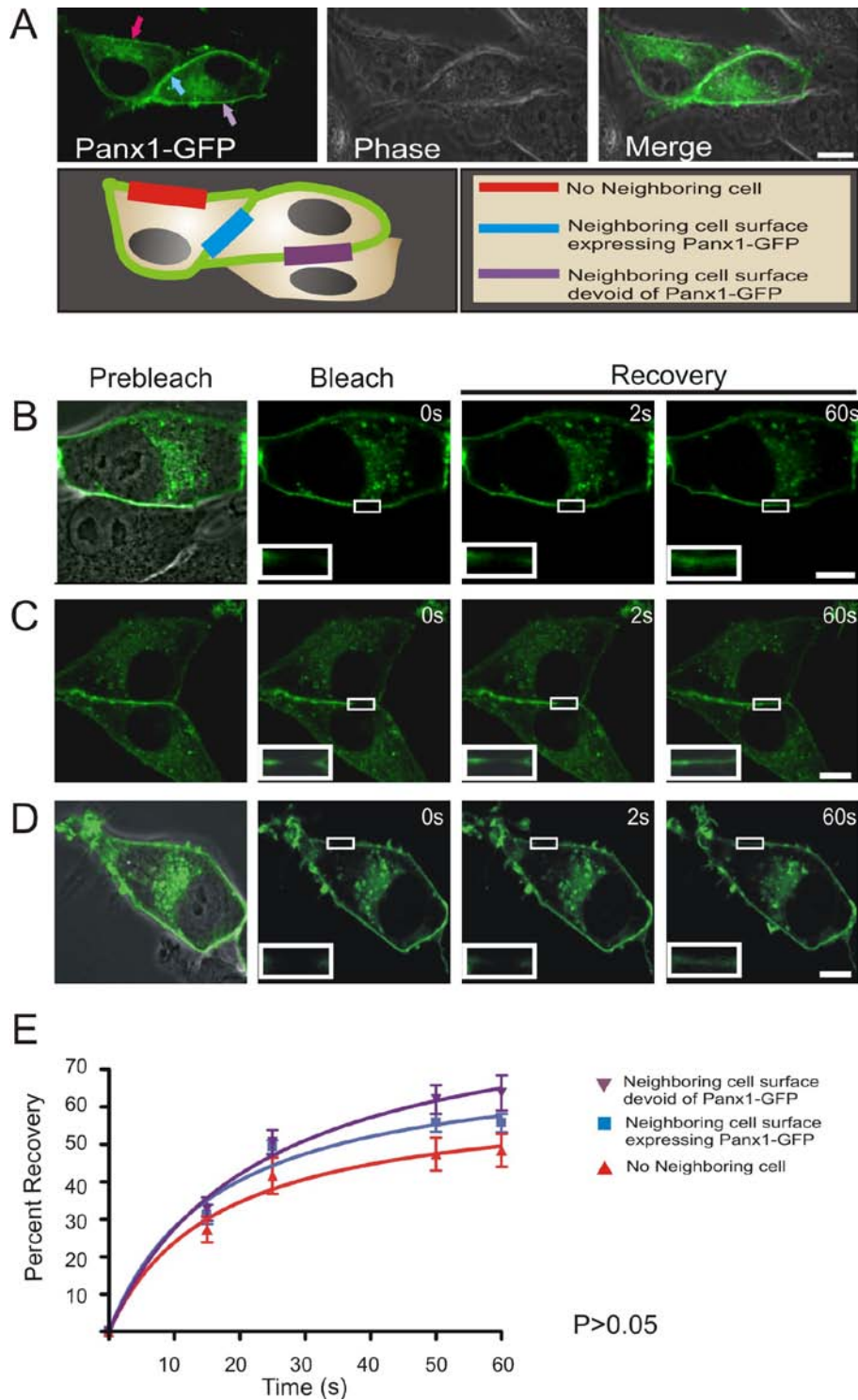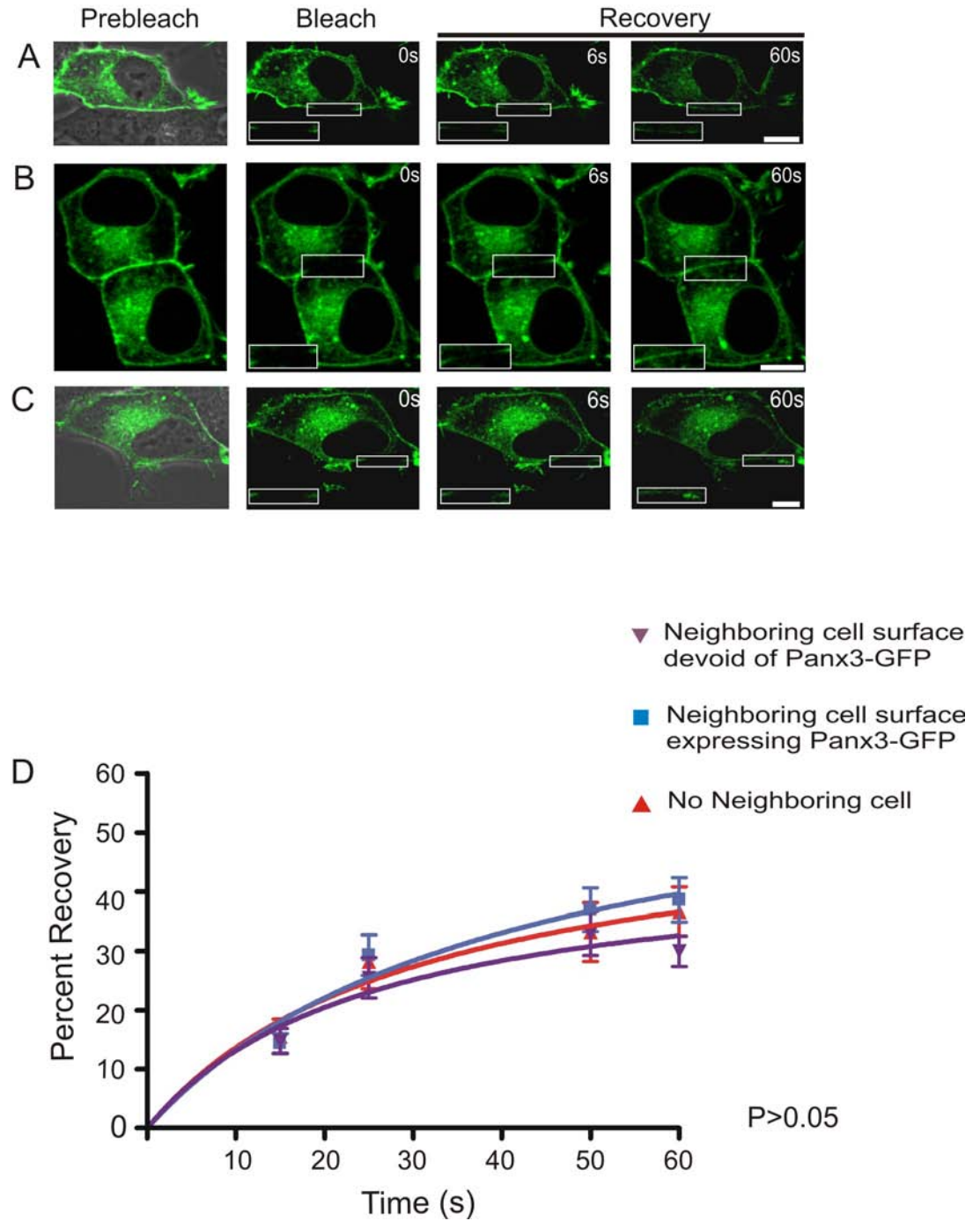
Figure 2.6 Panx3-GFP is highly mobile at all plasma membrane domains

Panx3-GFP was localized to three distinct plasma membrane domains of BICR-M1R$_k$ cells co-expressing Panx3 (A-C). Selected cell surface regions containing

Panx3-GFP were photobleached and fluorescence recovery back into the photobleached areas was assessed and normalized over the time course of 60s. The percent Panx3-GFP recoverable fraction was not found to be significantly different amongst all three plasma membrane domains examined (P>0.05) (D). Bars=10μm. n=12-25 per plasma membrane domain collected from three independent experiments. See Movie 2.2: http://www.jbc.org/

Movie 2.2   The cell surface population of Panx3-GFP is highly mobile

FRAP and rapid time-lapse imaging was performed at cell-cell interfaces where both cells co-expressed Panx3-GFP and Panx3. After photobleaching, Panx3-GFP rapidly migrated into the photo-bleached area. Intracellular vesicle-like structures carrying Panx3-GFP were evident as were bright fluorescent clusters at the cell surface. Panx3-GFP was also observed to be present in actively remodeling membrane protrusions. The movie represents 31 frames scanned every 2 seconds, with a total elapsed time of 62 seconds.

2.3.6 Cell surface population of Panx1-GFP and Panx3 is insensitive to nocodazole treatment

It has been documented that nocodazole disruption of microtubules impairs the continuous trafficking and regeneration of Cx43-GFP at the cell surface [88]. To investigate if trafficking and recovery of Panx1-GFP into the photobleached area is dependent on microtubules, Panx1-GFP expressing BICR-M1R$_k$ cells were exposed to nocodazole for 90 minutes. Nocodazole treatment resulted in characteristic morphological changes in the cells from spindle-shaped to more cuboidal with a notable disruption of the microtubule architecture (Figure 2.7A-C). However, the distribution of Panx1-GFP (Figure 2.7B) and Panx3 (Supplementary Figure 2.7.5B) at the cell surface remained relatively unaffected by the nocodazole treatment. Furthermore, FRAP studies revealed that Panx1-GFP migrated into the photobleached area similarly in both untreated and nocodazole-treated cells (Figure 2.7C, D). Interestingly, the inward progression of fluorescent recovery from the edges of the photobleached area towards the centre was not detected until 10 seconds post bleaching (Figure 2.7C, insert). Furthermore, FRAP analysis of Panx1-GFP in the presence of nocodazole treatment, revealed no significant difference in the recovered fraction when compared to the untreated cells (Figure 2.7D). Thus, nocodazole treatment does not visually affect the cell surface localization of Panx1-GFP, or the recovery into the photobleached area at the cell surface.
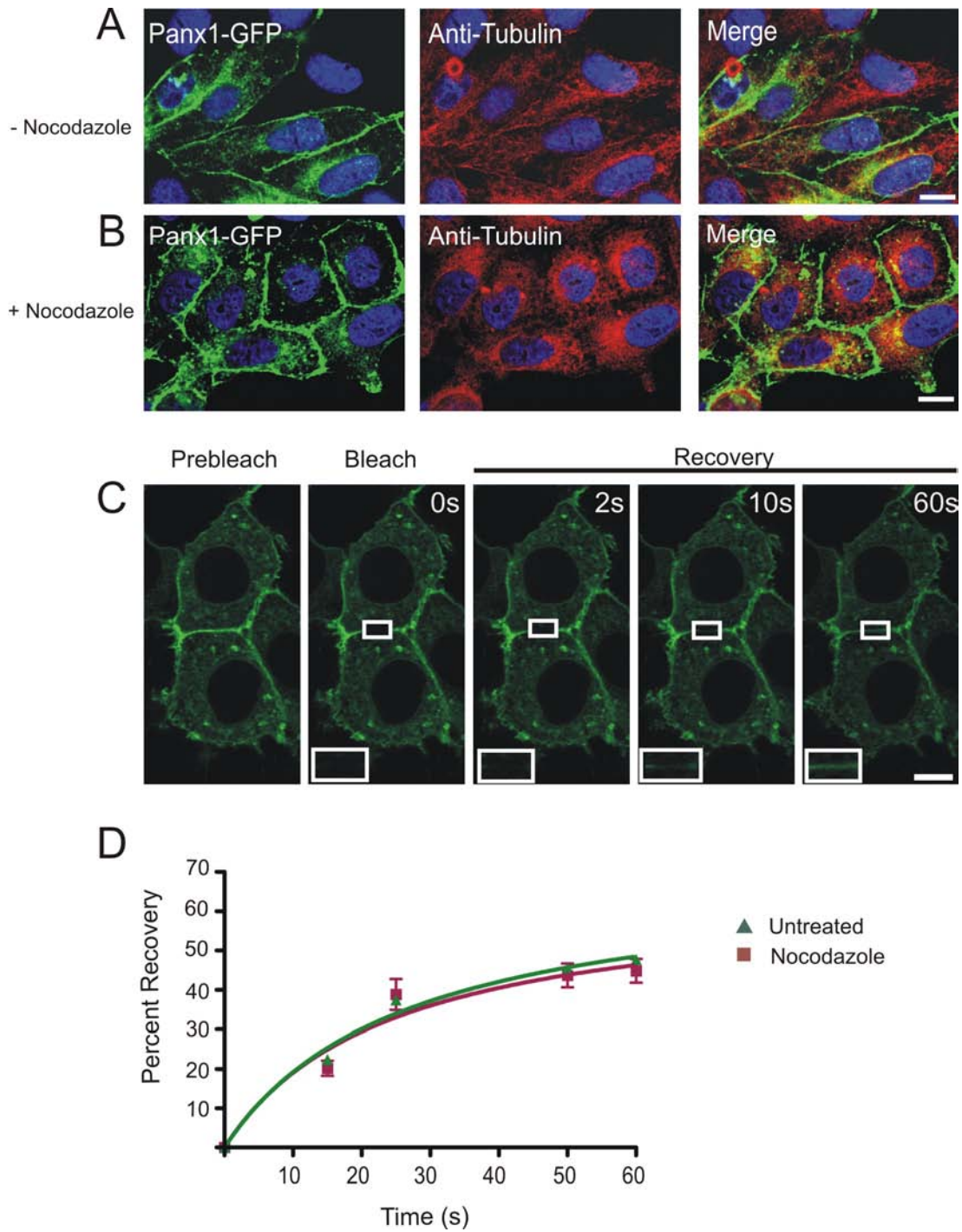
Figure 2.7 The cell surface population of Panx1-GFP is insensitive to nocodazole treatment

Untreated (A) or nocodazole-treated (B) Panx1-GFP expressing BICR-M1R$_k$ were immunolabeled for tubulin. As expected, nocodazole treatment collapsed

tubulin into paranuclear regions (A, B); however, the distribution profile of Panx1-GFP at the cell surface and in the intracellular compartments (A, B) remained relatively unchanged with collapsed tubulin (B). FRAP analysis in presence of nocodazole revealed that Panx1-GFP was able to recover into the photobleached area and the percentage of recoverable fraction was not significantly different from the untreated cells (C and D). Bars= 10μm. n = 5-10 per plasma membrane domains, data collected over four independent repeats.

2.3.7 The cell surface stability of Panx1-GFP and Panx3 is sensitive to cytochalasin B treatment while the mobility of Panx1-GFP transport vesicles is perturbed in the absence of intact microfilaments

We next wanted to assess the role of actin microfilaments in stabilizing Panx1 and Panx3 at the cell surface as well as evaluating their cell surface dynamic properties and transport of Panx1-GFP. Treatment of cytochalasin B (90 min) caused a re-distribution of F-actin from the cell periphery (Figure 2.8A, Supplementary Figure 5A) to the paranuclear region (Figure 2.8B, Supplementary Figure 5A), with a subsequent change in cell morphology. In cytochalasin B treated cells, Panx1-GFP and Panx3 were mainly localized in intracellular compartments (Figure 2.8B, Supplementary Figure 5A, arrowheads); while a small population remained evident at the cell surface (Figure 2.8B, Supplementary Figure 5A, arrows). These findings suggest that actin may play a crucial role in the cell surface stability of Panx1-GFP and Panx3. FRAP analysis of the remaining and detectable cell surface population of Panx1-GFP after cytochalasin B treatment (see Movie 2.3) revealed that Panx1-GFP was mobile but the recovery rate was slower and the amount of the recovered fraction was significant less (~15-20%), when compared to the untreated cells (Figure 2.8C). Furthermore, rapid time-lapse imaging on the same field of cells visualized before (see Movie 2.4) and after (see Movie 2.5) cytochalasin B treatment revealed that Panx1-GFP carrying vesicles were freely able to move and travel in the untreated cells, however, this movement was greatly perturbed when cells were treated with cytochalasin B with a ~60% decrease in vesicle
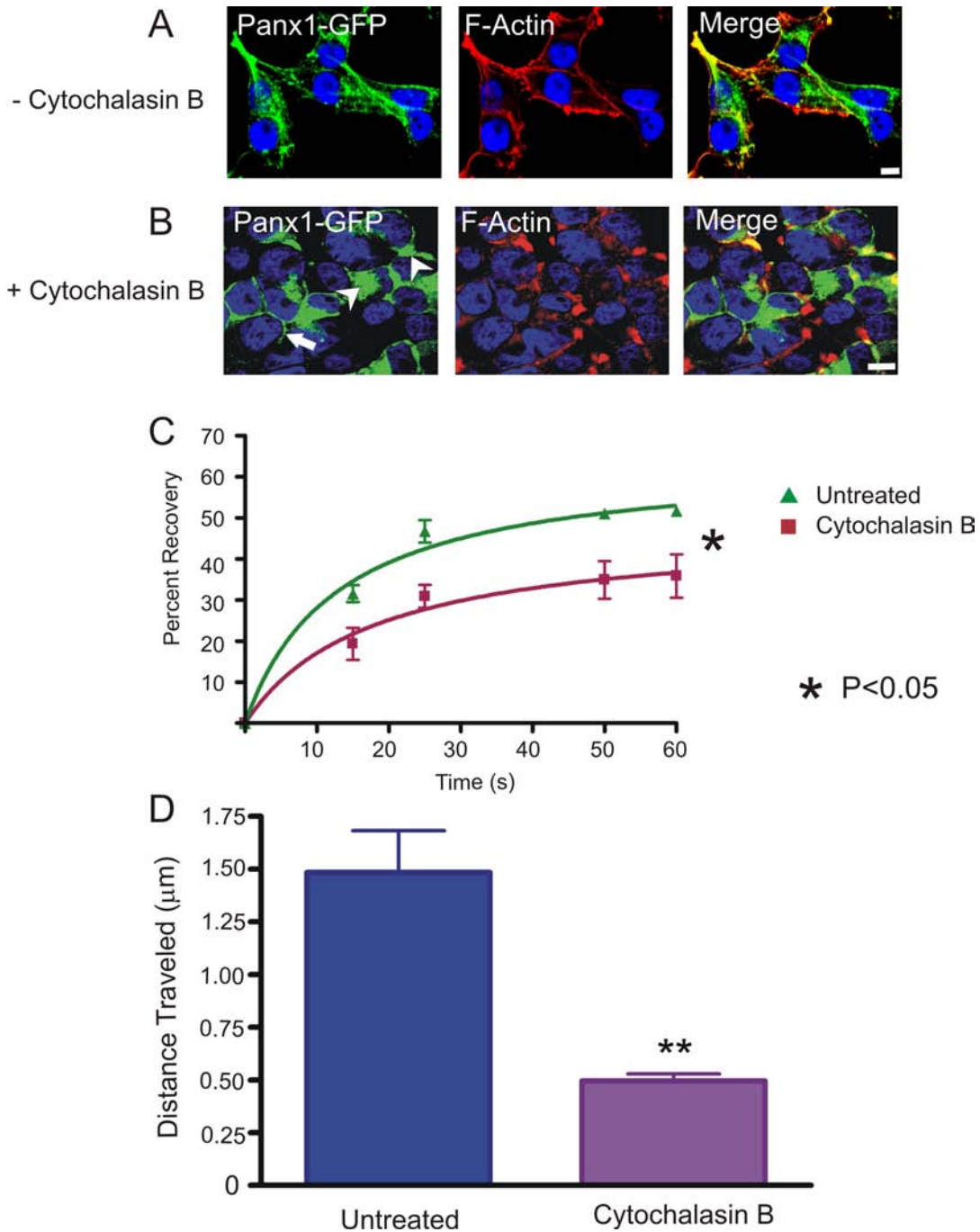
Figure 2.8 Effect of cytochalasin B on Panx1-GFP

Untreated (A) or cytochalasin B treated (B) Panx1-GFP expressing BICR-M1R$_k$ cells were labeled with phalloidin for F-actin localization. As expected, cytochalasin B caused the re-distribution of F-actin from the cell surface (A) to

the paranuclear region (B). The collapse of F-actin microfilaments coincided with the intracellular accumulation of Panx1-GFP (B, arrowheads) while, a small population of Panx1-GFP remained evident at the cell surface (B, arrows). FRAP analysis in the presence of cytochalasin B treatment revealed that the cell surface population of Panx1-GFP was significantly impaired from entering the photobleached area (P<0.05) (C) N=3. Quantification of the total distance traveled by Panx1-GFP carrying vesicles within the same field of cells analyzed before and after the cytochalasin B treatment indicated a significant (P< 0.05) reduction in vesicle mobility in cytochalasin B treated cells (D). Bars= 10μm. Representative of five independent experiments.

Movie 2.3   Panx1-GFP recovery in the photobleached area is reduced in response to the disruption of actin microfilaments

Panx1-GFP expressing BICR-M1R$_k$ cells pre-treated with cytochalasin B were subjected to FRAP and rapid time-lapse imaging at a cell surface where there was no neighboring cell (top of the frame). Recovery of Panx1-GFP into the photo-bleached area was minimal, becoming evident at roughly 20 seconds post photobleaching. The movie represents 61 frames scanned every 1 second, with a total elapsed time of 60seconds. See online at http://www.jbc.org/

Movies 2.4 and 2.5   Movement of Panx1-GFP carrying vesicles is reduced in response to the disruption of actin microfilaments

Rapid time-lapse imaging was performed on the same field of BICR-M1R$_k$ cells expressing Panx1-GFP before (Movie 4) and after cytochalasin B (Movie 5) treatment. Post 45 minutes of cytochalasin B treatment, we observed an apparent loss of membrane protrusions as well as a reduction in the movement of intracellular Panx1-GFP carrying vesicles. The movies represent 39 frames for untreated cells and 41 frames for cytochalasin B treated cells, scanned every 1.5 seconds. See online at http://www.jbc.org/

movement over a fixed interval of time (8.8s) (Figure 2.8D). Collectively, these studies suggest that microfilaments play a multifaceted role in pannexin stabilization at the cell surface and vesicular transport.

2.3.8 F-actin directly binds Panx1 at the carboxy terminus

To further examine the possible interaction of Panx1 with actin, lysates of wild-type BICR-M1R$_k$ cells engineered to express Panx1 or Panx1-GFP were subjected to immunoprecipitation of Panx1 prior to immunoblotting for Panx1 or β-actin. As expected, multiple glycosylated species of Panx1 (resolved below the IgG band) and Panx1-GFP were detected in the immunoprecipitates and cell lysates of Panx1 over-expressing cells but not wild-type BICR-M1R$_k$ cells (Figure 2.9A, top panel). Interestingly, β-actin was found to co-immunoprecipitate with Panx1 from both Panx1 and Panx1-GFP expressing BICR-M1R$_k$ cells (Figure 2.9A, bottom panel). To further validate the interaction of actin with Panx1, we conducted co-sedimentation assays where polymerized actin was mixed with GST fusion protein containing the carboxy terminal tail (C-tail) of Panx1. As observed by Sypro-stained gel, once polymerized, F-actin typically sediments in the pellet fraction. In the absence of polymerized actin, GST-Panx1 C-tail was found in both the soluble and pellet fraction (Figure 2.9B). However, when combined with F-actin, GST-Panx1 C-tail sediments preferentially in the pellet fraction (Figure 2.9B). As a control, GST alone did not sediment in the pellet fraction with or without F-actin (Figure 2.9B). Since the Panx1 C-tail fusion protein detection at ~43kD was partially masked by actin, we cleaved the C-tail of

Panx1 from the GST and performed a similar co-sedimentation assay. Further Panx1 immunoblots revealed the Panx1 C-tail at ~15kD in the pellet fraction (Figure 2.9C). These results suggest that F-actin binds directly to the carboxyl terminal of Panx1.
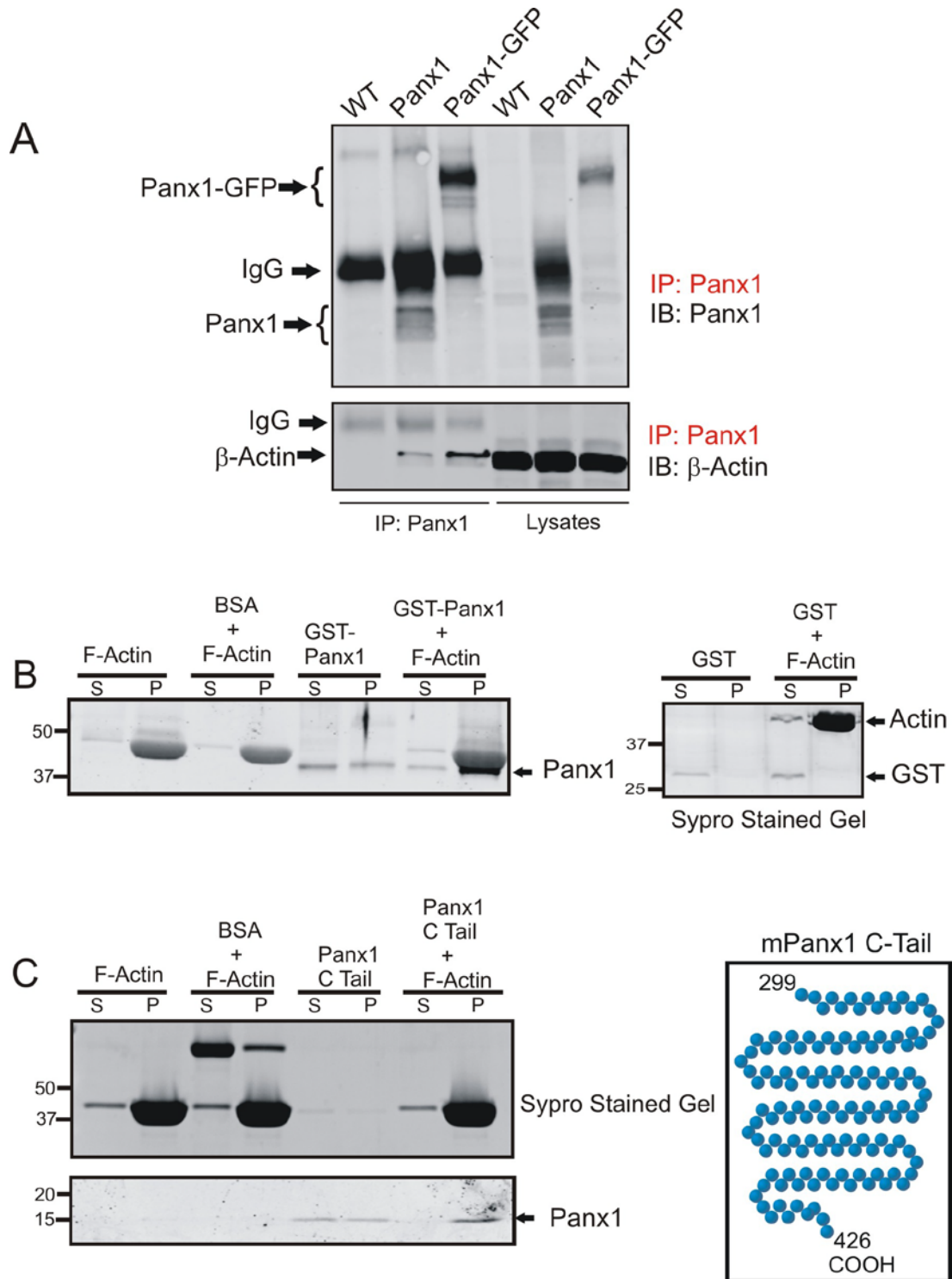
Figure 2.9 F-actin binds Panx1 at the carboxy terminus

Wild-type (WT), or Panx1 or Panx1-GFP expressing BICR-M1R$_k$ cells were lysed and subjected to immunoprecipitation (IP) for Panx1 prior to immunoblotting (IB)

the immunoprecipitates and cell lysates for Panx1 or β-actin. β-actin co-immunoprecipitated with Panx1 and Panx1-GFP (A). Monomeric actin was polymerized into F-actin, incubated with either GST-fusion protein containing the carboxy-terminal tail of Panx1 (B) or the carboxy-terminal tail of Panx1 alone (C) and separated into supernatant or pellet fractions (denoted by S and P, respectively) prior to immunoblotting for Panx1. Panx1 was found to co-sediment with F-actin in the pellet fractions (B and C). Parallel gels were stained with Sypro gel stain and BSA and GST were used as controls in the co-sedimentation assays. Representative of three independent repeats.

2.4 DISCUSSION

With the recent discovery of pannexins as a new family of channel or conduit forming proteins, there has been a growing interest to elucidate their biochemical properties, life-cycle and cellular roles. Previous reports have linked Panx1 channels to the release of ATP in neurons [66] and astrocytes [124], and in cellular response to pathological insults such as initiation of inflammatory action [76, 112], ischemia-induced death of neurons [78] and in tumor suppression [53]. Our understanding of Panx3 is even more rudimentary. While Panx3 has been shown to be a cell surface glycoprotein that forms conduits capable of dye uptake [25, 125], its cellular function remains largely unknown. It was our hypothesis that being integral membrane proteins with sequence relationships to invertebrate innexin gap junction proteins, Panx1 and Panx3 would exhibit similar characteristics to the well studied Cx43 gap junction protein in terms of the secretory pathway governing their trafficking, dynamic properties within the plasma membrane and interplay with the cytoskeletal network.

2.4.1 Trafficking of Panx1 and Panx3 to the cell surface

It has been well established that Cx43 is co-translationally inserted into the ER and oligomerizes into connexons in the *trans*-Golgi network before trafficking to the plasma membrane [13]. In the case of Panx1, treatment with EndoH and PNGaseF enzymes have revealed that the lower molecular weight species constitutes the core protein that gets glycosylated to the high mannose form in the ER before further glycosylation and processing in the Golgi apparatus and delivery to the cell surface [25, 47]. Although recent studies have extensively

focused on correlating glycosylation status with the delivery of Panx1 to the cell surface [47, 81], molecular mechanisms underlying the secretory pathway taken by Panx1 and Panx3 were largely unknown. To address if the transport of Panx1 and Panx3 from the ER to the Golgi apparatus is mediated through COPII vesicles, we transiently co-expressed Panx1 or Panx3 with the dominant-negative GTP-bound mutant Sar1^{H79F}. Stabilization of Sar1 in the dominant-negative GTP bound state has been previously shown to efficiently block COPII-mediated ER transport of proteins to the cell surface [126]. Our data demonstrated that Sar1^{H79F} expression severely inhibited the cell surface localization of Panx1 and Panx3, thus suggesting that COPII vesicular trafficking of these pannexin family members is required prior to their eventual delivery to the cell surface. This data also indicates that efficient GTP hydrolysis of Sar1 is crucial for regulating their transport from the ER compartment, as restriction of GTP hydrolysis of Sar1^{H79G} to GDP has been previously shown to arrest the cargo-containing vesicles at the ER exit sites [122]. Consistent with our findings, we previously showed that Sar1 function was necessary for delivery of Cx43 to the cell surface [88]. Our data supports the premise that the post-ER pool of Panx1 and Panx3 is correlated with pannexin processing to the highly complex glycosylation species; whereas the accumulation of the high mannose intermediate species of Panx1 and Panx3 is consistent with retention of Panx1 and Panx3 in the ER. Similar Sar1 GTPase dependency was observed for K$_{ATP}$ channels, where expression of dominant-negative mutants: Sar1^{H79G} (mutant incapable of hydrolysing GTP) and Sar1^{T39N} (mutant restricted in its ability to

exchange GDP for GTP) prevented proper channel processing and the cell surface expression of the channel [127].

ER to Golgi transport of Panx1 and Panx3, as well as their state of glycosylation, was further confirmed by the use of BFA which is known to inactivate Arf1 thereby inhibiting ER to Golgi transport [128]. Consistent with a previous study [81] we noticed a dramatic increase in the high mannose form of Panx1 in BFA-treated cells. Interestingly, we also observed an accumulation of the high mannose species of Panx3 in response to BFA treatment, consistent with the inhibition of both Panx1 and Panx3 being delivered to the Golgi apparatus for further processing. Vesicular trafficking of Panx1 and Panx3 would also strongly suggest that, like Cx43, both proteins are integral transmembrane proteins that get transported from ER membranes in COPII vesicles.

2.4.2 Mobility Dynamics of Panx1 and Panx3

In our study, we used Panx1-GFP and Panx3-GFP as tracer probes to elucidate the distribution profile and cell surface dynamics of Panx1 and Panx3. The distribution of Panx1-GFP at the plasma membrane appeared to be uniform with occasional Panx1 enriched domains consistent with previous findings using the untagged Panx1 [25]. In contrast, Panx3-GFP alone revealed an increased intracellular profile, as reported earlier [25], with some clear evidence of its localization to the cell surface that was confirmed by cell surface biotinylation assays. Since adequate delivery of Panx3-GFP to the cell surface was required to investigate its dynamics at the plasma membrane, we co-expressed it with untagged Panx3 and found an increased cell surface expression of Panx3-GFP.

It is possible that Panx3 co-oligomerized with Panx3-GFP to facilitate its delivery to the plasma membrane; if this holds true, it would also suggest that having a GFP tag at the carboxy terminal tail of Panx3 does not interfere with the intermixing of Panx3 subunits. A similar mechanism has been proposed for the cell surface rescue of a trafficking-defective, glycosylation-deficient mutant of Panx1 when co-expressed with either wild-type Panx1 or tetracysteine tagged Panx1, further indicating that tagging of pannexins does not impair its ability to assemble together with its untagged counterpart [81].

In our study, delivery of both Panx1-GFP and Panx3-GFP to the cell surface appeared to occur at multiple plasma membrane domains via intracellular vesicle-like structures that formed bright clusters upon apparent fusion with the plasma membrane. These clusters were found to be quite mobile and displaced laterally within the cell surface membrane, thus supporting a model of untargeted delivery of Panx1 and Panx3 to all cell surface micro-domains. In contrast, Cx43-GFP typically known to localize in punctate-like structures at the cell surface, has been documented to have both an arbitrary delivery to all plasma membrane domains [88, 96] as well as a preferred microtubule-dependent delivery to adherens junctions that reside in close proximity to the pre-existing gap junctions [129]. Interestingly, our data supports the premise that Panx1 and Panx3 are enriched in membrane protrusions at areas that are devoid of contacting cells, a situation not typically observed for Cx43 unless non-functional Cx43 mutant studies are performed [96]. Localization of pannexins in the finger-like membrane protrusions could suggest it may play a role in cell migration, as the process of

cell motility typically involves actin polymerization, and entails formation of fan like or pointed projections (lamellipodium and filopodia, respectively) at the leading edge [130]. Previously, the absence of Panx1 from the leading edge of a corneal epithelium wound in $P_2X_7^{-/-}$ mice was correlated with delayed corneal re-epithelialization and compromised wound healing [131]. Other channel forming proteins such as aquaporin-1 has been implicated in increased cell migration by localizing to the lamellipodia [132]; whereas, migration of lymphocytes [133] and embryonic nerve cells [134] have been correlated with voltage-dependent K^+ channels, thus supporting the role of channel forming proteins in regulating cell motility.

Our FRAP assessments of Panx1 and Panx3 mobility identified that, similar to Cx43 [96], lateral movement of Panx1-GFP and Panx3-GFP occurred from the outer edge to the centre of the photo-bleached areas. It is notable that while the recovery of fluorescence into the photobleached area is likely the result of lateral movement of pannexins due to the time course being examined, there is also likely a contribution from newly delivery fluorescent protein tagged pannexins to the cell surface. The relative rate of Panx1-GFP and Panx3-GFP recovery into the photobleached area was quite comparable in any of the examined plasma membrane micro domains, thus suggesting that the assembly state of these pannexin family members remains relatively unchanged with respect to its subcellular location within the plasma membrane. In our study, Panx1-GFP (and to a slightly lesser extent Panx3-GFP) exhibited over twice the mobility of Cx43-GFP, which are typically arranged in gap junction-like clusters [96]. Slow

recovery of Cx43-GFP was also reported in HeLa cells [135]. Given the relatively uniform cell surface distribution of Panx1 and Panx3 that appears to be untargeted to specific micro-domains, we speculate that these pannexins are not likely packaged into dense crystalline-like structures as reported for Cx43 [39]. Thus, the distribution and mobility of these pannexins are more in line with other channels and receptors such as Na^+ channels [136], and acetylcholine receptors [137].

The percent of fluorescence recovery after photobleaching for both Panx1-GFP and Panx3-GFP (representing the mobile fraction) reached a plateau between 40-60% with the remaining component representing the immobile fraction. Typically the size of the immobile fraction is dependent on the nature of the protein and the membrane microenvironment being assessed. For instance, the immobile fraction of Na^+ channels ranges from ~10% in the cell body to ~40% in the neurite terminals [136]. Likewise, the mobile fraction of glycine receptors ranges from ~50% in the neuronal cell body to ~70% in the processes [138]. In addition, the viscosity of the membrane microdomain [139], tethering of proteins with scaffolds/binding partners or interaction with cytoskeleton can all contribute to the size of the immobile fraction [140].

2.4.3 Cytoskeletal dependency of Pannexin trafficking and mobility

In order to assess the role of the cytoskeleton in pannexin trafficking and cell surface mobility dynamics, we used nocodazole and cytochalasin B to disrupt microtubules and microfilaments, respectively. Nocodazole-induced disruption of

microtubules did not significantly alter the cell surface distribution of either Panx3 or Panx1-GFP, which may not be totally unexpected given the predicted long half-life of Panx1 [25, 47]. This finding is quite distinct from Cx43, where enhanced growth of gap junctions [89], and Cx43 molecular movement into the photobleached gap junctions was minimal in nocodazole-treated cells [88] suggesting that Cx43 is much more dependent on microtubules than Panx1. In contrast, disruption of microfilaments revealed concomitant accumulation of paranuclear Panx1-GFP and Panx3 with collapsed actin microfilaments, while only a subpopulation of Panx1-GFP or Panx3 remained at the cell surface. The longer turnover dynamics of pannexins, and the rapid intracellular accumulation upon short term cytochalasin B treatment support the premise that actin provides stability to the cell surface population of Panx3 and Panx1. On the other hand, Cx43 gap junctions have been documented to remain considerably more independent to the assembly state of microfilaments [141]. Mobility assessment of the remaining cytochalasin B-insensitive subpopulation of Panx1-GFP at the cell surface revealed a rather smaller mobile fraction of ~35% in the absence of intact microfilaments. This surprising finding was somewhat distinct from Na, K-ATPase and reggie-1/flotillin-2 where the disruption of microfilaments caused an increase in the mobile fraction [142, 143]. The smaller mobile fraction of Panx1-GFP noticed in our study may be explained by the fact that transport vesicles carrying Panx1-GFP either to or from the plasma membrane were less mobile and this decrease may mechanistically account for the reduced fluorescent recovery into the photobleached area. The relative speeds of Panx1-GFP

carrying vesicles in untreated cells (~0.2 μm/sec) and cytochalasin B treated cells (~0.07 μm/sec) were also quite different. Although credited to trafficking on microtubules tracks, vesicles containing Cx43-GFP showed comparable average speeds of ~0.5 μm/sec in untreated HeLa cells [95].

2.4.4 Interaction of Panx1 with actin

Given the finding that actin microfilaments regulated the distribution and cell surface mobility of Panx1, we speculated a direct interaction between Panx1 and actin may exist. Since we were best equipped to address this question for Panx1 we first demonstrated that actin does in fact co-immunoprecipitate with Panx1. To further assess: 1) if Panx1 binds to monomeric or filamentous actin, 2) if Panx1 interaction to actin is direct, and 3) which domain of Panx1 might be responsible for interaction, we conducted co-sedimentation assay with a GST-Panx1 C-tail fusion protein. Here we show that Panx1 sediments preferentially in the F-actin fraction, the interaction appears to be direct and it is the carboxy terminal tail of Panx1 that seems responsible for interacting with actin. Comparatively, actin binding to Cx43 is thought to be facilitated via its interaction with zonula occludens-1 which is a known Cx43 binding partner [144]. Future studies will be needed to elucidate the Panx1 motif responsible for actin binding at the C-terminus, and whether actin also binds to Panx3.

 In summary, trafficking and assembly of pannexins is a precisely regulated process. Our study is the first to report that Panx1 and Panx3 transport is

dependent on Sar1-mediated COPII vesicles, cell surface Panx1 and Panx3 have dynamic mobility properties, and Panx1 directly interacts with F-actin.

2.5 ACKNOWLEDGEMENTS

2.7 SUPPLEMENTARY FIGURES
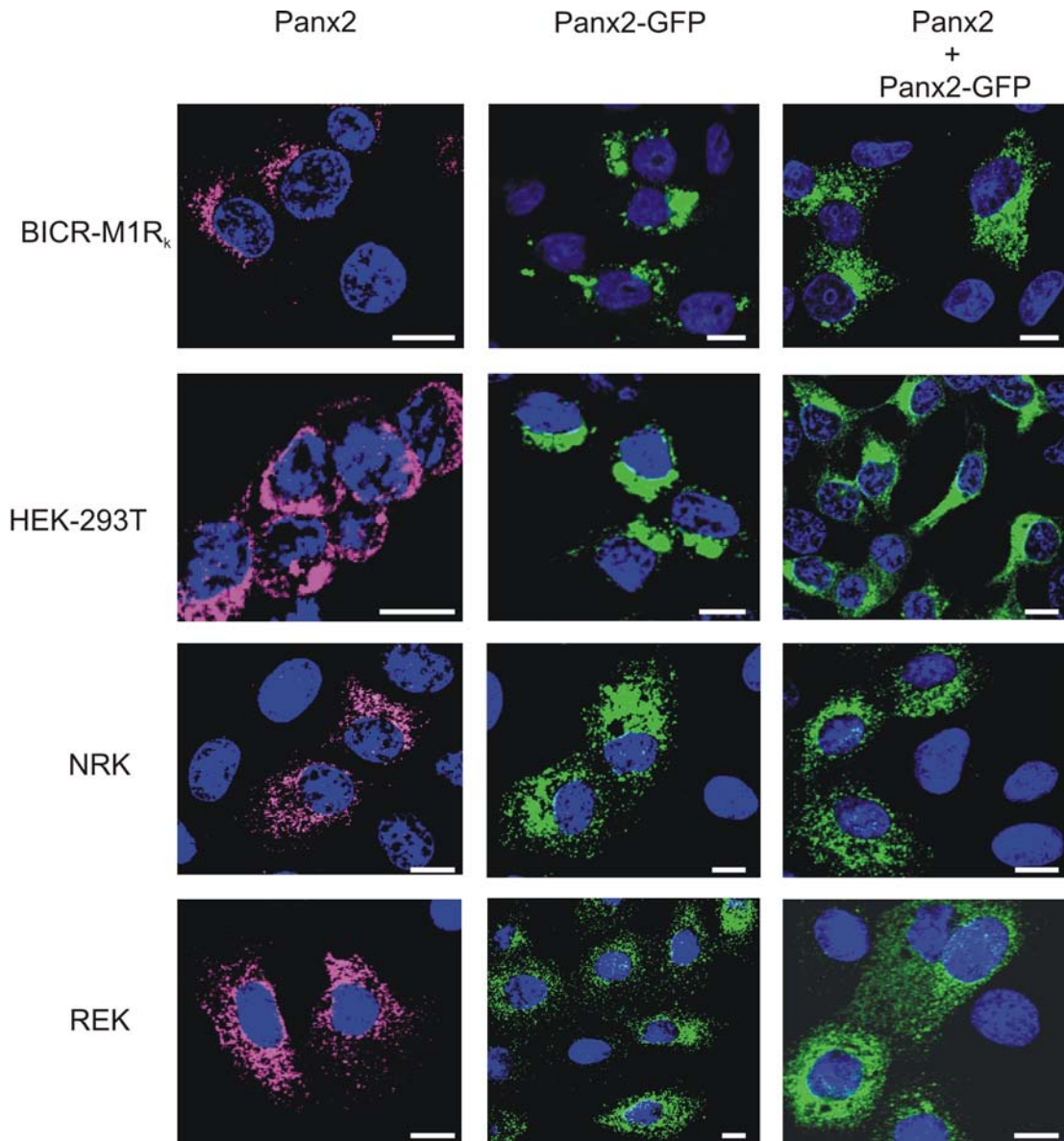
Supplementary Figure 2.7.1 Distribution profile of mouse Panx2

BICR-M1R$_k$, HEK-293T, NRK and REK cells were transiently transfected to express Panx2 and Panx2-GFP alone or together. Panx2 expressing cells were immunolabeled for Panx2. In all the cell types, both Panx2 and Panx2-GFP were primarily localized to intracellular compartments. Bars = 10 μm.
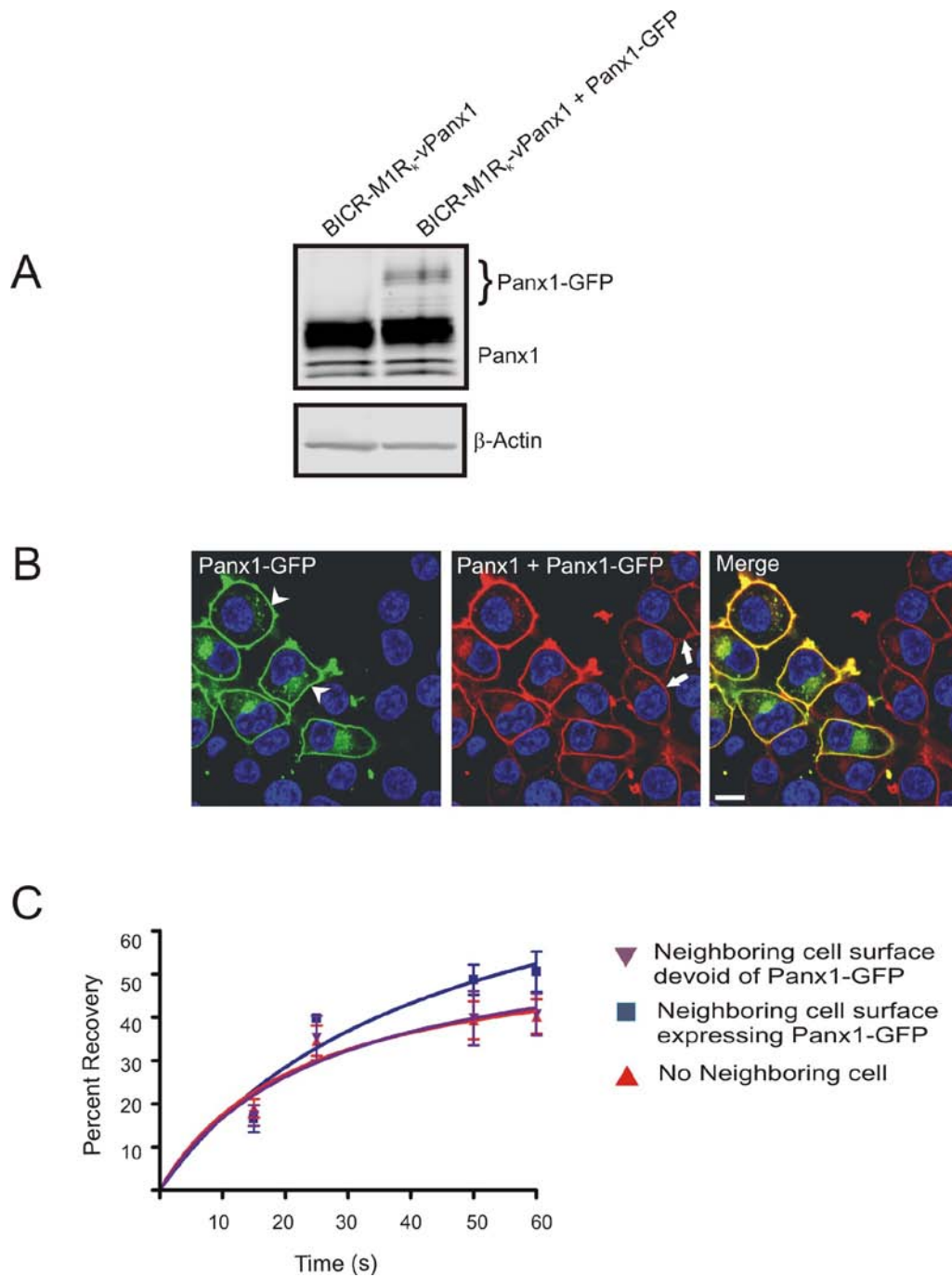
Supplementary Figure 2.7.2 Characterization of the cell surface dynamics of Panx1-GFP when expressed in Panx1-expressing BICR-M1R$_K$ cells

Panx1 over-expressing BICR-M1R$_k$ cells engineered to co-express Panx1-GFP were immunoblotted (A) and immunolabeled (B) with anti-Panx1 antibody. Like untagged Panx1, Panx1-GFP also resolved in a multiple banding profile, where

β-actin was used as a protein loading control (A). Immunolabeling of Panx1+Panx1-GFP cells identified the cell surface and intracellular distribution of GFP-tagged (B-arrowheads) and untagged (B-arrows) Panx1. Nuclei were stained with Hoechst 33342 (blue). Bar = 10 μm. Three distinct plasma membrane domains expressing Panx1-GFP were photobleached and fluorescence recovery revealed no significant difference amongst them (C). n = 8-10 per plasma membrane domain collected from three independent experiments.
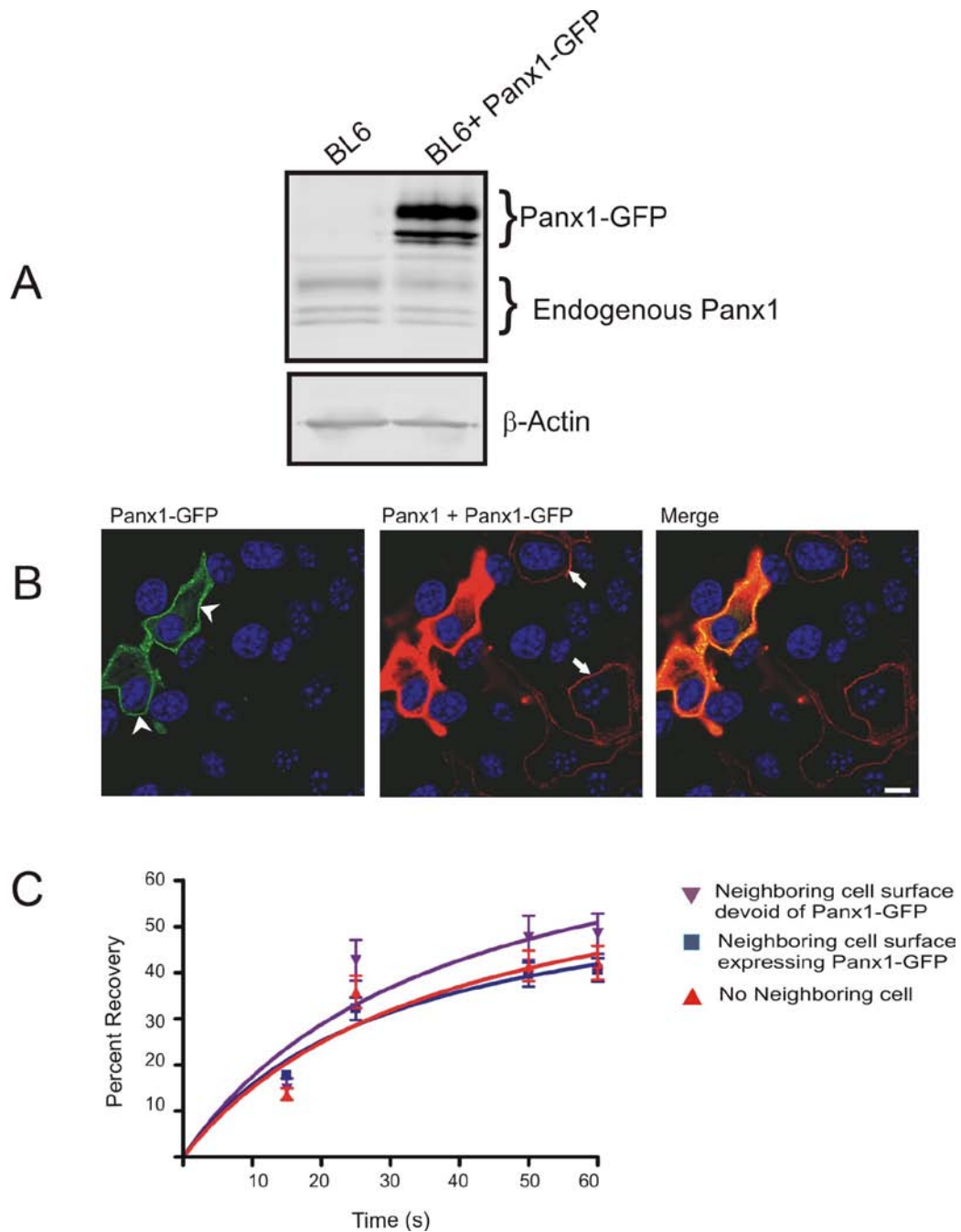
Supplementary Figure 2.7.3 Characterization of the cell surface dynamics of Panx1-GFP when expressed in Panx1-positive BL6 cells

BL6 cells expressing endogenous Panx1 were transiently transfected with Panx1-GFP and immunoblotted with anti-Panx1 antibodies (A). β-actin was used as a protein loading control (A). Exogenously expressed Panx1-GFP (B, arrowheads) and endogenously expressed Panx1 (B, arrows) exhibited a uniform

cell surface distribution. Nuclei were stained with Hoechst 33342 (blue). Bar = 10 μm. Photobleaching of Panx1-GFP at three plasma membrane domains revealed no significant difference in the percentage of recovery (C). n = 9-12 per plasma membrane domain collected from three independent experiments.
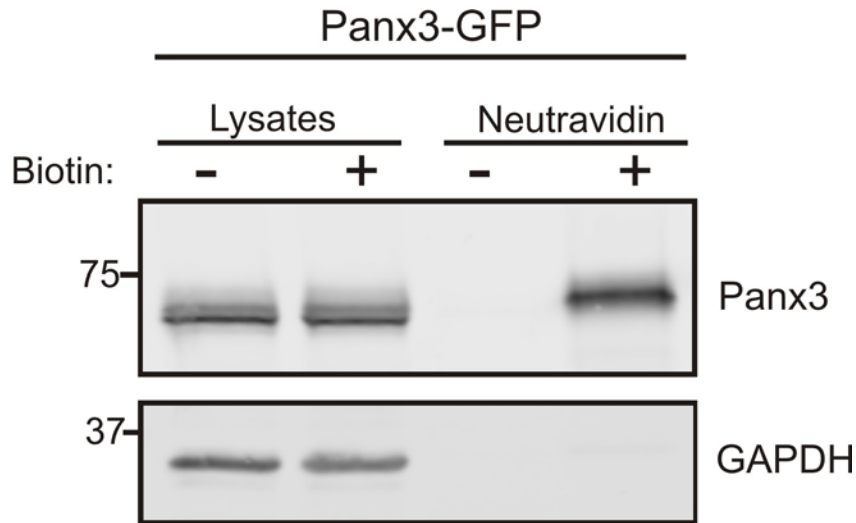
Supplementary Figure 2.7.4 Panx3-GFP is capable of trafficking to the cell surface

Cell surface biotinylation of BICR-M1R$_k$ cells transiently expressing Panx3-GFP indicated that Panx3-GFP can reach the cell surface. Cell lysates of Panx3-GFP with (+) or without (-) biotin were precipitated with neutravidin beads and immunoblotted for Panx3. GAPDH was used as a control to assess if biotin had entered the cell during the labeling procedure.
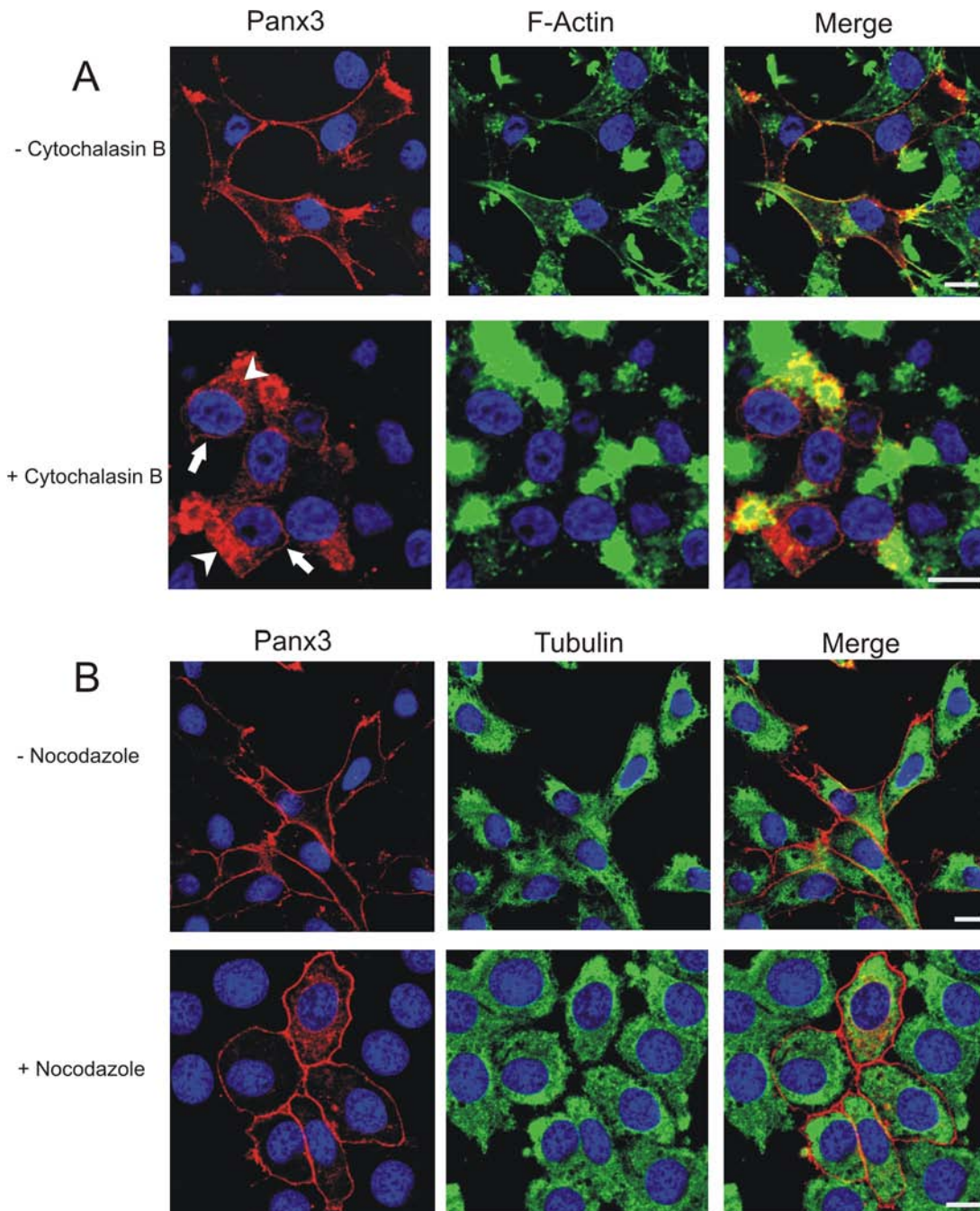
Supplementary Figure 2.7.5 The cell surface distribution of Panx3 is partially sensitive to cytochalasin B and insensitive to nocodazole treatment

BICR-M1R$_k$ cells transiently expressing Panx3 were treated with cytochalasin B (A) or nocodazole (B) and co-immunolabeled for Panx3 and tubulin or labeled for Panx3 together with phalloidin.   In cytochalasin B treated cells, Panx3 was

mainly localized to intracellular compartments (A, arrowheads), with some evidence of a cell surface pool (A, arrows); whereas nocodazole treatment caused no obvious difference in the cell surface distribution of Panx3 (B) Bar = 10 μm.

CHAPTER 3: The Carboxyl Terminal Tail of Panx1 Regulates Trafficking and Homomeric Interaction

3.0 OVERVIEW

This study was designed to characterize the role of the C-terminal domain of Panx1 in trafficking and oligomerization, by truncating the polypeptide at residue 307 and comparing its properties to full length Panx1.

_____

This chapter is currently in the process of being submitted for publication

3.1 INTRODUCTION

Pannexins were originally discovered due to their shared sequence homology with the invertebrate gap junction proteins, innexins [1]. The pannexin family is comprised of three members: Panx1, Panx2 and Panx3 [1]. Although the scope of physiological significance of pannexin family members is only beginning to emerge, it is well established that Panx1 holds importance in: forming conduits for ATP release [57, 145, 146], propagation of Ca^{2+} waves [60], and triggering neuronal and immunological inflammasome [49, 77, 147]. Additionally, activation of Panx1 channels has been implicated in ischemic cell death [78], and seizure-like activities [66]. In order to fulfill a wide spectrum of biological functions, a precise regulation of pannexin assembly and trafficking is required.

In general, glycosylation of integral membrane channel proteins can have important implications on proper folding and subunit assembly, cell surface expression, and function [148-150]. We and others have shown that Panx1 is N-linked glycosylated [25, 47] and exists as core (Gly0), high mannose (Gly1) and complex (Gly2) species [59]. The significance of Panx1 glycosylation on trafficking was first explored using site-directed mutagenesis of putative N-linked glycosylation sites [47]. While the Panx1^{N204Q} mutant was fully glycosylated and expressed all the three forms: Gly0, Gly1 and Gly2, the Panx1^{N254Q} mutant was not glycosylated and was expressed only as a Gly0 species [25, 47]. Moreover, the Panx1^{N254Q} mutant displayed trafficking defects suggesting that glycosylation played a role in proper trafficking of Panx1 to the cell surface.

Cell surface Panx1 exists in the form of hexamer channels, termed pannexons [47]. In MDCK cells, Panx1 has been shown to rescue the delivery of the Panx1[N254Q] mutant to the cell surface suggesting that they co-oligomerize [81]. Thus, the lack of glycosylation does not perturb the ability of Panx1[N254Q] subunits to fold properly and intermix with Panx1. Interestingly, despite the glycosylation deficiency and the low levels of the Panx1[N254Q] mutant at the cell surface, the mutant is still capable of forming functional single membrane channels that can take up dye [25]. A glycosylation deficient mutant of zebrafish Panx1 (zfPanx1-N246K), on the other hand, traffics to the cell surface, but displays impaired uptake of ethidium bromide compared to WT zfPanx1 [151].

The function of Panx1 channels has also been investigated by engineering specific point mutations in the polypeptide sequence and expressing these mutants in reference cell models. First, substitution of lysine→alanine at residues 248 and 265 in the second extracellular loop resulted in a loss of Panx1 channel function. Mutation of arginine at position 75 (in the first extracellular loop) to alanine, lysine, glutamine, or cysteine was further used to assess the inhibitory effects of ATP analogues on Panx1 channel currents [63]. Based on the single mutation analysis of these mutants, R75 was identified as a key ATP binding site for regulation of Panx1 channel activity [63]. When expressed in *Xenopus oocytes,* the C346S mutant formed constitutively leaky channels thereby causing cell death; whereas C136S or C436S mutants did not significantly alter Panx1 channel properties [152]. Although the C346S mutant was only partially glycosylated to the Gly1 form, as opposed to the full glycosylation states

achieved by the C136S and C426S mutants, all three mutants trafficked and localized to the cell surface [152]. Thus, these results suggest that partial glycosylation of Panx1 to the high mannose species (Gly1) is sufficient to drive a subpopulation to the cell surface, a notion further supported by our recent work demonstrating cell surface biotinylation of the Gly1 species of Panx1[N254Q] [59].

Clearly, engineering of mutations along several domains of Panx1 provide insights into Panx1 assembly, trafficking and channel function. While several studies have investigated at the effect of single amino acid substitutions within specific Panx1 motifs, mutants where entire Panx1 domains have been deleted have not be studied. We were particularly interested in the large 127 amino acid long C-terminal domain as this cytoplasmic domain is a prime candidate exposed for interacting with other regulatory proteins. In fact, we have previously shown that the Panx1 C-tail acts as a substrate for binding actin, which provides a multifaceted role in vesicular transport, cell surface mobility, and stability of Panx1 [153]. In the present study we expand our understanding of the role of the Panx1 C-terminus by investigating the trafficking and oligomeric potential of C-terminal truncated Panx1.

3.2 EXPERIMENTAL PROCEDURES

3.2.1 Cell culture and reagents

BICR-M1R$_k$ cells and human embryonic kidney (HEK)-293T, cells were cultured in high glucose DMEM (Invitrogen, Burlington, ON, Canada), supplemented with 10% fetal bovine serum, 100 units/ml penicillin, 100 μg/ml streptomycin, and 2 mM L-glutamine (all from Invitrogen, Burlington, ON, Canada).

3.2.2 Expression constructs and transfection

To truncate Panx1 carboxy tail at amino acid position 307, primers were designed with flanking sites for HindIII digestion- using the forward primer: 5'-GATAAGCTTACCATGGCCATCGCCCAC, and NotI digestion for reverse primer: 5'- TCAAGCGGCCGCACCACTTTGAGAATG. PCR products were digested with HindIII and NotI restriction enzymes, and inserted into the pcDNA3-mRFP vector (Addgene Plasmid Repository). Truncated Panx1 and RFP (denoted as Panx1^{T307}-RFP) were separated by a five-amino acid polylinker encoded by the nucleotide sequence (GGACCGGTCGCCACC). The resulting construct was validated by sequencing.

To create the Panx1-RFP construct, full length Panx1 (encoding 426 amino acids) was excised from a previously engineered pEGFP-N1 vector [25] using HindIII and BamHI restriction enzymes. Panx1 was fused with RFP in frame to the carboxyl terminus in the pcDNA3-mRFP vector by a thirty one amino acid polylinker encoding by the nucleotide sequence:

(CTGTCGACGGTACCGCGGGCCCGGGATCCACTAGTAACGGCCGCCAGTG

TGCTGGAATTCTGCAGATATCCATCACACTGGCGGCCGCTCGAG).

For transfection of Panx1^{T307}-RFP and Panx1-RFP, cells were grown overnight to

50-70% confluency in 35 mm dishes and transfected in Opti-MEM1 (Invitrogen)

media containing 2 μL of Lipofectamine 2000 (Invitrogen) and 5 μg of plasmid

DNA. For co-expression studies, HEK-293T cells were plated in 100 mm dishes

and 7-9 μg of Panx1 was co-transfected with 10-15 μg of either Panx1^{T307}-RFP

or Panx1-RFP in Opti-MEM1 media containing 15 μL of Lipofectamine2000.

Opti-MEM1 media was replaced with complete culture media 4 hours after

transfection at 37°C.

3.2.3 Immunocytochemistry

Cells were immunolabeled as previously described [153]. Briefly, cells grown on

a glass coverslips were fixed using ice-cold 80% methanol and 20% acetone for

20 minutes at 4°C and blocked in 2% blocking solution (Bovine Serum Albumin -

(BSA; Sigma)) for 30 minutes. Cells were incubated for 1 hour at room

temperature with affinity-purified polyclonal Panx1 antibody at a concentration of

2 μg/mL, a 100 fold dilution of monoclonal anti-GM130 antibody (BD

Transduction Laboratories), a 500 dilution of monoclonal anti-PDI antibody

(Stressgen) or a 200 fold dilution of polyclonal anti-RFP antibody (Abcam). Cells

were incubated with goat anti-rabbit or goat anti-mouse Alexa Fluor488 (1:500,

Invitrogen) for 45 minutes at room temperature. Cells were rinsed with PBS and

nuclei were stained with Hoechst 33342 and mounted. Immunolabeled cells were

imaged using a 63x oil objective lens mounted on a Zeiss LSM 510 META (Zeiss, Toronto, ON) system.

3.2.4 Co-Immunoprecipitation and immunoblotting

Protein lysates were collected from cells expressing Panx1^{T307}-RFP and Panx1-RFP with or without Panx1 using a lysis buffer as previously described [153]. Protein concentrations were measured using a BCA protein determination kit (Pierce). The co-immunoprecipitation assay was performed mainly as previously described [154]; briefly, 1 mg of each protein lysate was incubated with 10 µg/ml of anti-Panx1 CT-395 antibody and rocked overnight at 4°C. The following day, 30 µl (50% slurry) of protein A-Sepharose beads were added to the lysates and incubated for an additional 2 hours at 4°C. Thereafter, beads were collected by centrifugation at 4500 rpm for 2 minutes, washed three times to remove any nonspecific binding, and boiled for 5 minutes in 2x Laemmli buffer prior to resolving on 8-10% SDS-PAGE gels.

For cellular lysates control, a total of 30-40 µg of protein was used, and gels were transferred to a nitrocellulose membrane using the iBlot Dry Blotting system (Invitrogen). Nitrocellulose membranes were blocked in 3% BSA or 5% blotto milk (Santa Cruz Biotechonologies), and probed overnight with polyclonal affinity purified anti-Panx1 (0.2 µg/mL) or polyclonal anti-RFP (1:2,000) antibodies at 4˚C. Monoclonal anti-GAPDH antibody (1:10,000, Millipore) was used to assess protein loading. Since both the RFP and Panx1 antibodies were raised in rabbits, detection of co-immunoprecipitates was achieved using the Clean-Blot IP

Detection Reagent (horse radish peroxidase; Pierce Chemical) as a secondary antibody at 1:4,000 dilution for 45 minutes, in order to minimize the appearance of the IgG bands. Blots were incubated in reagents from SuperSignal West Femto chemiluminescent kit (Pierce Chemical) prior to scanning with the BioRad system. For cell lysates, detection of primary antibody binding was performed using mouse IgG IR dye 800 at 1:10,000 (Rockland Immunochemicals) or rabbit IgGAlexa 680 at 1:10,000 (Invitrogen) and scanning with the Odyssey infrared imaging system (Licor).

3.2.5 Deglycosylation assays

Enzymatic digestion of glycan chains using peptide N-glycosidase (PNGase) F and endo-β-*N*-acetylglucosaminidase (Endo) H were performed as previously described [59]. Briefly, 35 µg of HEK-293T cell lysates containing either Panx1^{T307}-RFP or Panx1-RFP were incubated in the presence or absence of 10U of *N*-glycosidase F and incubated for 1 hour at 37°C prior to immunoblotting using the RFP antibody. Similarly, for Endo H treatment, 35 µg of protein was incubated with or without 5000U of the enzyme for 1 hour at 37°C and samples were resolved on a 8% SDS PAGE before transferring to nitrocellulose membranes and probing with an anti-RFP antibody.

3.2.6 Cell surface biotinylation

HEK-293T cells ectopically expressing either Panx1^{T307}-RFP or Panx1-RFP were subjected to biotinylation 48 hours following transfection. To prevent any potential internalization of cell surface proteins, all reagents and cell cultures

were maintained on ice. Cell culture dishes were first rinsed three times with cold PBS to remove media and incubated thereafter either in PBS alone or in PBS containing 1 mg/ml of EZ-link Sulfo NHS-LC biotin (Pierce Chemical) for 20 minutes at 4°C.To quench any excess biotin, cell culture dishes were first rinsed and then incubated in PBS containing 100 mM glycine for an additional 15 minutes at 4°C. Proteins were then extracted from both unlabeled and biotin labeled dishes using the SDS lysis buffer (1% Triton X-100 and 0.1% SDS in PBS), and quantified using a BCA protein determination kit (Pierce). 1 mg of cell lysates from biotin labeled and unlabeled samples were incubated with 50 µl of NeutrAvidin-agarose beads (Pierce Chemical) overnight at 4°C. The following day, beads were washed with IP lysis buffer (150 mM NaCl, 10 mM Tris-HCl, pH 7.4, 1 mM EDTA, 0.5% NP-40, and 1% Triton X-100) containing 1 mM NaF and 1 mM Na_3VO_4, and suspended in 2x Laemmli buffer before boiling for 5 minutes and resolving on the SDS-PAGE. Total protein containing 30-40 µg of lysate was simultaneously resolved on the gel, transferred to nitrocellulose and probed for RFP and Panx1 expression.

3.2.7 Pharmacological inhibitors

HEK-293T cells expressing $Panx1^{T307}$-RFP and Panx1 together or individually were exposed to 10 µM of lactacystin (Sigma) and 200 µM of chloroquine (Sigma) for 20 hours prior to protein extraction. Total protein lysates of treated and untreated cells were then subjected to immunoblotting for RFP and Panx1.

3.3 RESULTS

In order to characterize the biological significance of the Panx1 C-tail, we truncated Panx1 at residue 307 that is approximately 10 amino acids downstream of where the fourth transmembrane domain is predicted to exit the plasma membrane. To facilitate detection of the Panx1 truncated mutant, the mutant was tagged with red fluorescent protein (RFP). To control for any possible adverse effect of the RFP tag, we also tagged full length Panx1 with RFP to be used in comparative studies.

3.3.1 RFP tagging does not modify the distribution profile of Panx1

RFP is a fluorescent protein derived from *Discosoma* coral that is spectrally distinct from the green fluorescent protein (GFP), originally cloned from *Aequorea* jellyfish [155]. In order to validate that the RFP tag does not modify the trafficking of Panx1, we compared it to the GFP-tagged version that previously showed similar cell surface delivery and localization patterns to untagged Panx1. Transfection of Panx1-RFP in BICR-M1R$_k$ cells stably expressing Panx1-GFP revealed relatively uniform co-localization at the cell surface and overlap in vesicle-like compartments distributed intracellularly (Figure 3.1A, arrowheads). Interestingly, similar to Panx1-GFP, RFP-tagged Panx1 was also found in plasma membrane protrusions (Figure 3.1B, arrows).
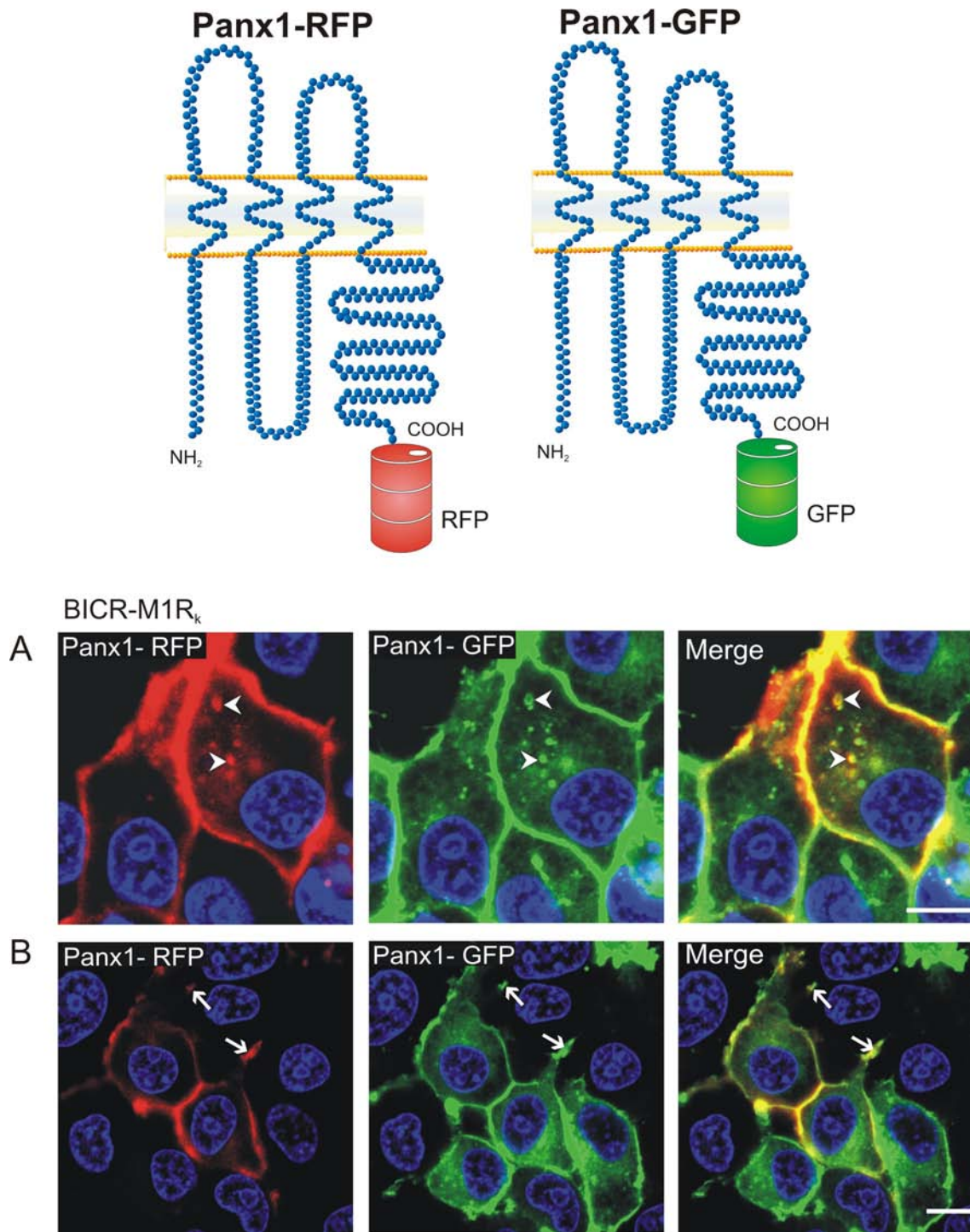
Figure 3.1 Panx1-RFP co-localize with Panx1-GFP

Over-expression of Panx1-RFP (red) in BICR-M1R$_k$ cells stably expressing
Panx1-GFP (green) resulted in their co-localization (yellow) in a relatively uniform

pattern at the cell surface and in vesicle-like structures (A, arrowheads). Panx1-RFP also co-localized (yellow) with Panx1-GFP at the plasma membrane protrusions (B, arrows). Nuclei were counterstained with Hoechst. Bar = 10 µm.

This suggests that like GFP, RFP tagging of the Panx1 carboxyl terminal tail also displays distribution characteristics similar to the untagged counterpart and therefore could be employed as a control to study the biological properties of Panx1^{T307}-RFP.

3.3.2 The C-tail of Panx1 is important for trafficking to the plasma membrane

Both Panx1^{T307}-RFP and Panx1-RFP were over-expressed in either BICR-M1R$_k$ or HEK-293T cells, as these cell lines are devoid of endogenous Panx1 [59, 153]. The high transfection efficiency of HEK-293T cells was deemed ideal for immunoblotting experiments; however, given their small spindle morphology, large nuclei and low cytoplasmic volume [59], they were not as suitable for immunolocalization studies as the larger BICR-M1R$_k$ cells.

When Panx1^{T307}-RFP was expressed in BICR-M1R$_k$ cells the mutant was found to primarily reside in intracellular compartments (Figure 3.2A). In contrast, full length Panx1-RFP was capable of trafficking and localizing to the cell surface in a relatively uniform manner (Figure 3.2B). As expected, the Panx1 CT-395 (from here on denoted as the anti-Panx1) antibody detected the full length Panx1-RFP but was unable to detect Panx1^{T307}-RFP due to the deletion of the antigenic epitope used to generate the antibody (Figure 3.2A and B). In comparison, the RFP antibody detected both Panx1^{T307}-RFP and Panx1-RFP (Figure 3.2C and D). Interestingly, the subcellular distribution profile of both Panx1^{T307}-RFP and Panx1-RFP was consistent between BICR-M1R$_k$ and HEK-293T cells (Figure 3.2E and F), eliminating any potential cell type differences.
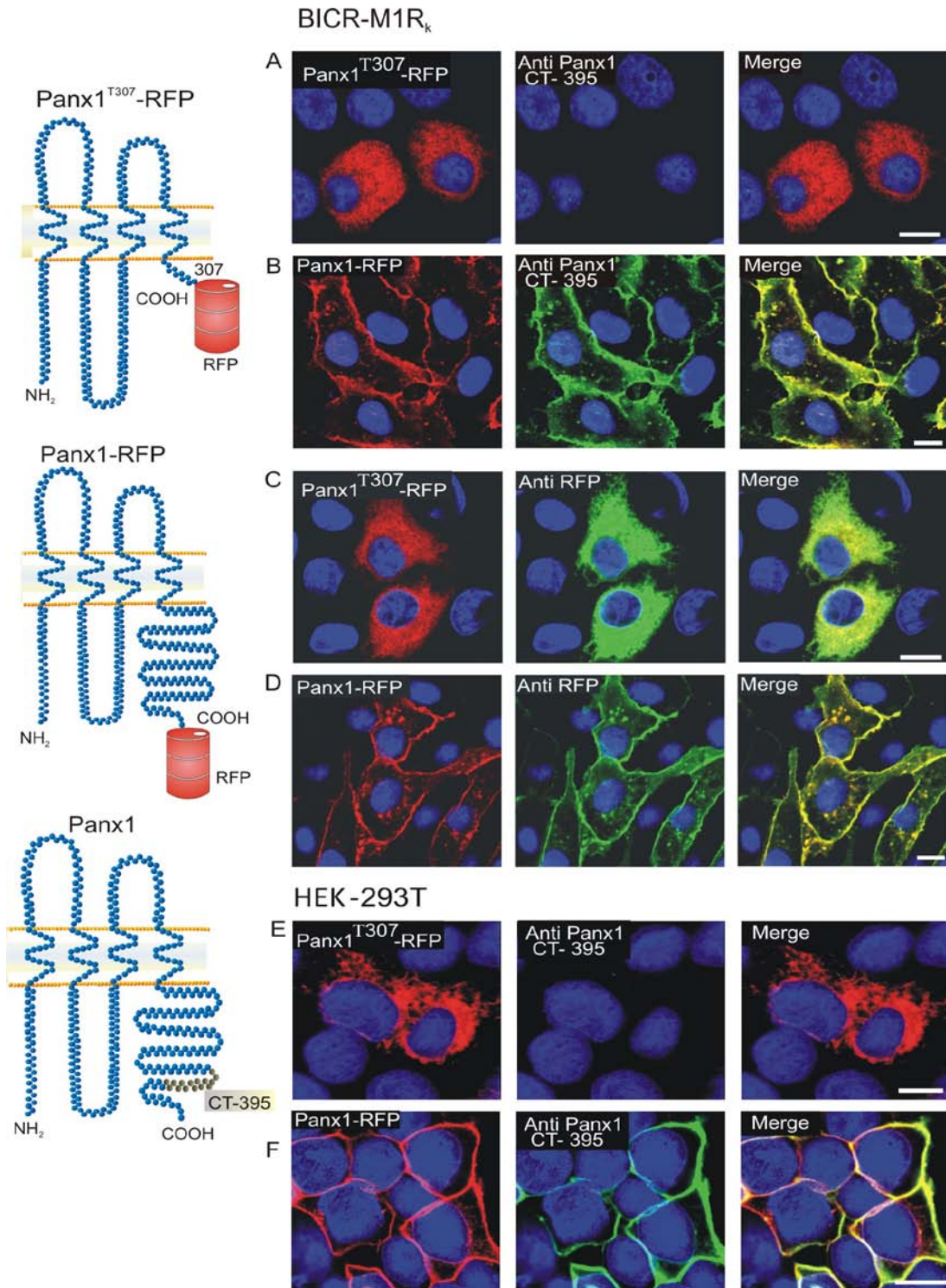
Figure 3.2 The C-tail of Panx1 is critical for trafficking to the cell surface
Panx1^{T307}-RFP was localized to the intracellular compartments (A, red) while
Panx1-RFP was found at the cell surface (B, red) in BICR-M1R$_k$ cells.

Immunolabeling with Panx1 detected Panx1-RFP and not Panx1^{T307}-RFP (A and B, green). As expected, the anti-RFP antibody localized both Panx1-RFP and Panx1^{T307}-RFP (C and D, green). The subcellular distribution of full length and C-tail truncated Panx1 remained consistent in HEK-293T cells (E and F, red). Nuclei were counterstained with Hoechst. Bar=10µm.

Collectively, these findings suggest that the C-terminal of Panx1 is critical for delivery and retention of Panx1 at the cell surface.

3.3.3 Panx1^{T307}-RFP is primarily retained within the ER compartment and glycosylated to a high mannose form

In order to identify the subcellular localization of Panx1^{T307}-RFP, cells were immunolabled for ER (PDI and calnexin) and Golgi (GM130) resident proteins. Although the distribution patterns of both Panx1^{T307}-RFP and PDI (an ER lumen protein) partially overlap, their localization patterns were not identical (Figure 3.3A). In contrast, the ER integral membrane protein marker, calnexin, revealed strong co-localization with Panx1^{T307}-RFP, particularly around the perinuclear region (Figure 3.3B). Not surprisingly, Panx1-RFP at the cell surface did not localize with either PDI or calnexin (Figure 3.3A and B). Additionally, labeling with the *cis*-Golgi matrix protein, GM130, revealed a distinct distribution profile from both Panx1^{T307}-RFP and Panx1-RFP (Figure 3.3C). Thus, in the absence of the C-tail it appears that Panx1 is largely retained in the ER compartment. As a glycoprotein, it is well documented that Panx1 exhibits multiple banding patterns reflecting the core unglycosylated protein: Gly0; a high mannose glycosylated species associated within the ER: Gly1; and the extensively glycosylated species that is modified in the Golgi apparatus prior to cell surface delivery: Gly2 [25, 47, 59]. To address if Panx1^{T307}-RFP also resolves as multiple species, lysates of HEK-293T wild-type cells, cells over-expressing full length Panx1 fusion proteins, and the C-tail truncated protein were subjected to immunoblotting using anti-RFP and Panx1 antibodies.
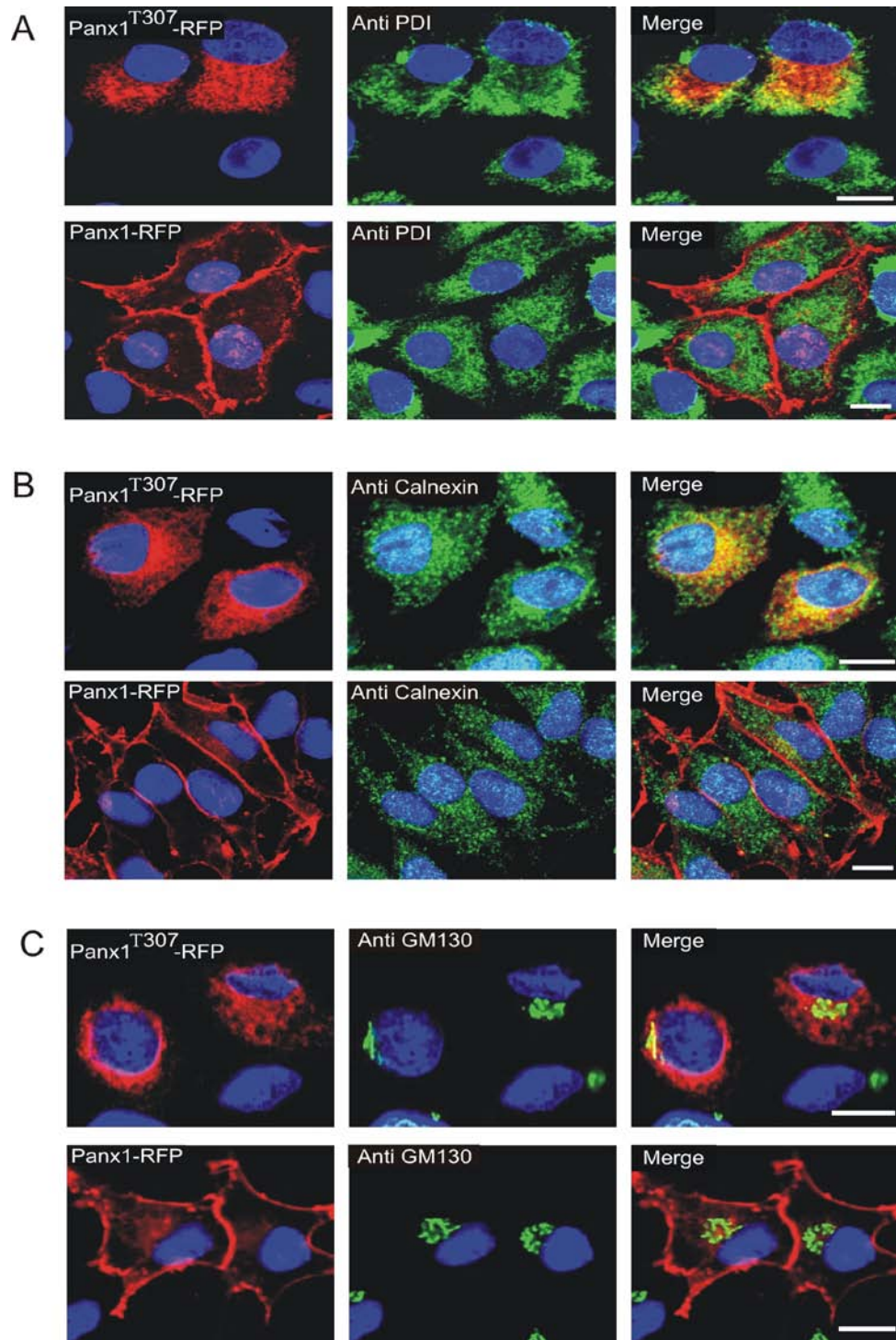
Figure 3.3 Characterization of the subcellular distribution of Panx1^{T307}-RFP

BICR-M1R$_k$ cells ectopically expressing Panx1^{T307}-RFP (red) or Panx1-RFP (red) were immunolabeled with antibodies against PDI, calnexin and GM130.

Panx1^{T307}-RFP expressing cells revealed an intracellular pattern that exhibited partial colocalization with resident proteins of the endoplasmic reticulum. The bulk of Panx1-RFP trafficked to the cell surface with no obvious co-localization with PDI (A, merge) or calnexin (B, merge). GM130 (green) was mainly localized around the perinuclear region. Nuclei were counterstained with Hoechst. Bar=10µm.

Owing to the fusion of RFP (~27-30kD), C-tail truncated Panx1 was detected as a doublet at a molecular weight of ~50kD, whereas full length Panx1 resolved as multiple bands at ~75-80kD (Figure 3.4A). Consistent with our immunolabeling data, the Panx1 CT-395 antibody did not detect Panx1^{T307}-RFP, but identified full length GFP and RFP -tagged Panx1 (~75-80KD), as well as occasionally some bands near 50kD, which are likely proteolytic products (Figure 3.4B). As expected, WT cells did not express any Panx1, however, some non-specific bands were observed above 50 kDa when probed with the RFP antibody (Figure 3.4A).

In order to determine whether the banding pattern of Panx1^{T307}-RFP was a result of glycosylation, we enzymatically digested the cell lysates using *N*-glycosidase F prior to immunoblotting. Within an hour, *N* glycosidase F treatment of Panx1-RFP removed glycan chains associated with the Gly1 and Gly2 species and shifted the banding pattern to the level of Gly0 (Figure 3.4C). Similarly, the upper band of Panx1^{T307}-RFP, likely the Gly1 species, also shifted to the lower band (Gly0) upon *N*-glycosidase F digestion (Figure 3.4D). To further assess the extent of glycosylation, both Panx1^{T307}-RFP and Panx1-RFP were subject to Endo H digestion, which selectively cleaves the high mannose form of a glycoprotein. Consistent with previously reported digestion of mouse [47, 59] and rat untagged Panx1 [47], Endo H treatment of Panx1-RFP revealed a shift in only the intermediate Gly1 band without reducing the Gly2 species (Figure 3.4E). Interestingly, the upper band of Panx1^{T307}-RFP was also sensitive to the Endo H treatment (Figure 3.4F).
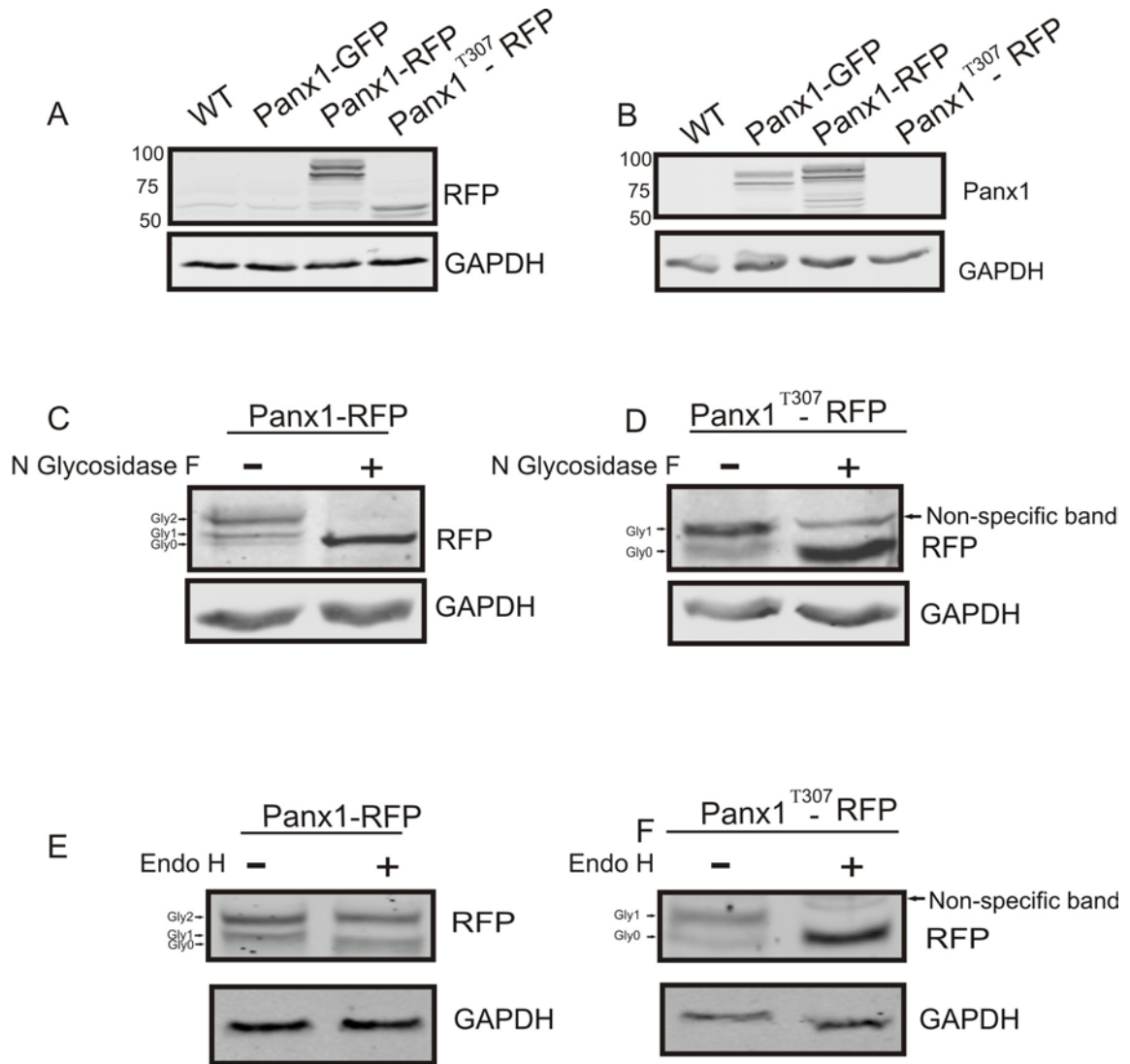
Figure 3.4 Panx1^{T307}-RFP exhibits glycosylation states distinct from Panx1-RFP

Protein lysates of HEK-293T WT cells and cells over-expressing Panx1-GFP, Panx1-RFP and Panx1^{T307}-RFP were immunoblotted for RFP tagged Panx1 (A and B). Panx1-RFP (A and B) resolved similar to Panx1-GFP (B) in a multiple banding profile, whereas Panx1^{T307}-RFP was detected primarily as a doublet ~50kD (A). Digestion of Panx1-RFP and Panx1^{T307}-RFP with *N*-glycosidase F (C and D) and Endo H (E and F) revealed that while Panx1-RFP can exist as a core (Gly0), high mannose (Gly1) and complex glycoprotein species (Gly2),

Panx1^{T307}-RFP primarily consists of core (Gly0) and   high mannose (Gly1) species. GAPDH was used as a protein loading control.

Taken together, these results suggest that in the absence of the C-tail, glycosylation of Panx1 is limited to a high mannose form.

3.3.4 Panx1 is incapable of rescuing Panx1^{T307}-RFP to the plasma membrane

Panx1 is reported to presumably oligomerize with the glycosylation-deficient mutant, Panx1^{N254Q}, to rescue its predominant intracellular distribution to the cell surface [81]. To examine whether the C-tail of Panx1 regulates homomeric interactions, we transiently co-expressed Panx1 with Panx1^{T307}-RFP. When Panx1 is ectopically expressed alone or in conjunction with Panx1-RFP, a relatively uniform cell surface distribution is revealed (Figure 3.5A and B). In contrast, the intracellular retained Panx1^{T307}-RFP was not rescued to the cell surface when co-expressed with Panx1; instead, a sub-population of Panx1 was detected intracellularly in the perinuclear region (Figure 3.5C). Thus, suggesting that intermixing of Panx1 with the C-tail mutant does not result in rescue of the mutant to the cell surface.

3.3.5 C-Tail of Panx1 is involved in glycosylation-dependent homomeric interactions

To further examine the potential role of the Panx1 C-tail in Panx1 oligomerization, lysates of HEK-293T cells, cell over-expressing Panx1 alone or in combination with either Panx1-RFP or Panx1^{T307}-RFP were subjected to immunoprecipitation for Panx1.
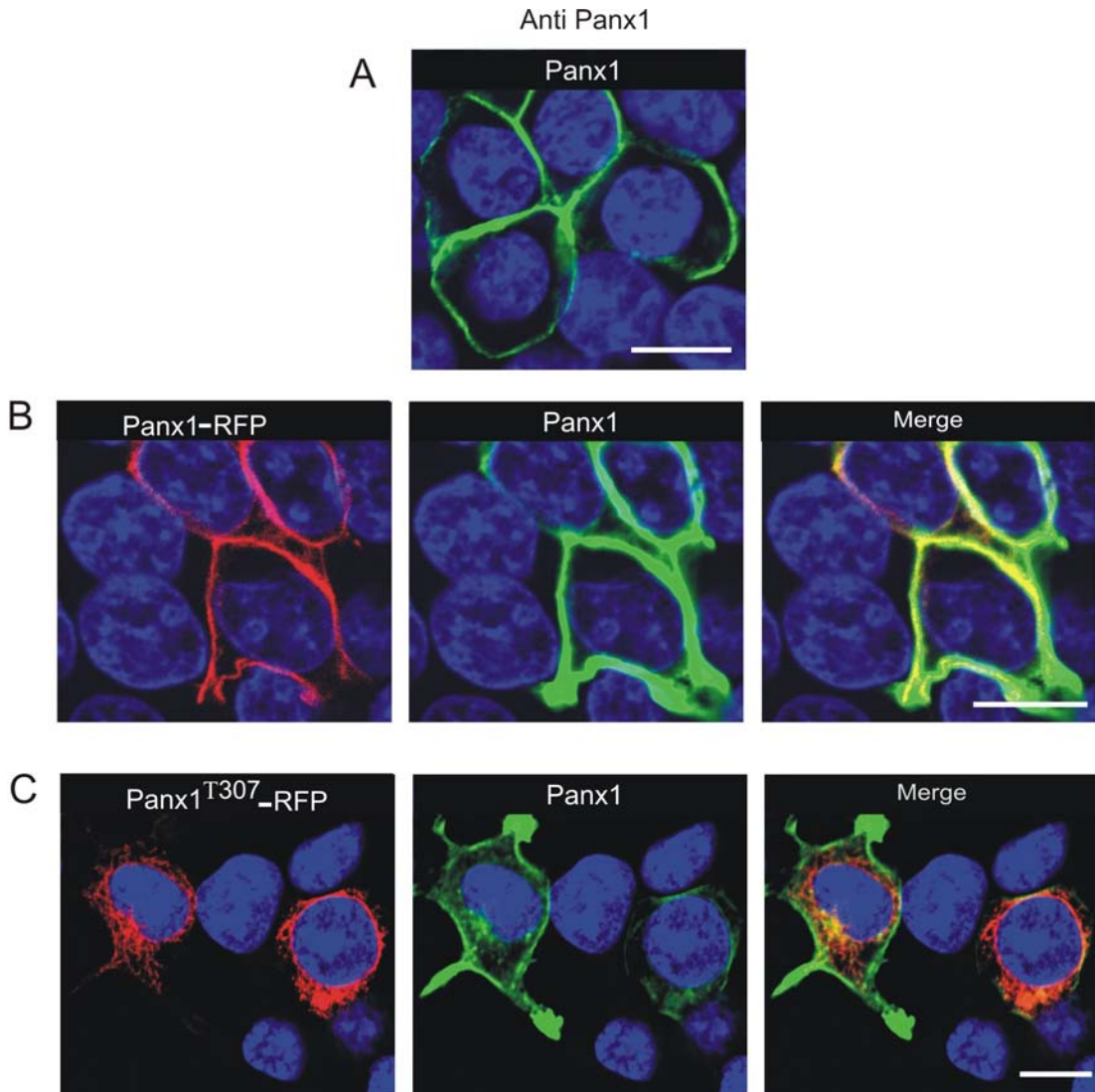
Figure 3.5 Panx1 expression did not relocalize Panx1^{T307} to the cell surface

HEK-293T cells transfected with Panx1 alone (A), or with Panx1-RFP (B, red) and Panx1^{T307}-RFP (C, red) were immunolabeled for Panx1 (green). When expressed alone (A) or with Panx1-RFP (B), Panx1 reached the cell surface and also colocalized with Panx1-RFP (B, merge). The intracellular localization pattern of Panx1^{T307}-RFP (red) was evident in the presence of Panx1 (green) (C). Nuclei were counterstained with Hoechst. Bar=10μm.

When immunoblotted with either RFP or Panx1 antibodies, immunoprecipitates of Panx1 co-expressed with Panx1-RFP revealed both the high mannose (Gly1) and complex glycosylated species (Gly2), with much lower detection of the core (Gly0) species (Figure 3.6A and B). In contrast, only trace amounts of the Gly1 species of Panx1^{T307}-RFP was found to co-immunoprecipitate with Panx1 (Figure 3.6A). Conversely, immunoblotting with the anti-Panx1 antibody revealed the Gly1 and Gly0 species with little evidence of the Panx1 Gly2 species when co-expressed with Panx1^{T307}-RFP (Figure 3.6B). Interestingly, total cell lysates also revealed little Gly2 species of Panx1 in the presence of Panx1^{T307}-RFP (Figure 3.6B). Collectively, these findings suggest that all three species of Panx1 can readily interact with Panx1-RFP. In contrast, when the C-tail of Panx1 is truncated, only a weak interaction exists with Panx1, with a preference for the core and high mannose species.

3.3.6 Panx1^{T307}-RFP has a dominant-negative effect on the maturation of Panx1 to the Gly2 Species

To determine the effect of Panx1^{T307}-RFP mutant on the maturation of Panx1 to the Gly2 species and delivery to the cell surface we conducted a cell surface biotinylation assay on live HEK-293T cells expressing Panx1^{T307}-RFP, and Panx1-RFP alone or in combination with Panx1. As depicted by Panx1 immunoblotting of NeutrAvidin pulled down fractions and cell lysates, all species of Panx1-RFP were capable of trafficking to the cell surface, with a preference for the Gly2 species when probed with anti-RFP antibody (Figure 3.7A).
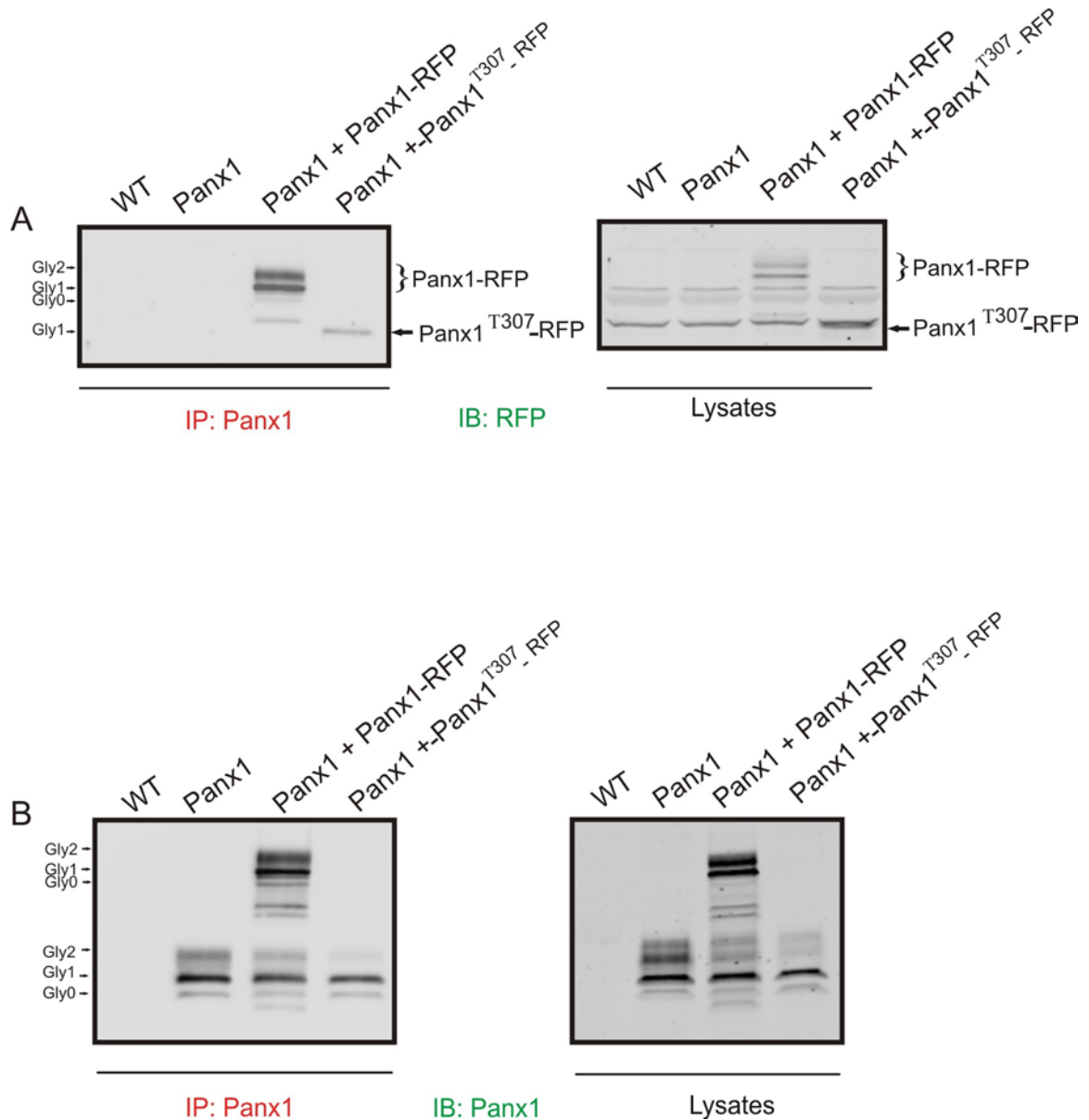
Figure 3.6 Truncation of the Panx1 C-tail limits the interaction with the full length Panx1

Immunoprecipitation of Panx1 was performed on cell lysates from WT HEK-293T cells and cells ectopically expressing either Panx1 alone or with Panx1-RFP and Panx1^{T307}-RFP. A robust interaction of the Gly1 and Gly2 species of Panx1-RFP with Panx1 was revealed when immunoblotted for RFP (A) and Panx1 (B). Panx1^{T307}-RFP also co-immunoprecipitated with Panx1, however, it was mainly the Gly1 species that was weakly pulled down (A). Co-immunoprecipitaton of

Panx1 with Panx1^{T307}-RFP revealed reduced interaction with the Gly2 species of Panx1 (B). Expression levels of all Panx1 variants were also assessed by probing the total protein lysate with RFP or Panx1 antibody.

In contrast, despite detectable Panx1^{T307}-RFP expression in the cell lysates, NeutrAvidin fractions contained virtually no Panx1^{T307}-RFP (Figure 3.7A).

As a control, the lack of immunolabeling of GAPDH suggests that biotin did not penetrate into the cell. When co-expressed with Panx1, a subpopulation of the highly glycosylated species of Panx1-RFP (Figure 3.7B and C), as well as all the three glycosylation forms of Panx1, reached the cell surface (Figure 3.7C). However, when co-expressed with Panx1^{T307}-RFP, there was a noticeable reduction in the cell surface population of all the three species of Panx1 (Figure 3.7C), with no clear evidence of plasma membrane expression of Panx1^{T307}-RFP, even in the presence of Panx1 (Figure 3.7B). These findings support the notion that the Panx1^{T307}-RFP mutant is acting dominantly to reduce the delivery of Panx1 to the cell surface.

3.3.7 Panx1^{T307}-RFP is preferentially degraded through the proteasomal pathway

Given the predominant intracellular distribution of Panx1^{T307}-RFP, we assessed whether Panx1^{T307}-RFP is targeted to proteasomal or lysosomal degradation using the pharmacological inhibitors lactacystin and chloroquine, respectively. Blocking the proteasomal pathway with lactacystin clearly showed a robust accumulation of both the Gly1 and Gly0 species of Panx1^{T307}-RFP, with no detectable change in protein expression upon chloroquine exposure (Figure 3.8A). On the contrary, inhibition of the lysosomal and not the proteasomal pathway revealed a pronounced increase in the Gly1 and Gly2 species of both Panx1-RFP (Figure 3.8A) and Panx1 (Figure 3.8B). In comparison to Panx1

alone (Figure 3.8B), co-expression with Panx1^{T307}-RFP showed an overall decrease in the Gly2 species of Panx1, with a noticeable reduction in the Gly1 species, upon chloroquine treatment (Figure 3.8C). When compared to Panx1^{T307}-RFP alone (Figure 3.8A), co-expression with Panx1 revealed an accumulation of the Gly1 species of Panx1^{T307}-RFP with the chloroquine treatment, without considerably altering the expression upon lactacystin treatment (Figure 3.8C).
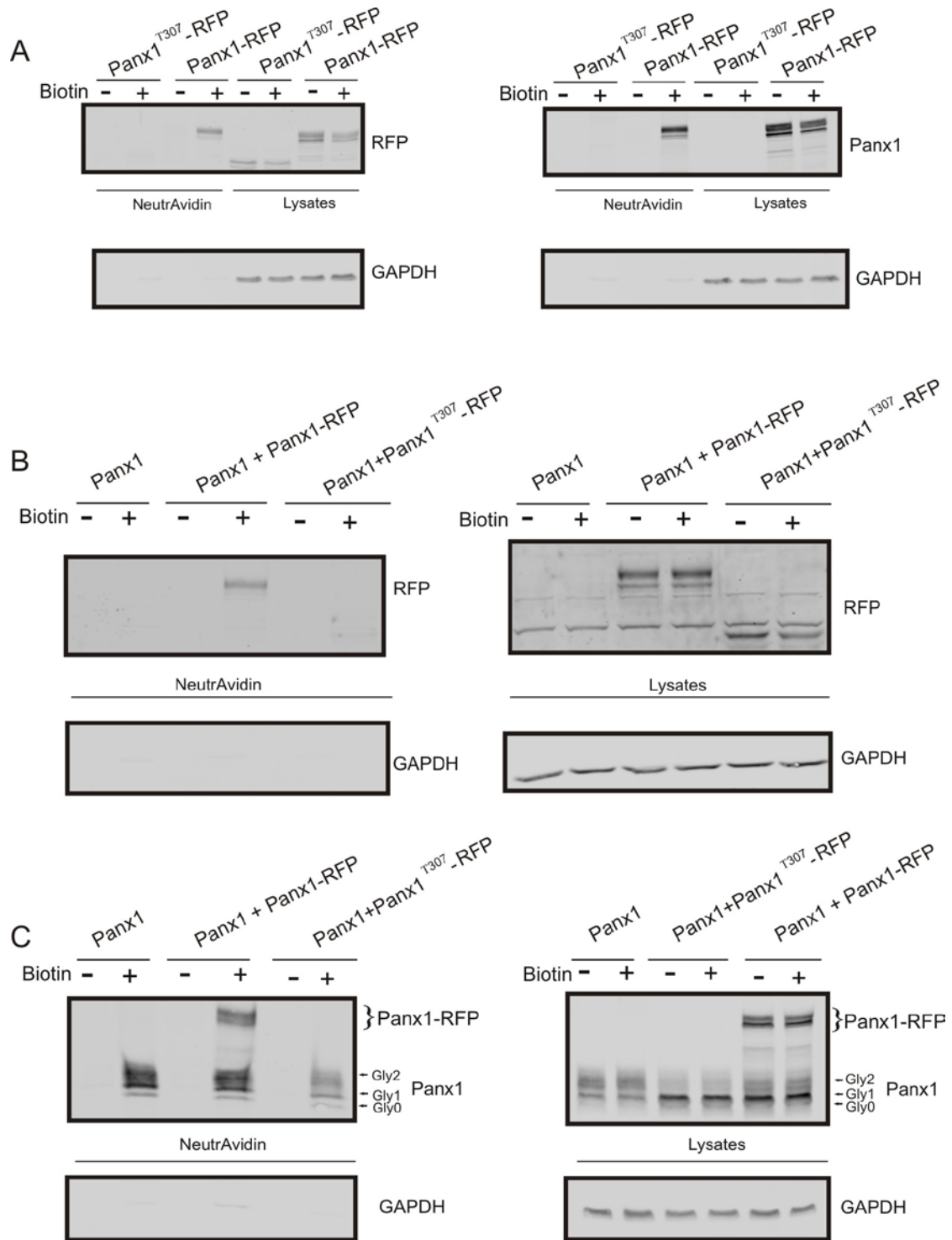
Figure 3.7 Panx1^{T307}-RFP reduces the cell surface expression of Panx1

Protein lysates of HEK-293T cells labeled with (+) or without (-) biotin were precipitated with NeutrAvidin beads prior to immunoblotting for RFP and Panx1.

Cell surface biotinylation of Panx1-RFP revealed that all glycosylated species of Panx1 trafficked to the cell surface, while no clear cell surface expression of Panx1^{T307}-RFP was detected (A). NeutrAvidin fraction displayed a pronounced cell surface expression of both Panx1-RFP and Panx1, when co-expressed together (C). Plasma membrane biotinylation of co-expressed Panx1 could not detect Panx1^{T307}-RFP at the cell surface (B); however Panx1^{T307}-RFP expression reduced the overall expression of Panx1 (C). Total protein lysates labeled with (+) or without (-) biotin were also assessed for expression levels of Panx1, Panx1-RFP and Panx1^{T307}-RFP. GAPDH (an intracellular protein) was used to detect any internalization of biotin.
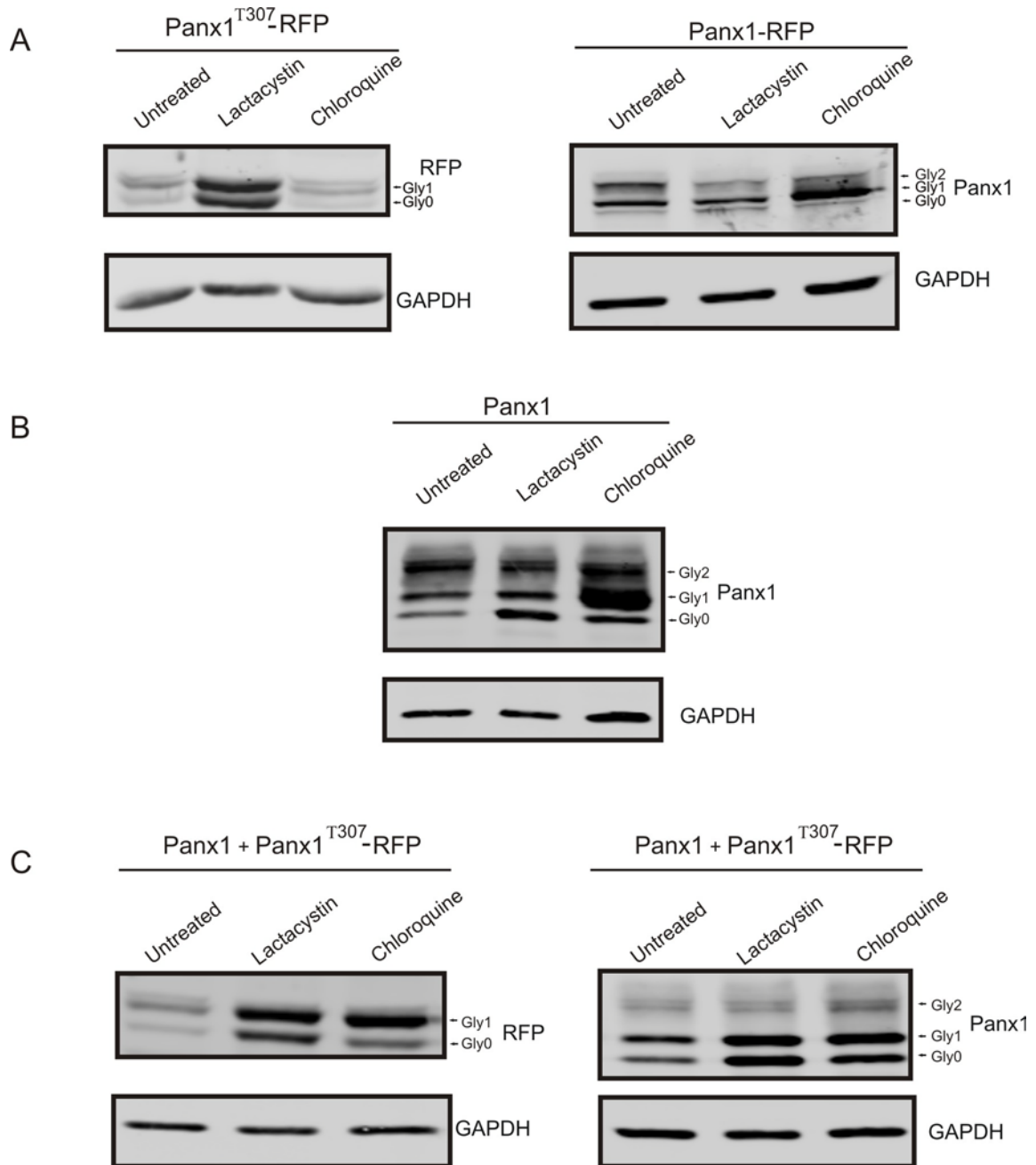
Figure 3.8 Panx1 is destined for proteasomal-mediated degradation in the absence of the C-tail

Panx1^{T307}-RFP, Panx1-RFP and Panx1 expressing HEK-293T cells were exposed to either proteasomal (lactacystin) or lysosomal (chloroquine) inhibitors for 20 hours prior to immunoblotting for RFP and Panx1. Expression of both the Gly0 and Gly1 species of Panx1^{T307}-RFP increased with lactacystin exposure,

with no detectable change upon chloroquine treatment (A). Lactacystin-treated cells expressing Panx1-RFP (A) or Panx1 (B), revealed a slight reduction in the expression of the Gly2 species; while chloroquine treatment resulted in the accumulation of the Gly1 and Gly2 species. Co-expression of Panx1 with Panx1^{T307}-RFP clearly reduced the Gly2 form of Panx1 (C). When co-expressed together, chloroquine treatment caused a reduction in the Gly1 form of Panx1, while Gly1 increased in cells expressing Panx1^{T307}-RFP (C). GAPDH was used as a protein loading control.

3.4 DISCUSSION

To identify the role of the Panx1 C-terminal domain in regulating Panx1 trafficking, glycosylation, oligomerization and degradation, the current study employed a Panx1 mutant that lacked the last 119 amino acid residues from the C-terminus. First we identified that in the absence of the C-terminal tail the mutant failed to traffic to and be retained at the cell surface. Second, the Panx1 truncated mutant was retained primarily within the ER where it was found as a core Gly0 protein or a high-mannose Gly1 species. Third, the Panx1 mutant failed to substantially interact with Panx1 suggesting that the C-terminal domain plays a role in Panx1 homomeric oligomerization. Finally, the ER-retained truncated mutant was subjected to proteasomal degradation, which is consistent with ER associated degradation.

3.4.1 Cell surface trafficking, post-translation modification and homomeric interaction of Panx1^{T307}-RFP

It has been well established that Panx1 traffics to the plasma membrane and distributes itself in a fairly uniform pattern, with some evidence of cell surface clustering [153]. Our results revealed that the deletion of the C-tail causes a shift in Panx1 localization, with a predominant retention in the ER. Similarly, truncation of the C-tail domain has been shown to perturb the cell surface trafficking of several other integral membrane proteins such as the human anion exchanger AE1 [156], the human sodium dependent vitamin C transporter 1 [157], the A1 adenosine G-protein coupled receptor [158] and Glut 1 and Glut 4 isoforms of glucose transporter [159], thus suggesting that an intact C-tail domain is required

to facilitate the adequate delivery of several proteins to plasma membrane. In addition, the cell surface trafficking of Panx1 is partially dependent on addition/processing of the glycan chains in the ER-Golgi compartments [47, 59]. Therefore, to determine if the lack of the cell surface localization of Panx1^{T307}-RFP was related to its glycosylation status we further assessed this possibility. Our results indicated that Panx1^{T307}-RFP exists as both core (Gly0) and high mannose (Gly1) species. Given that Panx1 is glycosylated on the second extracellular loop [25, 47], together with the fact that the Gly1 species of Panx1^{T307}-RFP was sensitive to Endo H treatment, our data suggests that deletion of the C-tail does not interfere with normal ER-based glycosylation events. It is quite likely that the trafficking defect is thus independent of ER-based glycosylation events but could still be related to proper Panx1 folding or oligomerization. This notion is somewhat similar to a case involving C-tail mutants of A1 adenosine G-protein coupled receptors, where incomplete modifications of the complex carbohydrate chains was correlated with defects in exiting the ER compartments of HEK-293 cells [158]. In addition, the ER retention of the C-tail truncated mutants of A1 receptors was also associated with incomplete folding and failed ER quality control [158]. It is well established that ER based chaperones, such as calnexin, mediate quality control by aiding in proper folding of glycoproteins, while restricting the trafficking of misfolded proteins [160]. In our studies, the strong co-localization of Panx1^{T307}-RFP and not Panx1-RFP with calnexin could possibly reflect the misfolded state of Panx1 in

the absence of its C-tail. Alternatively, failure of truncated Panx1 acquiring a proper oligomeric state could also be the cause for its ER retention [161, 162].

Misfolded mutant proteins often impair cell surface trafficking of their wild-type counterparts. One of the well characterized examples of this phenomenon is the ER retention of the Cl$^-$ ion channel cystic fibrosis transmembrane conductance regulator (CFTR) in the presence of its mutant counterpart ΔF508 [163]. Our cell surface biotinylation assay of cells co-expressing Panx1 and the truncated mutant did not reveal the mutant at the cell surface; however, the presence of the mutant clearly reduced the cell surface expression of all the Panx1 species. Interestingly, a similar ER variant-induced inhibition of the cell surface delivery of WT members of Wnt receptors was deemed to be due to impaired oligomerization [164]. Given that Panx1 oligomerizes as a hexamer prior to trafficking to the cell surface [47], we were interested in investigating if the partial retention of Panx1 in the presence of the mutant was due to potential co-interactions between the mutant and Panx1, while being residents of the ER. Interestingly, only a weak interaction between the Gly1 species of Panx1^{T307}-RFP and full length Panx1 was detected, thus suggesting the importance of the intact C-tail in mediating efficient oligomerization process of Panx1.

3.4.2 Fate of the C-tail truncated mutant of Panx1

It is widely accepted that misfolded or improperly assembled proteins retained in the ER are destined for premature degradation, if molecular chaperones are unable to correct their folding [159]. A proteasomal based degradation pathway is

linked to the degradation of incorrectly folded glycoproteins that are rejected by the quality control system of the ER [165], a process termed ER-associated degradation (ERAD). Proteasomal inhibition-induced accumulation of Panx1 in our studies, together with its localization in the calnexin-positive ER compartments suggests that this mutant is likely a substrate for ERAD. Interestingly and consistent with a study by Boassa et al., [47], our studies suggest that full length Panx1 is destined for lysosomal degradation. In particular, chloroquine-induced lysosomal inhibition of Panx1 revealed an increase in the more complex-mature form and the high mannose glycosylated species of Panx1. Since both glycosylated species of Panx1 (complex and high mannose) are capable of trafficking and residing at plasma membrane [59], its accumulation suggests that Panx1 cycling through the cell surface are destined for lysosomes for degradation. Alternatively, since a subpopulation of the high mannose species of Panx1 is also associated with the ER pool [47], its accumulation could either be a consequence of a negative-feedback mechanism, generated from the cell surface pool of Panx1 or inhibition of direct escape from ER-Golgi compartment to lysosomes. This hypothesis is somewhat supported by studies showing targeting of mutated prion proteins from the Golgi apparatus to lysosomes [166].

In keeping with our current findings, we propose a model where full length Panx1, capable of trafficking to the cell surface, is preferentially destined to lysosomes, as opposed to proteasomal dependent degradation of truncated mutant. This paradigm is shifted, however, when Panx1^{T307}-RFP and Panx1 are

co-expressed. An obvious increase in the high mannose species of Panx1^{T307}-RFP and Panx1 is noticed upon lysosomal and proteasomal inhibition, respectively. It is likely that oligomerization of Panx1 with Panx1^{T307}-RFP drives a subpopulation of Panx1^{T307}-RFP to lysosomes and a limited proportion of Panx1 to proteasomes.

3.4.3 Pathophysiological Significance

Adequate cell surface trafficking is imperative for Panx1 to form functional single membrane channels [25, 59]. A recent report showed that a single amino acid substitution from cysteine to serine at residue 346 on the C-tail alters Panx1 channel properties, such that it leads to the formation of constitutively leaky channels, thereby causing cell death [152]. Additionally, a point mutation in the Panx1 C-tail at position 337 perturbs the trafficking and distribution at the cell surface [47]. The physiological significance of the C-tail is further demonstrated by other channel forming proteins such as Cx43, where 97% of mice harboring a truncation of carboxyl-terminal (K258stop) die shortly after birth due to a defective epidermal barrier caused by impaired differentiation of keratinocytes [167]. With a growing significance of Panx1 in initiation and propagation of calcium waves [60], tumor suppression [53], release of interleukin-1β [147], keratinocyte differentiation [67], and ischemia induced cell death [78], our study provides strong evidence for a critical role for the carboxyl terminal tail in regulating Panx1 trafficking, oligomerization and degradation.

3.5 ACKNOWLEDGEMENTS

CHAPTER 4: Panx1 Exhibits Prolonged Turnover Kinetics and Internalization Pattern Distinct from the Connexin Family of Gap Junction Proteins

4.0 OVERVIEW

This study was designed to uncover the turnover kinetics and mechanism(s) responsible for Panx1 endocytosis. In particular, endocytic pathways mediated by clathrin-, caveolin- and dynamin were closely examined to determine their roles in the internalization of Panx1. A unique pattern of Panx1 turnover was characterized using rapid time-lapse imaging, while the degradation of Panx1 was explored using pharmacological inhibitors.

———————————

4.1 INTRODUCTION

Pannexins (Panxs) are the recently identified vertebrate homologues of the integral membrane invertebrate gap junction proteins, innexins [1, 21]. Although no sequence homology exists between pannexins and the vertebrate gap junction proteins, connexins (Cxs), pannexins were first proposed to belong to the gap junction superfamily of proteins based on their homology to innexins. Panx and Cxs exhibit tetraspanning transmembrane domains with intracellular amino and carboxy termini and two extracellular loops [108]. While there are 21 members of the connexin family, the pannexin family is comprised of only three members: Panx1, Panx2 and Panx3, which are commonly examined in humans, mice and rats [21]. Similar to Cx43, Panx1 is ubiquitously expressed in several murine tissues, while Panx2 is expressed predominantly in the central nervous system, and Panx3 is localized to the skin and cartilage [21, 25].

It has been reported that Panx1 oligomerizes into hexamers that traffic to the plasma membrane to form cell surface channels [47]. We and others have demonstrated that Panx1 achieves three states of glycosylation: Gly0 (core, unglycosylated), Gly1 (high mannose form) and Gly2 (complex form) [25, 47]; and assembles as single membrane channels that are mechano-sensitive [25, 57]. In addition, limited evidence also exists to support the formation of Panx1 intercellular channels [26, 53, 54].

Homomeric single-membrane Panx1 channels have a large conductance of 550 pS [57], which is correlated with ionic dysregulation during ischemic conditions, subsequently leading to neuronal necrosis [78]. Furthermore, *N*-methyl-D-

aspartate receptor (NMDAR)-induced opening of Panx1 channels has been implicated in hippocampal epileptiform seizure-like activity [66]. Other studies have associated Panx1 channel activation with apoptosis of *Xenopus* oocytes by forming a pore unit with the death complex of the P2X7 receptor [72]. More recently, Panx1 was characterized as a target for caspase 3 and 7 cleavage that resulted in a constitutively open channel [79]. In the same study, Panx1 channels were further shown to mediate phagocyte recruitment by releasing nucleotide signals from apoptotic cells [79]. In light of several physiological roles for Panx1, it is critical to determine pathways that may regulate its turnover and degradation.

In the case of Cx43, a unique turnover mechanism exists where gap junction plaques are internalized into one of the two contacting cells as large double membrane structures called connexosomes [101]. In addition, several studies have identified an association between Cx43 and clathrin-coated pits [102-104], where the down regulation of clathrin-adaptor protein complex 2 (AP2) as well as dynamin GTPase significantly reduced Cx43 gap junction internalization [102]. Cx43 has been shown to interact with caveolin (Cav)-1 [168] and Cav-2 to form complexes in membrane rafts at the plasma membrane that further regulate the level of gap junctional intercellular communication (GJIC) [154]. While more than one pathway exists in mediating Cx43 turnover, it has yet to be investigated whether pannexins follow the same routes of internalization.

We and others have reported that Panx1 exhibits slower turnover rates than Cx43 [25, 81]. While Cx43 biosynthesis, cell surface delivery, removal from the plasma membrane and degradation is completed with a half-life of only 1-3 hours

[82], use of pharmacological blockers have suggested that Panx1 levels at the cell surface remain relatively unchanged over a period of 8 hours [25]. Rapid turnover kinetics for Cx43 is of physiological importance for cell and tissue homeostasis through the regulation of GJIC. This notion is clearly demonstrated by a several fold increase in Cx43 expression in the myometrium prior to the labor onset, followed by rapid clearing post labor [169, 170]. Similarly, it is hypothesized that Panx1 turnover kinetics may also be critical in governing key physiological roles in cells. While Cx43 is targeted for both lysosomal and proteasomal degradation [105, 106, 171, 172], one report has suggested that Panx1 is destined for lysosomal degradation [47]. However, it is not currently known which glycosylated species of Panx1 undergoes lysosomal-mediated degradation. Thus, in the current study, we examine whether dynamin- and/or caveolin-dependent pathways are involved in Panx1 internalization, how Panx1 internalizes as assessed by rapid time-lapse imaging, and which Panx1 species are destined for lysosomal degradation.

4.2 EXPERIMENTAL PROCEDURES

4.2.1 Cell culture and reagents

BICR-M1R$_k$ cells, originally derived from rat mammary tumors, were a gift from Dieter Hulser, (Stuttgart, Germany [96]) and engineered to stably over-express Panx1, as previously described [25]. Cells were maintained at 37°C in high glucose DMEM (Invitrogen, Burlington, ON, Canada), supplemented with 10% fetal bovine serum, 100 units/ml penicillin, 100 μg/ml streptomycin, and 2 mM L-glutamine (all from Invitrogen, Burlington, ON, Canada), and sub-cultured using 0.25% trypsin/1 mM EDTA solution (Invitrogen).

4.2.2 Transfections

GFP-tagged WT and K44A DynII expression constructs were kindly provided by Dr. Mark A McNiven, (Mayo Clinic College of Medicine, MN) and used for conducting transient transfections of BICR-M1R$_k$ cells expressing Panx1. Cells grown in 35 mm dishes overnight to ~50-70% confluency were transfected in Opti-MEM1 media containing 1 μg of WT or K44A DynII GTPase cDNA constructs with 2 μL Lipofectamine 2000. Opti-MEM1 media was replaced with complete media 4 hrs post transfection.

4.2.3 Immunocytochemistry

Panx1 expressing BICR-M1R$_k$ cells grown overnight on glass coverslips were fixed with either 3.7% formaldehyde or 80% methanol and 20% acetone. Formaldehyde fixed cells were permeabilized in 1% blocking solution (Bovine Serum Albumin-(BSA; Sigma)) containing 0.1% Triton-X-100. Since antibodies

against Panx1, clathrin and Cav-1 were all raised in rabbits, a 488 fluorophore conjugated Panx1 antibody was engineered as per manufacturer's directions (Pierce Chemical) for dual labeling of Panx1 with these markers. For immunolabeling of Panx1 expressing cells for clathrin or Cav-1, cells were first incubated with either a 200 fold dilution of polyclonal anti-clathrin heavy chain antibody (Abcam), or a 100 fold dilution of polyclonal anti-Cav-1 antibody (BD Biosciences Transduction Laboratories) for 1 hr at room temperature, followed by incubation with goat anti-rabbit Alexa Fluor555 (1:500, Invitrogen) for 45 min at room temperature. Thereafter, cells were washed with PBS and incubated with Panx1_488 antibody for an additional 45 min at room temperature before staining nuclei with Hoechst 33342 (Invitrogen). For double labeling of Panx1 expressing cells for AP2 or Cav-2: cells were first labeled with affinity-purified polyclonal Panx1 antibody at a concentration of 2 μg/mL for 1 hr, followed by incubation with goat anti-rabbit Alexa Fluor555 (1:500, Invitrogen) for 45 min at room temperature. Next, cells were labeled with either monoclonal anti-AP2 (Sigma) or monoclonal anti-Cav-2 (BD Biosciences Transduction Laboratories) at a 100 fold dilution followed by incubation with goat anti-mouse Alexa Fluor488 (1:500, Invitrogen). DynII was labeled using a 50 fold dilution of anti-DynII antibody (Santa Cruz) for 1 hr prior to using Texas Red conjugated donkey anti-goat (1:200, Jackson Immuno Research Laboratories) as a secondary antibody. Once immunolabeled, cells were mounted on glass slides and imaged using a LSM 510 META confocal microscope (Zeiss) using a 63x oil lens.

4.2.4 Pharmacological inhibitors

Brefeldin A (BFA), cycloheximide (CHX), dynasore, methyl-β-cyclodextrin (MβC) and chloroquine were all purchased from Sigma. Cells were treated for 20-32 hr with 5 µg/ml BFA and for 1-24 hr with 10 mM MβC. For cycloheximide treatment, 20 µg/ml was used to inhibit all protein synthesis, and cells were lysed at 2, 4, 6 and 8 hours following the exposure. Dynasore treatment was used at a concentration of 40 µM, consistent with previous studies [102]. Post treatment, cells were fixed for immunocytochemistry and lysed for immunoblotting and co-immunoprecipitation assays.

4.2.5 Immunoblotting and co-immunoprecipitation

Immunoblotting and co-immunoprecipitation assays were performed based on our previously described protocol [153]. Briefly, cells were lysed in buffer containing 150 mM NaCl, 10 mM Tris-HCl, pH 7.4, 1 mM EDTA, 0.5% NP-40, and 1% Triton X-100, supplemented with protease inhibitor cocktail (one tablet per 10 mL buffer, Roche) and phosphatase inhibitors (1 mM NaF and 1 mM Na$_3$VO$_4$). Protein concentrations were measured using a BCA protein determination kit (Pierce), and 20-30 µg of total protein lysate was resolved on a 10% SDS-PAGE gel. Protein samples were transferred onto nitrocellulose membranes using the iBlot Dry Blotting system (Invitrogen) and blocked with 5% Blotto Milk (Santa Cruz Biotechnologies) or 3% BSA (Sigma) for 1 hr prior to incubating with anti-Panx1 (0.2 µg/mL), anti-clathrin (1:1000, Abcam), anti-AP2 (1:500, Sigma), anti-DynII (1:250, Santa Cruz), anti-Cav-1 (1:2000) or anti-Cav-2 (1:2000 BD Biosciences Transduction Laboratories), and anti-GAPDH (1:5000,

Millipore) antibodies. Primary antibody binding was detected using mouse IgG IR dye 800 at 1:10,000 dilution (Rockland Immunochemicals) or rabbit IgG Alexa 680 at 1:10,000 dilution (Invitrogen) and blots were scanned with the Odyssey infrared imaging system (Licor).

For co-immunoprecipitation assays, 800-1000 µg of cell lysates were incubated overnight in presence of 10 µg/ml anti-Panx1 antibody at 4°C, and immune complexes were pulled down using 30 µl (50% suspension) of protein A-Sepharose beads. Beads were washed in 1x lysis buffer, boiled for 5 min in 30 µl of 2x Laemmli buffer, resolved by SDS-PAGE, and immunoblotted with specific antibodies to detect Panx1, clathrin, AP2, Cav-1, Cav-2 and DynII. Although primary antibodies were detected using mouse IgG IR dye 800 at 1:10,000 (Rockland Immunochemicals) or rabbit IgG Alexa 680 at 1:10,000 (Invitrogen), detection of co-immunoprecipitates was achieved using the Clean-Blot IP Detection Reagent (horse radish peroxidase; Pierce Chemical) as a secondary antibody at a 4000 fold dilution for 45 minutes, in order to minimize the appearance of the IgG bands in some instances.

4.2.6 Transferrin uptake

Cells expressing WT DynII or K44A mutant grown on glass bottom dishes were rinsed and incubated in DMEM media containing 20 mM Hepes and 2 mg/ml BSA for 1 hr at 37°C. Cells were incubated for 1 hr in presence of 10 µg/ml of dynasore. Media was then replaced with media containing 10 µg/ml of transferrin-Alexa 555 (Invitrogen) and cells were incubated for additional 45 min

at 4°C to block any uptake. Thereafter, cells were imaged either immediately (to capture 0 min of uptake) or post 30-40 min after incubation at 37°C.

4.2.7 Rapid time-lapse imaging

BICR-M1R$_k$ cells expressing GFP-tagged Panx1 were sub-cultured on glass bottom dishes and treated with 5 µg/ml of BFA in culture media for 20 hr at 37°C. Prior to imaging, cells were rinsed and replenished with Opti-MEM1 media containing fresh BFA. Rapid time-lapse imaging was performed in a temperature and C0$_2$ controlled humidity chamber, staged on a Zeiss LSM 510 META confocal microscope. A region of interest was selected and vesicles budding from the plasma membrane were monitored at 30 s time intervals for a total period of 23 min.

4.3 RESULTS

4.3.1 Panx1 exhibits a longer turnover rate than Cx43

We have previously demonstrated that Cx43-positive BICR-M1R$_k$ cells serve as a good cell reference model for examining the turnover mechanisms of Cx43 [109], and thus this cell system has been employed in this study to investigate the internalization process of Panx1. In order to follow the fate of an existing cell surface population of Panx1, we used BFA to block the transport of newly synthesized proteins to the plasma membrane. BFA-treated cells over-expressing Panx1 were fixed at various time points prior to immunolabeling for Cx43 and Panx1. In untreated cells, Cx43 was visualized as punctate structures at cell-cell appositions with some intracellular distribution, whereas Panx1 was localized in a relatively uniform pattern at the cell surface (Figure 4.1A). Within 3 hrs of BFA exposure, most of the Cx43 puncta were cleared from the cell surface and newly synthesized protein was retained in an ER-like pattern. In contrast, Panx1 was localized predominantly at the cell surface with minimal distribution in the intracellular compartment (Figure 4.1A). At 32 hrs of BFA treatment, some clearing of Panx1 from the cell surface was evident with increased accumulation in an ER-like pattern (Figure 4.1A). To further compare the kinetic properties between pannexins and connexins, Panx1 and Cx43 expression was examined in cells under conditions in which protein synthesis was inhibited by CHX.
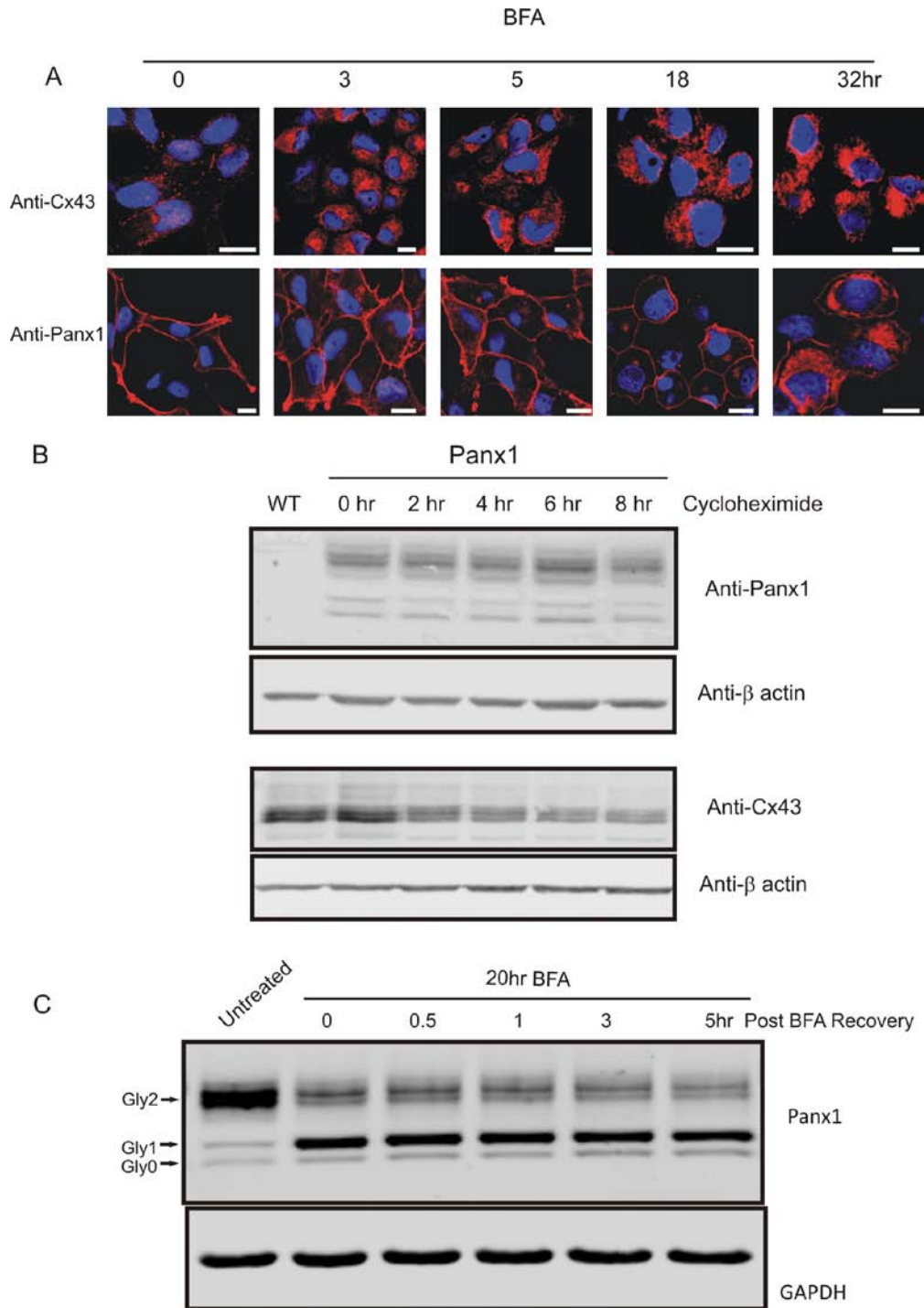
Figure 4.1 Turnover kinetics of Cx43 and Panx1

Panx1 expressing, Cx43-positive BICR-M1R$_k$ cells were treated with BFA for up to 32 hr prior to immunolabeling for Cx43 or Panx1 (A, red). Note the loss of

Cx43 from the cell surface within 3 hr of BFA treatment while Panx1 was observed at the cell surface for over 18 hr. Nuclei were stained with Hoechst. Bar=10μm. Cells exposed to CHX for 2, 4, 6 and 8 hr were immunoblotted for Panx1 and Cx43 (B). When compared to untreated cells (0 hr), immunoblot analysis of Panx1 revealed no difference between the banding profile at 2, 4, 6 and 8 hr of CHX treatment (B); whereas, the level of Cx43 consistently diminished following CHX exposure (B). Upon BFA treatment, Panx1 revealed the accumulation of the Gly1 species with a reduction of the Gly2 species, which remained the same for up to 5 hr upon BFA washout (B). β-actin and GAPDH were used as protein loading controls.

In agreement with the BFA results and when compared to untreated cells, immunoblot analysis of Panx1 levels revealed no difference between the banding profiles at 2, 4, 6 and 8 hrs of CHX treatment (Figure 4.1B), whereas there was an overall time-dependent decrease in Cx43 levels following CHX exposure (Figure 4.1B). These results clearly suggest Panx1 retention at the cell surface is much longer than Cx43.

The rapid turnover and intracellular accumulation of Cx43 can be reversed within 1 hr of BFA removal [109]. Based on this information, we investigated if the recovery dynamics of Panx1 BFA treatment was the same as Cx43 or different. BFA treatment of Panx1 expressing cells for 20 hrs reduced the higher glycosylated (Gly2) species, with a subsequent increase in the high mannose (Gly1) form of Panx1 (Figure 4.1C). However, 5 hr washout of BFA was insufficient to return the ratio of the three Panx1 glycosylated species back to normal (Figure 4.1C). Collectively, these results suggest that not only is Panx1 long lived at the cell surface but trafficking of Panx1 through the secretory pathway is relatively slower than that of Cx43.

4.3.2 Panx1 is co-expressed but does not co-immunoprecipitate with clathrin or AP2

Clathrin mediated endocytosis (CME) is a well documented process that is initiated by the recruitment of clathrin and adaptor proteins (such as AP2) to the plasma membrane before forming a coat around the endocytic vesicles and budding off [173]. Internalization of Cx43 has previously been correlated, in part, with the CME pathway [102]. In order to investigate if Panx1 is internalized

through a clathrin driven pathway, we first immunolabeled Panx1 expressing BICR-M1R$_k$ cells with antibodies directed against the clathrin heavy chain and Panx1. Panx1 was distributed at the cell surface in a relatively uniform pattern; while, clathrin was assembled in a punctate-like pattern at the cell surface with some intracellular distribution (Figure 4.2A). Panx1 co-distributed with clathrin (Figure 4.2A) and AP2 (Figure 4.2B) at the cell surface. The plasma membrane co-distribution of Panx1 with AP2 was not noticeably altered in the presence or absence of BFA (Figure 4.2B and C). Additionally, immunoprecipitation of Panx1 from WT and Panx1 over-expressing cells did not pull down either clathrin or AP2, which were expressed in total lysates at ~180 kDa and ~105-110 kDa, respectively (Figure 4.2D). As expected, Panx1 was immunoprecipitated in cells over-expressing Panx1 but not in WT cells (Figure 4.2D). This indicates that although Panx1 may co-exist in the same compartment with either clathrin or AP2, they do not interact.

4.3.3 Panx1 co-distributes but does not co-immunoprecipitate with Cav-1 and Cav-2

Several channels have been reported to localize to the lipid rafts/ caveolae to regulate their functional status [174-176]. Caveolae are specialized invaginated domains that are formed by the caveolin family of integral membrane proteins, which consists of three members: Cav-1, Cav-2 and Cav-3 [177]. Similar to Panx1, Cav-1 is ubiquitously expressed in several tissues, whereas Cav-2 is co-expressed with Cav-1 in various tissues and Cav-3 is primarily restricted to muscle [178].
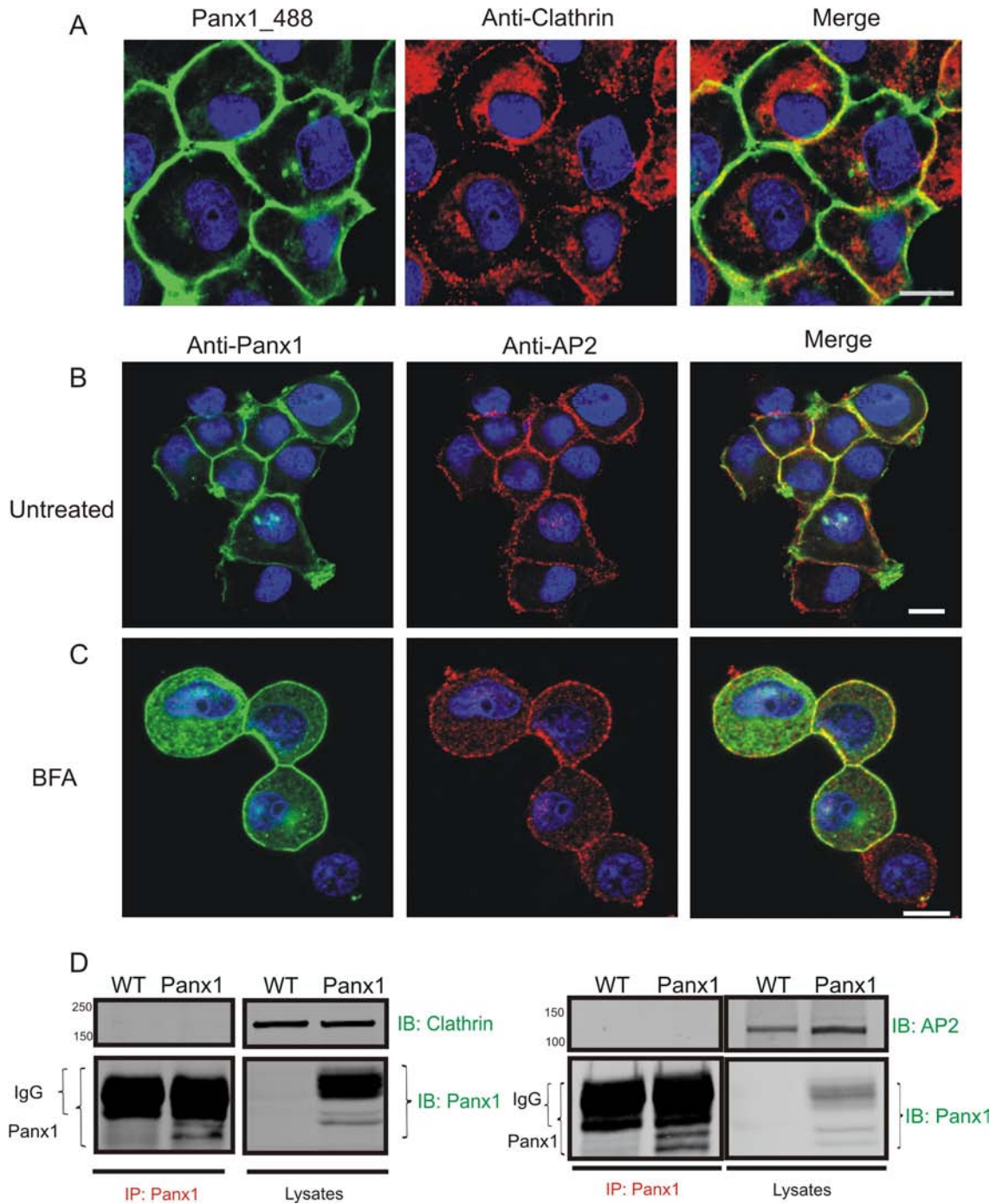
Figure 4.2 Panx1 co-distributes, but does not co-Immunoprecipitate with clathrin or AP2

Panx1 expressing BICR-M1R$_k$ cells were immunolabeled for clathrin heavy chain (A) or anti-AP2 (B, C). 488-fluorophore conjugated Panx1 antibody detected Panx1 (green) with clathrin (red) at the cell surface (A, merge). Double

immunofluorescent-labeling revealed the co-distribution of Panx1 (green) with AP2 (red) at the cell surface before and after a 20 hr BFA exposure (C). Nuclei were stained with Hoechst. Bar=10μm. Immunoprecipitates of Panx1 from WT and Panx1 expressing cells were immunoblotted for Panx1, clathrin and AP2. Panx1 (~43-50kD) was successfully pulled down from Panx1 expressing cells (under and below the IgG band); however, clathrin (~192kD) or AP2 (~105-110kD) did not co-immunoprecipitate with Panx1 (B). IB: immunoblot; IP: immunoprecipitation, WT: wild type cells; Panx1: Panx1 expressing cells.

In order to determine whether caveolins play a role in Panx1 turnover, we investigated the localization profile and interaction status of Panx1 between Cav-1 and Cav-2. Two different fixative methods, formaldehyde and acetone/methanol, were employed to detect the intracellular and cell surface populations of Cav-1/Cav-2, respectively [154]. In formaldehyde fixed cells, Panx1 co-distributed with Cav1 (Figure 4.3A) and co-localized with Cav-2 (Figure 4.3C) in the intracellular compartment, presumably the Golgi complex. Conversely, fixation with acetone/methanol revealed co-expression of Panx1 with Cav-1 (Figure 4.3B) and Cav-2 (Figure 4.3D) mainly at cell-cell appositions. To examine the potential interaction of Panx1 with Cav-1 and Cav-2, a co-immunoprecipitation assay was conducted. Panx1 but not Cav-1 was pulled down in the immunoprecipitates of Panx1 (Figure 4.3E). Reciprocally, Cav-1 but not Panx1 was detected in the immunoprecipitates of Cav-1 (Figure 4.3F). While Panx1 was detected in the immunoprecipitates of Panx1 expressing cells, Cav-2 remained undetected (Figure 4.3G). Conversely, Cav-2 but not Panx1 was expressed in the immunoprecipitates of Cav-2 (Figure 4.3H). As expected, total cells lysates revealed Panx1 expression only in over-expressing and not the WT cells, whereas Cav-1 (Figure 4.3E and F) and Cav-2 (Figure 4.3G and H) were detected in both WT and Panx1 over-expressing cells.
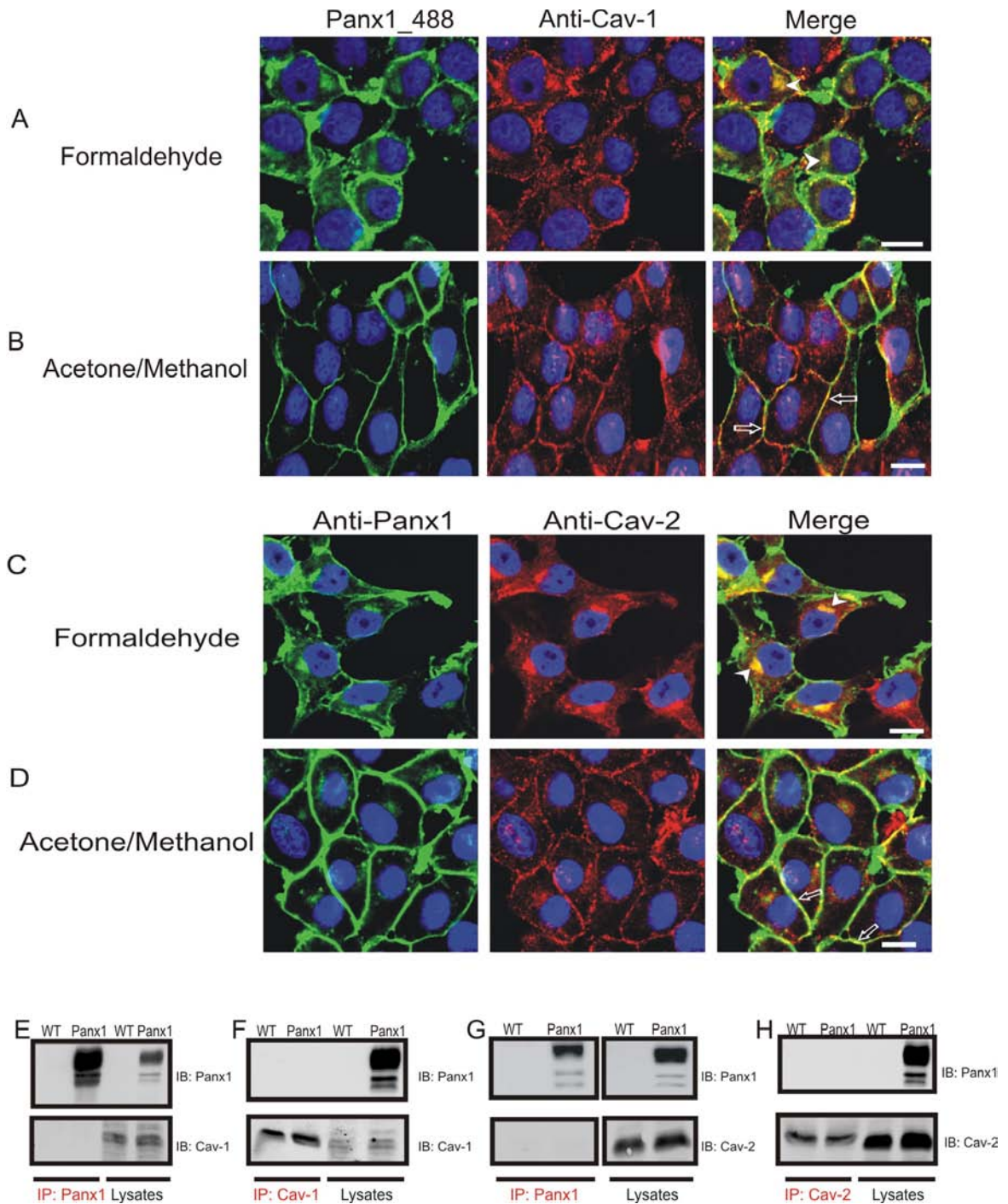
Figure 4.3 Subcellular distribution and interaction of Panx1 with Cav-1 and Cav-2

BICR-M1R$_k$ cells endogenously expressing Cav-1 and Cav-2, and stably expressing Panx1 were fixed with formaldehyde or acetone/methanol prior to immunolabeling. Panx1 (green) was found to co-distribute with intracellular and

plasma membrane localized Cav-1 and Cav-2 (red) (A-D).   Immunoprecipitates of Panx1 (E and G) from WT and Panx1 expressing cells were immunoblotted for Panx1, Cav-1 and Cav-2. Panx1 was detected only in the immunoprecipitates of Panx1 (E and G) and not in the Cav-1 (F) or Cav-2 (H) immunoprecipitates. Conversely, Cav-1(F) and Cav-2 (H) were found in their respective immunoprecipitates and not in the Panx1 immunoprecipitates (E and G). IB: immunoblot; IP: immunoprecipitation, WT: wild type cells; Panx1: Panx1 expressing cells.

While caveolins become detergent insoluble upon integrating into membrane rafts, these rafts can be disrupted with the cholesterol-depleting agent MβC [154]. We exposed Panx1 expressing cells to MβC for various time points to disrupt caveolin enriched membrane rafts. No substantial difference in the Panx1 banding pattern (Figure 4.4A) or localization profile (Figure 4.4B) was detected in presence of MβC. Interestingly, the highly phosphorylated species of Cx43, typically associated with the cell surface and detergent-insoluble pool [154], diminished within 1 hr of MβC treatment (Figure 4.4A). Overall, our results indicate that while Panx1 co-distributes in the same intracellular and cell surface compartments as Cav-1 and Cav-2, there is no clear evidence of their co-interaction. Additionally, cholesterol extraction from the plasma membrane does not noticeably alter the overall Panx1 expression.

4.3.4 Panx1 internalization is independent of dynamin GTPase

The dynamin GTPase is a common player in mediating caveolar fission, as well as budding the clathrin coated vesicles from the plasma membrane [179]. The mammalian dynamin family comprises of three members: dynamin I, II and III, where dynamin I is brain-enriched, dynamin II is ubiquitously expressed and dynamin III is mainly found in testis but also has some enrichment in brain especially in postsynaptic areas [180-183]. It is well accepted that a dominant-negative GTP hydrolyzing mutant of dynamin (K44A) interferes with the function of endogenous dynamin by blocking vesicular internalization prior to pinching off cell membrane [184]. Therefore in order to investigate the role of dynamin in
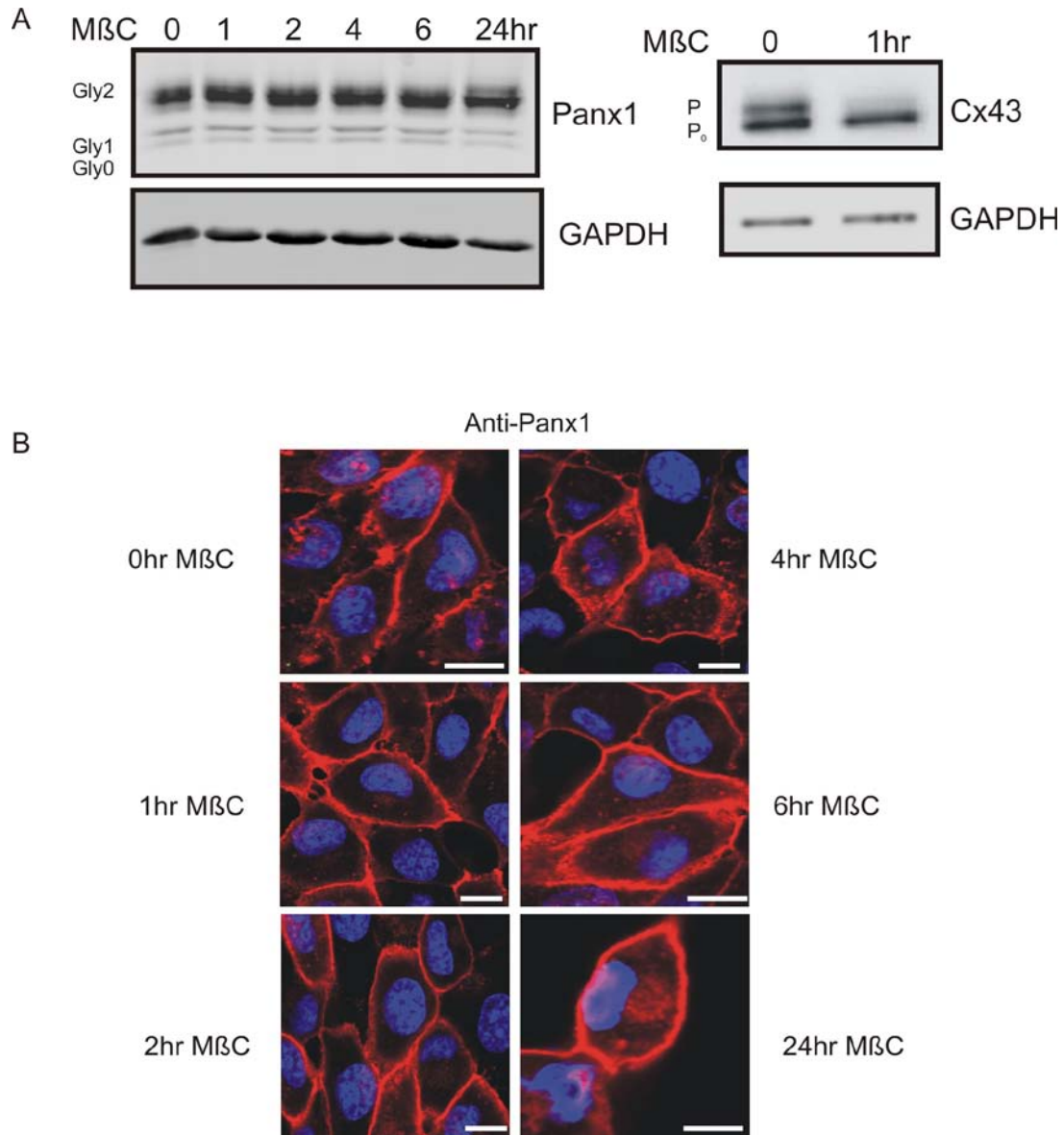
Figure 4.4 Characterization of methyl-β-cyclodextrin treatment on Panx1 expression levels and distribution profile

Western blots revealed that the expression levels of the Panx1 glycosylation species remained unaltered after a 24 hr treatment with MβC (A); while the highly phosphorylated form of Cx43 was reduced within 1 hr of MβC exposure (A). The cell surface distribution of Panx1 (red) remained relatively uniform during the 24 hrs of MβC treatment (B). Nuclei were counterstained with Hoechst. Bar=10μm. GAPDH was used as a protein loading control.

Panx1 internalization, we transfected previously generated GFP-tagged WT and K44A DynII in Panx1 over-expressing cells. As expected, an antibody generated against DynII detected both the WT (Figure 4.5A) and K44A DynII mutant (Figure 4.5B), dispersed intracellularly and at the cell surface. Some evidence of Panx1 co-localization with the WT (Figure 4.5C) and the K44A (Figure 4.5D) DynII mutant at the plasma membrane was noticed in untreated cells. Cells co-expressing Panx1 and WT DynII revealed consistent co-distribution at the cell surface with a slight increase in the intracellular localization of Panx1 (Figure 4.5E). Conversely, in the presence of BFA, cells co-expressing Panx1 and the K44A DynII mutant revealed less intracellular accumulation of Panx1 when compared to cells expressing only Panx1 in the same culture environment (Figure 4.5F). It was unclear if the increased intracellular expression of Panx1 in the absence of the K44A DynII mutant was due to uninhibited turnover of the cell surface population of Panx1 or the BFA-induced ER accumulation of Panx1. Therefore, we assessed the effect of the WT and K44A DynII mutant over-expression, and dynasore (a pharmacological inhibitor of dynamin GTPase) on the glycosylation species of Panx1. It was predicted that if dynamin GTPase plays a role in Panx1 internalization, then an increase in the Gly2 expression of Panx1 would be seen in the presence of the K44A DynII mutant or dynasore. In the untreated group, expression of Panx1 alone or in presence of the WT or K44A DynII revealed no significant difference among all the three glycosylated species of Panx1 (Figure 4.6A and B). In contrast, BFA treatment significantly reduced the Gly2 species with a subsequent increase in the Gly1 species of
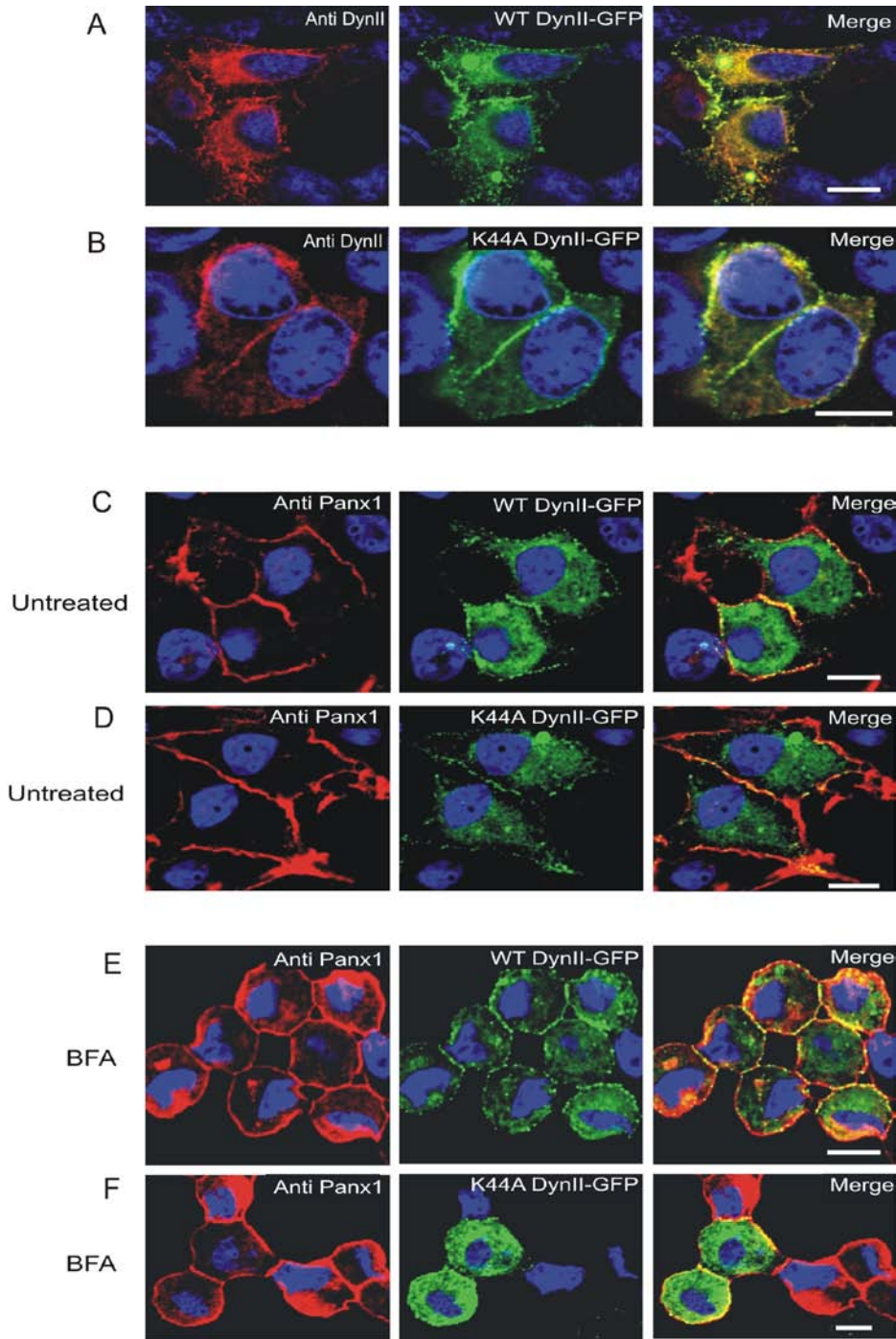
Figure 4.5 Assessment of Panx1 distribution in the presence of WT and K44A mutant DynII

Cells stably expressing Panx1 were transiently transfected with WT or K44A DynII expression constructs. Immunolabeling with anti-DynII antibody (red)

detected the GFP-tagged WT (green) and K44A (green) DynII mutant at the cell surface and within intracellular compartments (A and B). In untreated cells, WT and K44A DynII localized with Panx1 primarily at the cell surface (C and D). BFA treatment induced similar intracellular and cell surface distribution of Panx1 in the presence of WT (E) or K44A DynII (F). Nuclei were counterstained with Hoechst. Bar=10µm.

Figure 4.6 Characterization of dynamin GTPase on Panx1 expression, interaction and transferrin uptake

Protein lysates of untreated and BFA treated cells expressing Panx1 alone or in combination with WT and K44A DynII, were subjected to immunoblotting using
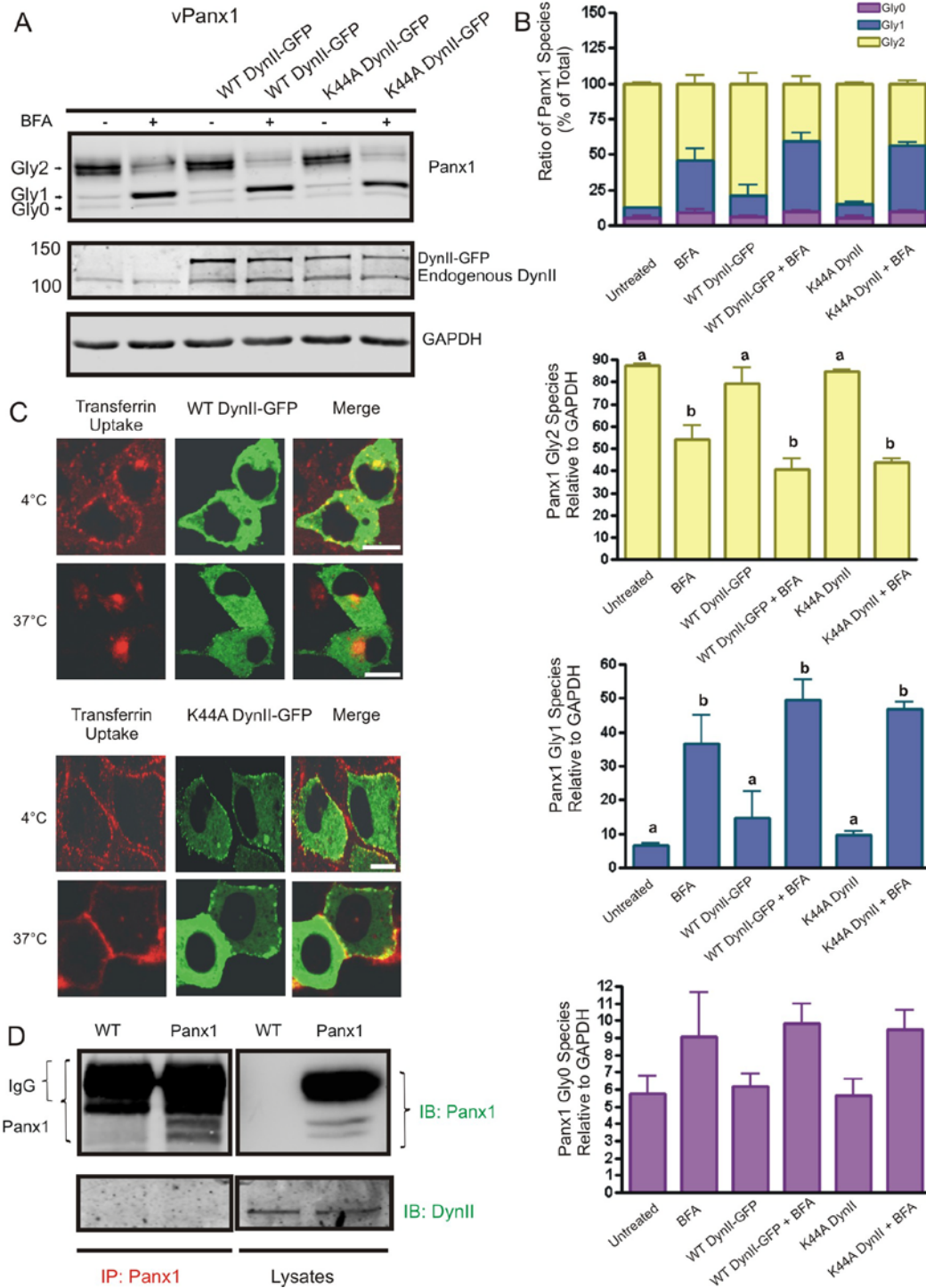
anti-Panx1 and anti-DynII antibodies. A significant reduction of the Panx1 Gly2 species and accumulation of the Gly1 species was observed when cells were exposed to BFA (A and B). The overall Panx1 expression levels remained unaltered with the co-expression of WT and K44A DynII (A and B). Transient transfection of WT and K44A DynII resulted in their expression at approximately equal levels (A). In contrast to the WT DynII, temperature sensitive uptake of transferrin-Alexa 555 in live cells was greatly reduced in the presence of K44A DynII (C). Immunoprecipitates of Panx1 from WT and Panx1 expressing cells were probed with anti-Panx1 and anti-DynII antibodies. Panx1 but not DynII was detected in the immunoprecipitates of Panx1 (D). GAPDH was used as a protein loading control. For statistical analysis, ratios between glycosylation species of Panx1 (Gly0, Gly1, Gly2) and GAPDH loading control were taken and a one-way ANOVA was performed followed by Tukey's post test (where 'a' is significantly different to 'b' and 'c'). Y-axis reflects arbitrary numbers. Bar=10µm.

Panx1 in all groups (Figure 4.6A and B). In comparison to the WT DynII, no significant increase in the Gly2 species of Panx1 was observed when co-expressed with the K44A DynII (Figure 4.6A and B).

To ensure that cells adequately expressed functional exogenous DynII constructs, we assessed the protein levels and transferrin uptake capabilities of the WT and K44A DynII. Over-expression of the GFP-tagged WT and K44A DynII revealed a band at approximately 125-130 kDa (Figure 4.6A). When maintained at 4°C, live cells expressing WT or K44A DynII revealed transferrin distribution at cell-cell appositions (Figure 4.6C). Following incubation at 37°C, the WT DynII showed a clear accumulation of transferrin in the intracellular compartment, while K44A DynII restricted the ability of transferrin uptake (Figure 4.6C). Given the role of dynamin in vesicular budding [184], it was not surprising to find that Panx1 did not interact with DynII (Figure 4.6D). Parallel with the DynII K44A study, treatment with dynasore alone did not significantly enhance the expression of the Panx1 Gly2 species (Figure 4.7A and B). When treated together with BFA, dynasore did not show any additive effect on the BFA-induced expression levels of the Panx1 Gly2 and Gly1 species (Figure 4.7A and B). As expected, dynasore treatment limited the transferrin uptake when incubated at 37°C (Figure 4.7C). Overall, our results indicate that Panx1 internalization is unique and independent of the dynamin-mediated pathway.
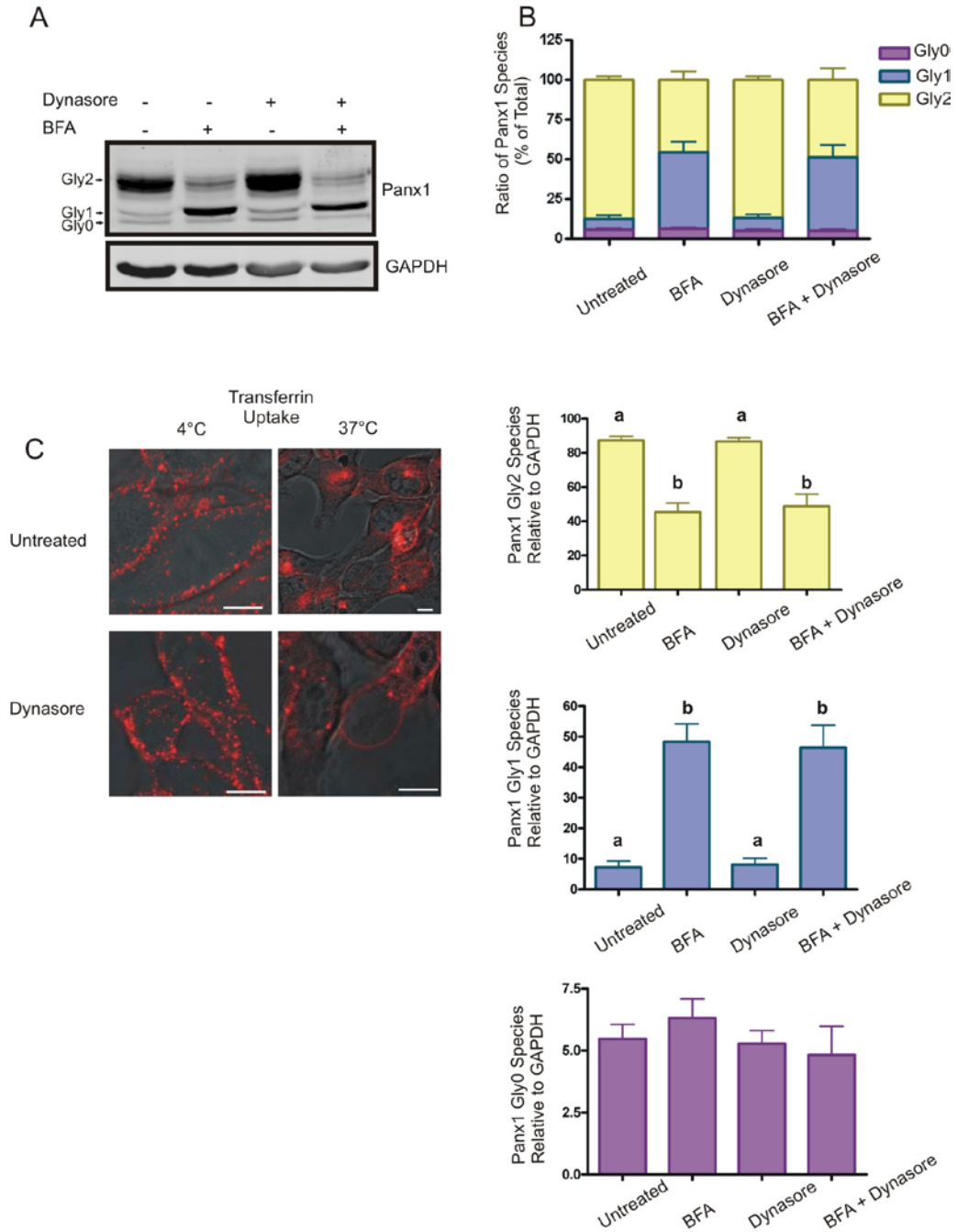
Figure 4.7 Panx1 protein expression levels remains unaltered in the presence of dynasore

Panx1 expressing cells were treated in the presence or absence of dynasore together with or without BFA for 20 hrs prior to immunoblotting for Panx1. Treatment with BFA alone caused a significant reduction in the Gly2 species of Panx1 with a marked accumulation of the Gly1 form; while dynasore treatment

alone did not change this protein banding profile (A and B). Together, dynasore did not cause any additive effect to the BFA induced reduction and accumulation of the Gly2 and Gly1 expression, respectively (A and B). GAPDH was used as a protein loading control. Exposure to dynasore successfully blocked the uptake of transferrin-Alexa 555 in live cells at 37°C (C) indicating its effectiveness at inhibiting endocytosis. For statistical analysis, ratios between glycosylation species of Panx1 (Gly0, Gly1, Gly2) and GAPDH loading control were taken and a one-way ANOVA was performed followed by Tukey's post test (where 'a' is significantly different to 'b' and 'c'). Y-axis reflects arbitrary numbers. Bar=10μm.

4.3.5 Panx1 follows a unique pattern of internalization

To examine the internalization of Panx1 in live cells, we exposed Panx1-GFP over-expressing BICR-M1R$_k$ cells to BFA for 20 hrs prior to capturing rapid-time lapse images.

BFA treatment revealed three distinct distribution profiles of Panx1: a) intracellular accumulation around the perinuclear region, b) some evidence of uniform distribution at the cell surface, and c) bright clusters at the plasma membrane (Figure 4.8). Over time, bright clusters of Panx1-GFP at the cell surface formed peculiar tubular-like extensions that stretched away from the plasma membrane toward intracellular compartments (Figure 4.8 arrowhead, see Movie 4.1). Additionally, Panx1-GFP containing extensions (570 s, Figure 4.8) appeared to collapse back onto the plasma membrane (720 s, Figure 4.8). Overall, these tubular-like extensions were very slow in internalizing from the cell cell surface ranging from ~ 30-45 mins. Over 30 tubular-extensions were visualized in 12 random cells assessed over three independent BFA exposures and image capturing sessions. Our imaging data suggests that Panx1 is removed from the cell surface along unique tubular-like extensions.

4.3.6 Panx1 is destined for the lysosomal mediated degradation

In contrast to untreated cells, long term exposure to the pharmacological lysosomal inhibitor, chloroquine, revealed a sustained expression of the cell surface associated Gly2 species, with a pronounced accumulation of the Gly1 form of Panx1 (Figure 4.9). The subcellular distribution of Panx1 in the presence
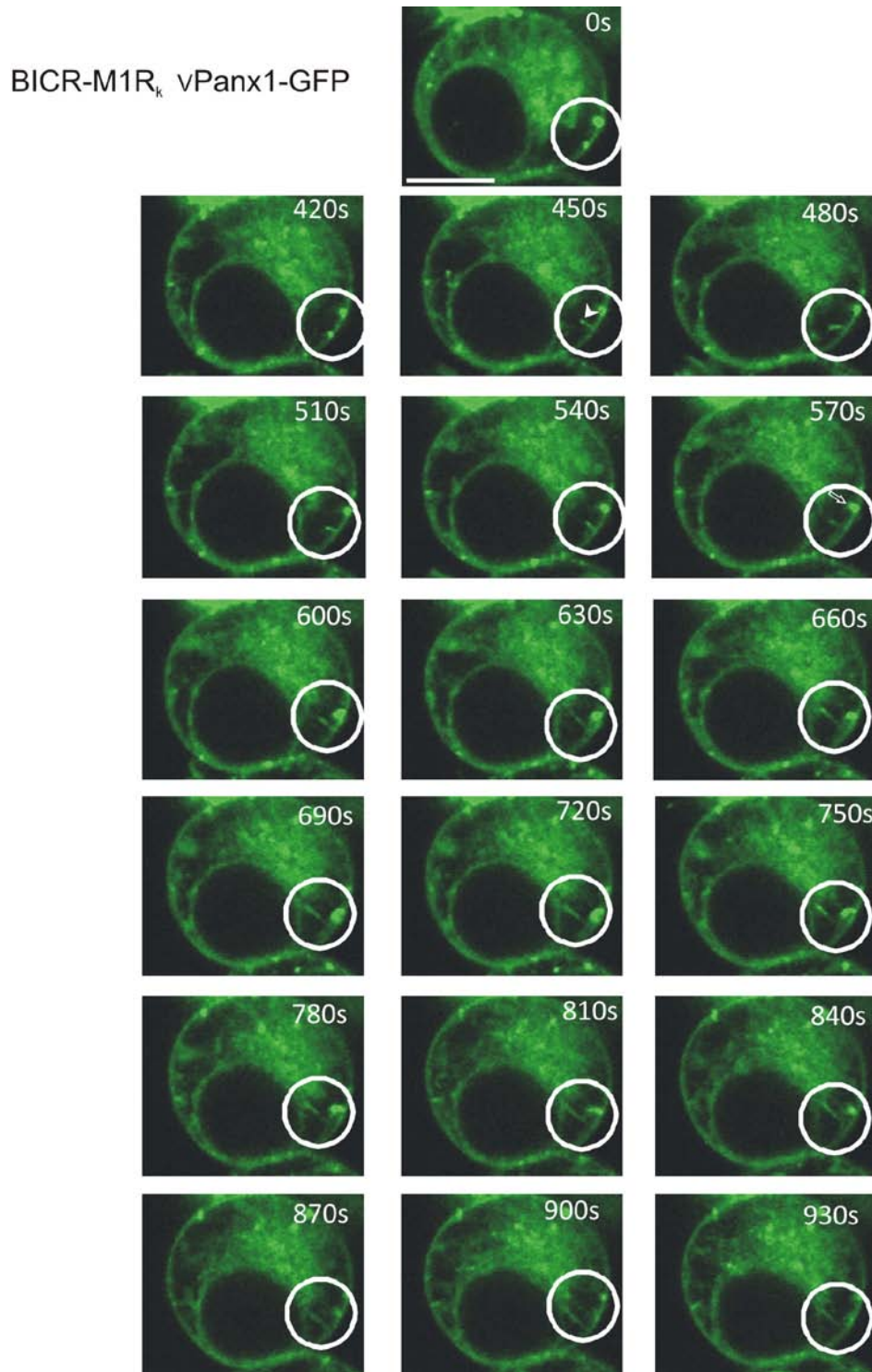
Figure 4.8 Panx1-GFP internalizes in dynamic tubular-like extensions

Cells stably expressing Panx1-GFP were treated with BFA for 20 hrs prior to performing rapid-time lapse imaging in the presence of BFA. Images were

acquired every 30 s for the total time of 23 min, however, only a subset of time frames are displayed (see Movie 4.1). Panx1-GFP internalized by clustering at the plasma membrane (420 s) followed by a dynamic tubular-like extension (arrowhead, 450s) that stretched to bud away from the cell surface towards the intracellular compartment (600-930s). Minimal extensions of other nearby cluster (unfilled arrow, 570 s) were noticed to collapse back on to the cell surface instead of detaching itself (720 s). Bar=10µm.

Movie 4.1 Panx1-GFP follows a unique pattern of internalization through dynamic tubular-like extensions

Rapid time-lapse images of BFA-treated Panx1-GFP expressing cells were captured to assess the mechanisms of Panx1 internalization. Panx1-GFP was localized in a relatively uniform manner with some evidence of bright clustering at the cell surface that occurred prior to endocytosis. These clusters first extended in a tubular-like morphology away from the cell surface and then detached. The movie sequence was captured every 30 s over 46 frames representing a total elapsed time of 23 min. The movie was accelerated to play in 10.12 s.

of chloroquine paralleled its banding profile, as a sub-population was noticed around the perinuclear region (presumably lysosomes [47]), with a clear evidence of the cell surface expression (Figure 4.9). As expected, BFA treatment reduced the Gly2 species with a subsequent increase in the Gly1 form of Panx1 (Figure 4.9), which was consistent with the loss of the cell surface distribution coinciding with an accumulation in an intracellular compartment (Figure 4.9). Inhibition of the lysosomal pathway in the presence of BFA resulted in a slight increase in expression of the Panx1 Gly2 species when compared to BFA treatment alone (Figure 4.9). This finding suggests that accumulation of the existing cell surface pool of Panx1 is a result of blocking its internalization and degradation through the lysosomal pathway.

A

B
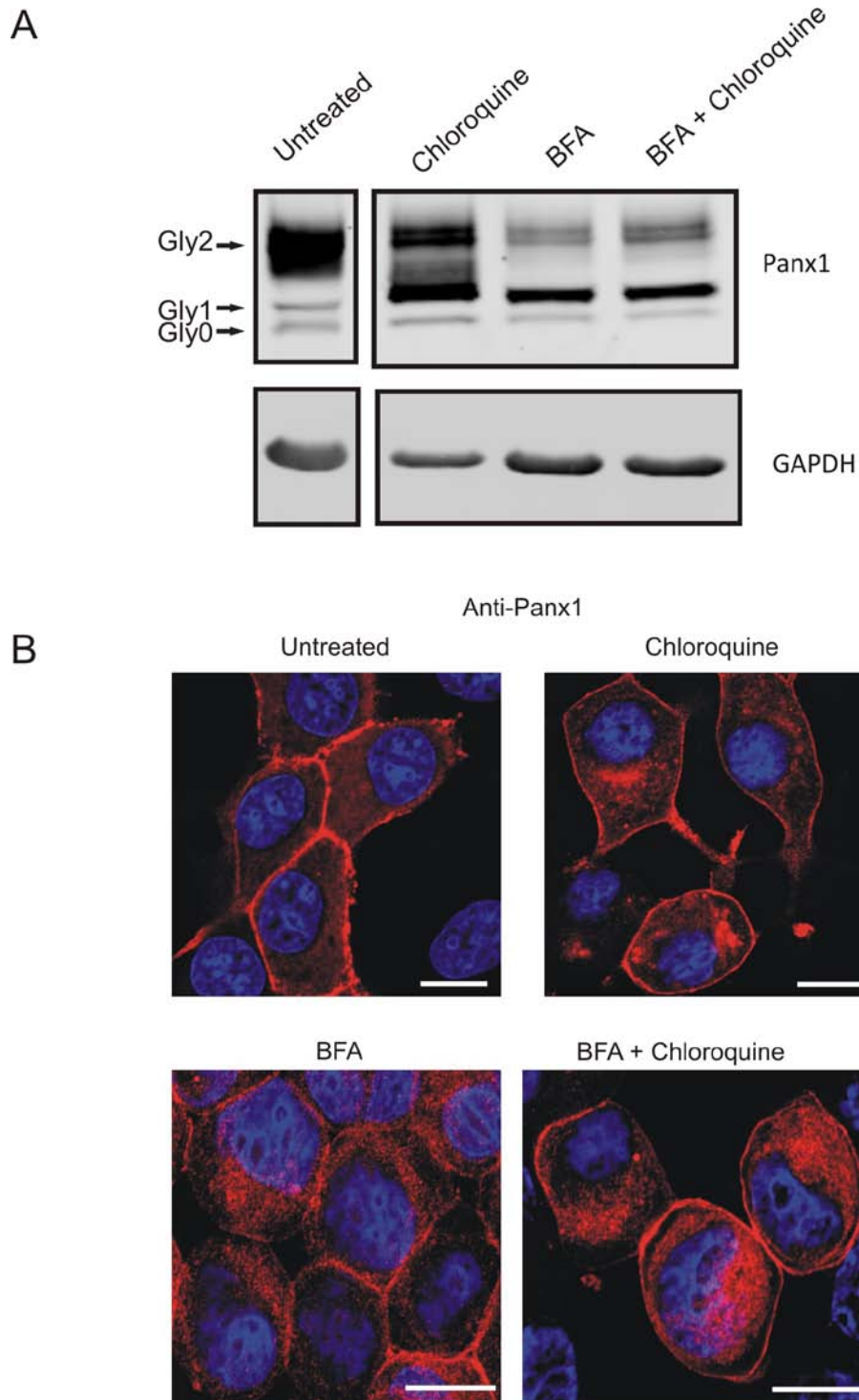
Figure 4.9 Panx1 is degraded by lysosomes

Panx1 expressing cells were exposed to BFA and the lysosomal inhibitor (chloroquine) alone or together for 20hr prior to immunoblotting (A) and

immunolabeling (B) for Panx1.   Chloroquine treatment caused a sustained expression of the Gly2 species of Panx1 with an accumulation of the Gly1 form (A) which was marked by a increased intracellular distribution of Panx1(B, red). BFA-induced reduction of the Panx1 Gly2 species (A) was correlated by the increased loss of the cell surface population of Panx1 with a subsequent accumulation in the intracellular compartment (B, red). When treated together, a subtle rescue of the Panx1 Gly2 species was observed in the presence of the lysosomal inhibitor, chloroquine (A). BFA treatment along with chloroquine also resulted in the increased cell surface distribution of Panx1 (B, red). GAPDH was used as a protein loading control. Nuclei were counterstained with Hoechst. Bar=10µm.

4.4 DISCUSSION

The focus of this study was to elucidate the turnover kinetics and mechanisms for internalization and degradation of Panx1. Our data strongly indicates that Panx1 has a long life at the cell surface, follows a unique pattern of internalization that is independent of endocytic pathways mediated by clathrin, caveolins and dynamin GTPase, and undergoes lysosomal-based degradation.

One of the distinguished characteristics of most connexin family members is that their physiological regulation is not only at the level of gating the channels open or closed [58] but also at the level of gap junction formation and removal [13]. The latter level of regulation is possible because most connexins, including Cx43, have an unprecedented short half-life for polytopic plasma membrane proteins. In this regard, our studies in which protein synthesis or trafficking were blocked by pharmacological agents revealed prolonged localization of Panx1 at the cell surface, compared to Cx43 gap junctions. Thus, indicating that Panx1 has a much longer half-life than Cx43.

While the highly phosphorylated P_2 form of Cx43 [109] is often identified at the plasma membrane, it is predominantly the complex glycosylated Gly2 form of Panx1 [47, 59] that is destined for cell surface delivery. The rapid turnover of Cx43 in response to BFA is correlated with the loss of the highly phosphorylated (P_2) species with an accumulation of the lower species (P_0) of Cx43 [109]. In our studies, a parallel phenomenon occurred where the high mannose Gly1 species of Panx1 increased at the expense of the Gly2 species. Since it was possible to rescue the trafficking of intracellular accumulated Cx43 and rebuild the normal

gap junction complement upon BFA removal [109], we wanted to follow the glycosylation status of Panx1 upon BFA washout as a measure of its recovery from intracellular retention. Interestingly, at no time following BFA removal did Panx1 levels at the cell surface return to normal, suggesting that Panx1 has delayed trafficking to the cell surface. Alternatively, it is possible that the prolonged exposure to BFA permanently impairs the reorganization of the Golgi apparatus thus limiting the rescue of the Panx1 Gly2 expression. Nonetheless, our data strongly supports the conclusion that Panx1 half-life while at the cell surface is many hours longer than what is documented for Cx43.

While the internalization mechanisms of connexins, particularly Cx43, have been extensively studied, the endocytic pathways governing Panx1 turnover have not yet been identified. Whereas, internalization of Cx43 as double membrane structures [101] termed connexosomes [13] has previously been linked to the CME pathway, while our study is the first to investigate the role of clathrin in Panx1 endocytosis. Our data indicates that although Panx1 co-distributes in the same cell surface micro-domain as clathrin, its physical interaction with the clathrin heavy chain could not be detected. Consistently, while AP2 co-distributed with Panx1 at the cell surface they also failed to interact. These finding are in contrast to other channels types such as chloride channels [185] or renal outer medullary K^+ channels (ROMK) [186], where clathrin-mediated internalization is marked by co-localization and co-interaction with clathrin and AP2. Since our study only revealed localization of Panx1 and AP2 in the same compartment without direct interaction, it is likely that Panx1 endocytosis is independent of

clathrin and thus distinct from Cx43 and other channel forming proteins. As there is growing evidence of clathrin-independent pathways for internalization of plasma membrane proteins that rely on caveolae and glycolipid rafts [187], our next approach was to identify if Panx1 turnover is mediated by caveolin-driven pathway.

Several channels such as K^+ [188], Ca^{2+} [189] and Cl^- [190] are reported to localize to glycolipid rafts/caveolae for their regulation by caveolins. Our first assessment revealed localization of Panx1 with Cav-1 and Cav-2 at the cell surface and within intracellular compartments. While the plasma membrane localization of Panx1 with Cav-1 and Cav-2 suggests the presence of Panx1 in the lipid rafts- presumably in preparation for internalization, the formaldehyde-fixed detection of Panx1 with Cav-1 and Cav-2 in the intracellular compartment argues for a distinct role. In the case of Cx43, the intracellular distribution with Cav-1 and Cav-2, suggested that caveolins might facilitate the delivery of Cx43 from the Golgi apparatus to cell surface [154]. It is possible that, like Cx43, caveolins might be involved in the secretory pathway of Panx1. Alternatively, intracellular co-distribution of caveolins with Panx1 could also reflect the role of caveolins in recycling Panx1 from the cell surface to the perinuclear region. This notion is in keeping with the previously reported caveolin-mediated internalization of the seven transmembrane receptor protein: autocrine motility factor from the plasma membrane and its targeting to the ER compartment [191, 192]. Interestingly, Cav-1 has been identified as a negative regulator of the endocytic pathway to the ER compartment, thus providing a more stabilizing role of

caveolae at the plasma membrane [187]. The reduced intracellular localization of Panx1 with Cav-1 (in comparison to Cav-2) could support the role of Cav-1 in maintaining Panx1 at the cell surface instead of its internalization-an argument that clearly needs further investigation. Our study has shown that distinct from Cx43, Panx1 does not interact with Cav-1 or Cav-2 [154]. Furthermore, the cholesterol depleting agent, MβC, known to disrupt the integrity of membrane rafts [193] and association of Cx43 with Cav-1/Cav-2 [154], did not noticeably alter the Panx1 expression or its cell surface localization. Taken together, our results suggest that turnover of Panx1 is independent of caveolin driven pathway.

As large dynamin GTPase (~100 kDa) has implications in clathrin-dependent internalization [194], and caveolar driven fission of the plasma membrane [195], we investigated if this molecular player could contribute in Panx1 endocytosis. To identify the role of dynamin GTPase in Panx1 internalization, we utilized the GTP binding and hydrolyzing mutant, K44A DynII, in the presence or absence of BFA. Although Panx1 co-distributed with K44A DynII at the cell surface, blocking of the ER-Golgi transport with BFA did not reveal a substantial accumulation of Panx1 at the cell surface. It was also interesting to observe that while K44A DynII and dynasore blocked the expected transferrin uptake, it did not significantly increase the expression of the cell surface species of Panx1. This finding differs from the previously documented accumulation of Cx43 plaques [102], and enhancement of ROMK (renal outer medullary potassium) channel currents in response to K44A DynII over-expression [186]. Thus, our data suggests that

Panx1 is internalized in a unique manner that is independent of dynamin GTPase.

Our rapid time-lapse imaging of Panx1-GFP following a long term exposure to BFA suggested that clustering of Panx1 at the cell surface is a pre-requisite for its turnover. Within several minutes, dynamic tubular-like extensions carrying Panx1 pinched off. This pattern of Panx1 internalization was quite distinct from the rapid internalization of the double membrane structure of Cx43 that bud from preexisting gap junction plaques, and enter one of the two neighboring cells [101]. The tubular morphology of Panx1 extensions is quite intriguing and hints to the possibility of its internalization via pathways independent of clathrin, caveolin and dynamin GTPase. Glycosyl-phosphatidyl-inositol anchored proteins enriched early endosomal compartments (GEECs) is one such example that results from fusion of uncoated tubulovesicular clathrin-independent carriers (CLICs) directly stemming from the plasma membrane [196]. Another feature of the CLICs/GEECs endocytic pathway is its independence from dynamin [197] and dependence on actin polymerization machinery that is regulated by the Rho family GTPase, Cdc42 [198]. As one of the documented binding partners of Panx1 [153], it is possible that actin might regulate the endocytic process of Panx1. One of the proposed models for actin-dependent endocytosis is the elongation of plasma membrane invaginates into a tubular structure through active polymerization, followed by scission via myosin motor proteins [199, 200]. Such association of actin and myosin II has been reported for endocytosis of Cx43 double membrane structures (e.g. connexosomes) [201], and needs to be

further investigated in the case of Panx1. Another candidate that has been linked to actin remodeling is endosomal-associated GTPase, ADP, ribosylation factor 6 (Arf6) [202, 203]. The Arf6-mediated pathway is not only independent of dynamin and clathrin [204] but is also implicated in the endocytosis and recycling of K^+ channels [205]. Interestingly, the Arf6 dependent pathway also includes the formation of tube-like structures that are eventually used for recycling the cargo back to the plasma membrane [206]. Although the Arf6 pathway needs further investigation, it is tempting to speculate that the observed collapse of Panx1-GFP tubules back onto the plasma membrane might take advantage of this mechanism.

Once internalized, degradation of Cx43 is linked to both lysosomal [106] and proteasomal pathways [171], while consistent with the previous report, our current study suggests a role of lysosomes in Panx1 degradation [47]. In our studies, while BFA blocked the cell surface trafficking of Panx1, consistent with increased Gly1 levels, it did not interrupt Panx1 turnover from the cell surface, as revealed by the loss of the Gly2 species. Surprisingly, chloroquine induced a robust increase in the Panx1 Gly1 species, which correlated with Panx1 localizing to the perinuclear region. It is possible that long term blockage of lysosomal function initiated a negative-feedback mechanism causing Panx1 to bypass normal targeting to the cell surface trafficking and direct trafficking to lysosomes. Collectively, the sustained expression of the Gly2 species in the presence of chloroquine, together with a subtle rescue of the BFA-induced loss

of the Gly2 species, supports that Panx1 typically cycles through the plasma membrane en route to lysosomes for final degradation.

In summary, since Panx1 forms large pore channels implicated in: neuronal necrosis [78], epileptic seizure-like activity [66] and initiation of the death complex with the P2X7 receptor [72], our study was designed to characterize mechanisms related to Panx1 turnover and degradation as potential regulatory mechanisms of overall Panx1 function. Our study is the first to show that the turnover of Panx1 is slow and is mediated via unique tubular-like extensions.

4.5 ACKNOWLEDGEMENTS

CHAPTER 5: DISCUSSION and CONCLUSIONS

5.1 DISCUSSIONS and CONCLUSIONS

Objective 1: To characterize the subcellular distribution of Panx1 and Panx3, to identify the secretory pathway involved in Panx1 and Panx3 cell surface trafficking, to analyze the mobility dynamics of GFP-tagged Panx1 and Panx3 at the cell surface and to assess the role of the cytoskeleton in Panx1 trafficking and cell surface dynamics.

Our study was the first to reveal that ectopically expressed Panx1 and Panx3 trafficked to the cell surface via the ER-Golgi in a Sar1-mediated COPII-dependent manner [153]. Once at the plasma membrane both pannexin members predominantly localized in a relatively uniform manner, as well as in dynamic cell surface protrusions [153]. Distinct from Cx43 [96], Panx1 and Panx3 were highly mobile at all plasma membrane domains [153]. In addition, Panx1 and Panx3 revealed no interdependency on microtubules for their cell surface delivery or mobility [153], as reported for Cx43 [88]. Interestingly, intact microfilaments facilitated the free movement of Panx1 carrying vesicles and provided overall stability at the cell surface [153]. This study also identified actin as a novel direct binding partner of Panx1 at the carboxyl terminal tail [153].

Objective 2: To identify the role of the carboxyl terminal tail in Panx1 trafficking and homomeric interactions.

To investigate the role of the carboxyl terminal tail (C-tail) of Panx1 in trafficking and homomeric interactions, we truncated the polypeptide at residue 307 (Panx1^{T307}) and ectopically expressed the mutant in BICR-M1R$_k$ and HEK-293T, cells devoid of Panx1. Truncation of the Panx1 C-tail dysregulated its cell surface delivery resulting in the mutant being retained predominantly in the ER.

Furthermore, enzyme-based de-glycosylation experiments revealed that the Panx1^{T307} mutant was glycosylated, albeit, to only the high mannose species. Interestingly, co-expression of Panx1 could not rescue the delivery of the Panx1^{T307} mutant to the cell surface and these species had limited co-interaction. Thus, these results suggest that the Panx1 C-tail plays a role in oligomerization. While our study fully supports the previously reported lysosomal-mediated degradation of full length Panx1 [47], our data also supports proteasomal-based degradation of mutant Panx1.

Objective 3: To explore the pathways for Panx1 internalization and degradation.

Using the pharmacological inhibitors of protein synthesis (cycloheximide) and protein trafficking (BFA), we discovered that Panx1 had a much longer predicted half-life compared to Cx43 [25]. To uncover the mechanism(s) responsible for Panx1 internalization, this study focused on determining the putative involvement of clathrin-, caveolin- and dynamin- mediated pathways. Although co-distribution of Panx1 with clathrin and adapter protein (AP2) was observed at the cell surface, no interaction was detected. This suggested that clathrin-mediated internalization may not play a role in Panx1 internalization. Similarly, Panx1 also co-distributed with caveolin (Cav)-1 and Cav-2 at the cell surface as well as within intracellular compartments. However, co-immunoprecipitation assays together with methyl-β cyclodextrin-induced disruption of membrane rafts supported the position that Panx1 internalization was independent of caveolins. Inhibition of dynamin (DynII) GTPase (characterized in budding off membrane-bound vesicles) by a dominant-negative GTP hydrolyzing mutant, K44A DynII

and the pharmacological inhibitor, dynasore, further revealed that Panx1 turnover was independent of dynamin. Interestingly, rapid time lapse imaging revealed a novel internalization pattern of Panx1 along dynamic tubular extensions. Although Panx1 degradation through the lysosomal pathway was previously reported [47], we found that the high mannose species of Panx1 is accumulated in the presence of the chloroquine-mediated inhibition of lysosomes. This finding was also correlated with increased perinuclear Panx1 distribution and sustained cell surface localization of Panx1. While Cx43 gets degraded through both lysosomal and proteasomal pathways [105], our study strongly supports the premise of Panx1 degradation through lysosomes.

5.2 CONTRIBUTIONS of the RESEARCH

Prior to this study, the dynamics, regulatory binding partners, pathways and compartments involved during the life-cycle of pannexins were essential unknown. The overall goal of this study was to investigate if pannexins share similar properties to Cx43 gap junctions based on their trafficking, mobility, turnover and degradation characteristics. These studies were the first in the field to combine GFP tagging and rapid time-lapse imaging to closely monitor and address the dynamic properties of pannexins in live mammalian cells. In these studies we showed that except for sharing a common secretory pathway, Panx1 and Panx3 are quite distinct from Cx43. Basically, Panx1 and/or Panx3 exhibited a: a) relatively uniform cell surface distribution, b) extensive and rapid mobility at the cell surface, c) prolonged turnover kinetics, and d) unique internalization

properties within dynamic tubular extensions that were independent of pathways mediated by clathrin, AP-2, Cav-1, Cav-2 and DynII.

5.2.1 Compared to Cx43, Panx1 and Panx3 exhibit distinct subcellular distribution properties, cell surface dynamics and cytoskeletal dependency

While an uniform cell surface distribution of Panx1 and Panx3 is the predominant phenotype observed when these pannexins are expressed in reference cell models, additional studies have highlighted other subcellular distribution profiles that include diffused localization throughout the cell body and punctate cell surface localization [36, 59, 125, 153]. Endogenously expressed Panx1 revealed three distinct profiles: a) the relatively uniform cell surface pattern at the cell surface of melanoma cells (B16-BL6) [153], and Madin-Darby canine kidney cells [47], b) a cell surface punctate pattern as observed in: human facial epidermis [25] and Hensen, Claudius and Boettcher cells of the rat cochlea [36], and c) diffused cell body localization as seen in an mouse osteoblast cell line (MC3T3-E1) [125], spiral limbus and spiral prominence in the rat cochlear lateral wall [36], and murine spleen [25]. Whereas endogenous expression of Panx3 was found to be within intracellular compartments in rat cochlear bone [36], mixed patterns of localization were found both at the cell surface and cytoplasmic localization in murine chondrocytes and chondrogenic cell lines (ATDC5) [37]. The differential distribution profiles of Panx1 and Panx3 suggest that they may have distinct cellular roles. While the uniform cell surface distribution of Panx1 supports the function of cellular communication with the extracellular environment -through formation of non-junctional membrane

channels [25, 55], the intracellular localization of pannexins suggests that they serve alternate roles. In the study conducted by Vanden Abeele et. al., [54], intracellular localized Panx1 was proposed to regulate ER-based calcium homeostasis. However, later we showed that Panx1 dysregulated keratinocyte differentiation while Panx3 maintained the epidermal integrity of murine skin [67]. In addition, our current study revealed a unique enrichment of Panx1 and Panx3 in dynamic cell surface protrusions, at areas that are devoid of contacting cells [153]. While similar distribution of Panx3 in cellular extensions supported its role in ATP release and chondrogenic differentiation [37], this phenomenon was not typically observed for Cx43, unless non-functional Cx43 mutant was ectopically expressed [96]. Collectively, these results support our hypothesis that the pannexin family of proteins exhibits a more diverse subcellular localization than connexins, broadening their potential cellular roles.

The cell surface clustering of Cx43 and the relatively uniform distribution of Panx1 and Panx3 [153] also supports that these families of proteins acquire different states of assembly. In fact, the rapid lateral movement of Panx1 and Panx3 in all plasma membrane microdomains [153], suggests that pannexins are likely not packaged into dense crystalline-like structures, as reported for Cx43 [39]. Pannexin channel packing and cell-cell interactions may be inhibited by steric hindrance provided by the bulky carbohydrate moieties at the extracellular domain, prohibiting the close proximity of the two adjacent cells. Electron micrographs of Panx1 at the cell surface depicting 20-50 nm of intercellular spacing, as opposed to 2-4 nm for Cx43 [47], further supports this notion. The

greater mobile fraction of Panx1 and Panx3 in comparison to Cx43 [153], could also suggest less interactions with scaffolding proteins and cytoskeletal elements.

 In our study, nocodazole-induced disruption of microtubules did not significantly alter the cell surface distribution of Panx1 and Panx3 [153]. However, this finding was quite distinct from Cx43, where the regeneration of gap junction plaques and cell surface mobility was minimal upon nocodazole exposure [88, 89], suggesting that the delivery of Cx43 was much more dependent on microtubules, as compared to Panx1 and Panx3. On the other hand, disruption of microfilaments revealed concomitant intracellular accumulation of Panx1 and Panx3 leaving only a subpopulation at the cell surface. In contrast, Cx43 gap junctions remain relatively more independent to the assembly states of microfilaments [141], thereby suggesting that the connexin and pannexin family of proteins have distinct dependency on cytoskeletal elements for their cell surface transport, mobility and stability.

5.2.2 The carboxyl terminal tail of Panx1 facilitates its trafficking and homomeric interaction

Several studies have identified the effect of single amino acid substitutions within specific motifs of Panx1 [25, 47, 63, 151, 152], however, deletion of an entire Panx1 domain has never been investigated. We were particularly keen on identifying the role of the C-tail, as this cytoplasmic exposed domain was considered a prime candidate for interaction with other regulatory proteins. In fact, our work identified that Panx1 C-tail serves as a substrate for direct binding

with actin that may provide multifaceted functions in Panx 1 transport, cell surface mobility and stability [153].

Using a truncated mutant of Panx1 lacking the last 119 amino acids from the C-tail, our study suggested that the C-tail was important in trafficking, homomeric interactions and targeted degradation through lysosomes. First, we identified that in the absence of the C-tail, Panx1 mutant failed to traffic to the cell surface. Second, the Panx1 C-tail truncated mutant was retained primarily within the ER where it was found as a core (Gly0) or high-mannose (Gly 1) species. Third, the Panx1 C-tail mutant failed to substantially interact with the full length Panx1, suggesting a role of the C-tail in homomeric oligomerization. Finally, the ER-retained truncated mutant was directed to proteasomes for degradation, thus supporting the involvement of the endoplasmic reticulum associated degradation (ERAD) pathway. Since ERAD is associated with premature degradation of misfolded proteins [159, 165], we speculate that the C-terminus may also play an important role in the proper folding of Panx1.

5.2.3 Distinct from Cx43, Panx1 exhibits a longer half-life and internalizes via unique tubular-like extensions

In these studies, we showed that the internalization of the cell surface pool of Panx1 exceeds the 1.5-3 hrs of Cx43 turnover [25] with an estimated half-life in excess of 10 hours. While removal of Cx43 from the cell surface involved internalization of the entire or fragments of gap junctions as connexosomes [13] into one of the two contacting cells [101], the removal of Panx1 form the cell surface appeared to follow tubular extensions. Mechanistically, rapid Cx43

internalization was aided by several molecular players such as: dynamin, clathrin, AP-2, actin and myosin [102, 104, 201]. However, the internalization of Panx1 as noted in our study was independent of clathrin, AP-2, dynamin and caveolin-driven pathways. Given the direct association of the Panx1 C-tail with microfilaments, it is possible that the internalization of Panx1 might be actin-mediated. Our studies also supported the lysosomal degradation of internalized Panx1. Since Panx1 channel function is linked to neuronal necrosis, epileptic seizures-like activity and activation of death complex of P2X7 receptor [66, 72, 78], our study provides a means of regulating the channel function by processes of internalization and degradation.

5.3 LIMITATIONS and FUTURE DIRECTIONS

5.3.1 Limitations

In order to identify the dynamic properties of pannexins in live cells, we tagged Panx1 and Panx3 with GFP. Although, Panx1-GFP revealed trafficking and localization pattern similar to its wild-type (WT) counterpart, the GFP tagging of Panx3 caused a severe trafficking defect [25] with only a trace amount available at the cell surface. This posed a limitation in collecting quantifiable data for Panx3 mobility at distinct microdomains of plasma membrane. To overcome this setback, we co-transfected the untagged Panx3, as it facilitated the adequate delivery of Panx3-GFP to the cell surface for assessment of the mobile fraction. The comparable percentage (40-50%) of mobile fractions of Panx3-GFP (co-expressed with Panx3) and Panx1-GFP (co-expressed with Panx1) further

suggested that co-expression with the WT counterpart does not hinder the mobility of pannexin family members at the plasma membrane.

In addition, while tagging of Panx1 C-tail truncated mutant with RFP identified its role in trafficking, we were unable to parallel our findings using the untagged counterpart due to the lack of a quality antibody. It was expected that our previously generated antibodies against Panx1 extracellular domain [59], would serve as a tool to detect the C-tail truncated mutant of Panx1; however, our antibody detection was deemed to be inadequate. Therefore, to control for any possible adverse effects of the RFP tag, we also tagged the full length Panx1 with RFP to be used in comparative studies. Since RFP tagging of full length Panx1 exhibited similar distribution characteristics as the untagged counterpart, it was employed as a control to study the biological properties of the Panx1 C-tail.

5.3.2 Future Directions

Based on our studies, it is clear that pannexins are a distinct family of proteins, as compared to connexins. Part of this distinction may arise from differential regulation, based on protein-protein interactions. While Panx1 was identified to directly interact with actin, it remains to be investigated which motif within the Panx1 C-tail binds to actin. Consistent with other reports [207, 208], one possible approach for identifying the actin binding site within Panx1 is by using serial truncations of the C-tail. In addition, it would be interesting to determine if Panx3 also interacts with actin, as its cell surface localization is also perturbed in response to disrupted microfilaments [153]. Although our studies identified a role of microfilaments and microtubules in the plasma membrane distribution of

Panx3, it has yet to be examined if these cytoskeletal elements play a role in the cell surface mobility of Panx3.

It has been postulated that the overall cellular function of pannexins can be regulated, in part, by appropriate trafficking and turnover to/from the plasma membrane. While deletion of almost the entire Panx1 C-tail provided evidence for its role in the cell surface trafficking, future research should focus on determine if there are any targeting motifs within the C-tail that regulate Panx1 trafficking. In addition, investigating the role of the C-tail should also be extended to Panx3. Our studies also suggest that Panx1 is a long-lived protein; however, it remains to be determined if Panx3 also exhibits a prolonged half-life. While Panx1 internalization was associated with unique tubular-like extensions budding away from plasma membrane, the underlying mechanism remains unclear. Since the endocytosis of Panx1 was found to be independent of clathrin, AP-2, dynamin and caveolin-driven pathways, we speculate that the Panx1 binding protein, actin might play a role in its internalization. One of the proposed models of actin-mediated internalization is the elongation of plasma membrane invaginates into a tubular structure through active polymerization, followed by scission via myosin motor proteins [199, 200]. Since such association of actin and myosin II has also been reported for endocytosis of Cx43 as connexosomes [201], future studies should pursue this hypothesis to investigate how Panx1 is internalized via tubular extensions.

In summary, our studies support the hypothesis that in comparison to Cx43, Panx1 and Panx3 exhibit distinct subcellular distributions, cell surface mobilities,

and cytoskeletal dependencies, while Panx1 possesses unique turnover dynamics, and mechanistic pathways leading to its internalization and degradation.

6.0 REFERENCES

1. Panchin, Y., I. Kelmanson, M. Matz, K. Lukyanov, N. Usman, and S. Lukyanov, *A ubiquitous family of putative gap junction molecules.* Current Biology, 2000. **10**(13): p. R473-R474.

2. Yen, M.R. and M.H. Saier, Jr., *Gap junctional proteins of animals: the innexin/pannexin superfamily.* Prog Biophys Mol Biol, 2007. **94**(1-2): p. 5-14.

3. Bruzzone, R., T.W. White, and D.L. Paul, *Connections with connexins: the molecular basis of direct intercellular signaling. [Review] [535 refs].* Eur. J. Biochem., 1996. **238**(1): p. 1-27.

4. Goodenough, D.A., J.A. Goliger, and D.L. Paul, *Connexins, connexons, and intercellular communication.* Annu. Rev. Biochem., 1996. **65**: p. 475-502.

5. Kumar, N.M. and N.B. Gilula, *The gap junction communication channel.* Cell, 1996. **84**(3): p. 381-8.

6. Constantin, B. and L. Cronier, *Involvement of gap junctional communication in myogenesis.* Int Rev Cytol, 2000. **196**: p. 1-65.

7. El-Sabban, M.E., L.F. Abi-Mosleh, and R.S. Talhouk, *Developmental regulation of gap junctions and their role in mammary epithelial cell differentiation.* J Mammary Gland Biol Neoplasia, 2003. **8**(4): p. 463-73.

8. Nishimura, T., C. Dunk, Y. Lu, X. Feng, A. Gellhaus, E. Winterhager, J. Rossant, and S.J. Lye, *Gap junctions are required for trophoblast proliferation in early human placental development.* Placenta, 2004. **25**(7): p. 595-607.

9. Dewey, M.M. and L. Barr, *Intercellular Connection between Smooth Muscle Cells: the Nexus.* Science, 1962. **137**(3531): p. 670-2.

10. Makowski, L., D.L. Caspar, W.C. Phillips, and D.A. Goodenough, *Gap junction structures. II. Analysis of the x-ray diffraction data.* J Cell Biol, 1977. **74**(2): p. 629-45.

11. Kumar, N.M. and N.B. Gilula, *Cloning and characterization of human and rat liver cDNAs coding for a gap junction protein.* J Cell Biol, 1986. **103**(3): p. 767-76.

12. Paul, D.L., *Molecular cloning of cDNA for rat liver gap junction protein.* J Cell Biol, 1986. **103**(1): p. 123-34.

13. Laird, D.W., *Life cycle of connexins in health and disease.* Biochem. J., 2006. **394**(Pt 3): p. 527-43.

14. Sasakura, Y., L. Yamada, N. Takatori, Y. Satou, and N. Satoh, *A genomewide survey of developmentally relevant genes in Ciona intestinalis. VII. Molecules involved in the regulation of cell polarity and actin dynamics.* Dev Genes Evol, 2003. **213**(5-6): p. 273-83.

15. Phelan, P., J.P. Bacon, J.A. Davies, L.A. Stebbings, M.G. Todman, L. Avery, R.A. Baines, T.M. Barnes, C. Ford, S. Hekimi, R. Lee, J.E. Shaw, T.A. Starich, K.D. Curtin, Y.A. Sun, and R.J. Wyman, *Innexins: a family of invertebrate gap-junction proteins.* Trends Genet, 1998. **14**(9): p. 348-9.

16. Barnes, T.M., *OPUS: a growing family of gap junction proteins?* Trends Genet, 1994. **10**(9): p. 303-5.

17. Krishnan, S.N., E. Frei, G.P. Swain, and R.J. Wyman, *Passover: a gene required for synaptic connectivity in the giant fiber system of Drosophila.* Cell, 1993. **73**(5): p. 967-77.

18. Phelan, P., L.A. Stebbings, R.A. Baines, J.P. Bacon, J.A. Davies, and C. Ford, *Drosophila Shaking-B protein forms gap junctions in paired Xenopus oocytes.* Nature, 1998. **391**(6663): p. 181-4.

19. Starich, T.A., R.K. Herman, and J.E. Shaw, *Molecular and genetic analysis of unc-7, a Caenorhabditis elegans gene required for coordinated locomotion.* Genetics, 1993. **133**(3): p. 527-41.

20. Watanabe, T. and D.R. Kankel, *The l(1)ogre gene of Drosophila melanogaster is expressed in postembryonic neuroblasts.* Dev Biol, 1992. **152**(1): p. 172-83.

21. Baranova, A., D. Ivanov, N. Petrash, A. Pestova, M. Skoblov, I. Kelmanson, D. Shagin, S. Nazarenko, E. Geraymovych, O. Litvin, A. Tiunova, T.L. Born, N. Usman, D. Staroverov, S. Lukyanov, and Y. Panchin, *The mammalian pannexin family is homologous to the invertebrate innexin gap junction proteins.* Genomics, 2004. **83**(4): p. 706-16.

22. Holland, L.Z. and J.J. Gibson-Brown, *The Ciona intestinalis genome: when the constraints are off.* Bioessays, 2003. **25**(6): p. 529-32.

23. Alexopoulos, H., A. Bottger, S. Fischer, A. Levin, A. Wolf, T. Fujisawa, S. Hayakawa, T. Gojobori, J.A. Davies, C.N. David, and J.P. Bacon, *Evolution of gap junctions: the missing link?* Curr Biol, 2004. **14**(20): p. R879-80.

24. Shestopalov, V.I. and Y. Panchin, *Pannexins and gap junction protein diversity.* Cell. Mol. Life Sci., 2008. **65**(3): p. 376-394.

25.   Penuela, S., R. Bhalla, X.-Q. Gong, K.N. Cowan, S.J. Celetti, B.J. Cowan, D. Bai, Q. Shao, and D.W. Laird, *Pannexin 1 and pannexin 3 are glycoproteins that exhibit many distinct characteristics from the connexin family of gap junction proteins.* J. Cell Sci., 2007. **120**(21): p. 3772-3783.

26.   Bruzzone, R., S.G. Hormuzdi, M.T. Barbe, A. Herb, and H. Monyer, *Pannexins, a family of gap junction proteins expressed in brain.* Proc. Natl. Acad. Sci. U S A, 2003. **100**(23): p. 13644-9.

27.   Dvoriantchikova, G., D. Ivanov, Y. Panchin, and V.I. Shestopalov, *Expression of pannexin family of proteins in the retina.* FEBS Lett., 2006a. **580**(9): p. 2178-82.

28.   Dvoriantchikova, G., D. Ivanov, A. Pestova, and V. Shestopalov, *Molecular characterization of pannexins in the lens.* Mol. Vis., 2006b. **12**: p. 1417-26.

29.   Ray, A., G. Zoidl, P. Wahle, and R. Dermietzel, *Pannexin expression in the cerebellum.* Cerebellum, 2006. **5**(3): p. 189-192.

30.   Ray, A., G. Zoidl, S. Weickert, P. Wahle, and R. Dermietzel, *Site-specific and developmental expression of pannexin1 in the mouse nervous system.* Eur. J. Neurosci., 2005. **21**(12): p. 3277-3290.

31.   Sohl, G., S. Maxeiner, and K. Willecke, *Expression and functions of neuronal gap junctions.* Nat. Rev. Neurosci., 2005. **6**(3): p. 191-200.

32.   Vogt, A., S.G. Hormuzdi, and H. Monyer, *Pannexin1 and Pannexin2 expression in the developing and mature rat brain.* Mol. Brain Res., 2005. **141**(1): p. 113-120.

33.   Weickert, S., A. Ray, G. Zoidl, and R. Dermietzel, *Expression of neural connexins and pannexin1 in the hippocampus and inferior olive: a quantitative approach.* Molecular Brain Res., 2005. **133**(1): p. 102-109.

34.   Zappala, A., D. Cicero, M.F. Serapide, C. Paz, M.V. Catania, M. Falchi, R. Parenti, M.R. Panto, F. La Delia, and F. Cicirata, *Expression of pannexin1 in the CNS of adult mouse: Cellular localization and effect of 4-aminopyridine-induced seizures.* Neuroscience, 2006. **141**(1): p. 167-178.

35.   Zoidl, G., E. Petrasch-Parwez, A. Ray, C. Meier, S. Bunse, H.-W. Habbes, G. Dahl, and R. Dermietzel, *Localization of the pannexin1 protein at postsynaptic sites in the cerebral cortex and hippocampus.* Neuroscience, 2007. **146**(1): p. 9-16.

36.   Wang, X.-H., M. Streeter, Y.-P. Liu, and H.-B. Zhao, *Identification and characterization of pannexin expression in the mammalian cochlea.* The Journal of Comparative Neurology, 2009. **512**(3): p. 336-346.

37.	Iwamoto, T., T. Nakamura, A. Doyle, M. Ishikawa, S. de Vega, S. Fukumoto, and Y. Yamada, *Pannexin 3 regulates intracellular ATP/cAMP levels and promotes chondrocyte differentiation.* J Biol Chem, 2010. **285**(24): p. 18948-58.

38.	Bauer, R., B. Loer, K. Ostrowski, J. Martini, A. Weimbs, H. Lechner, and M. Hoch, *Intercellular communication: the Drosophila innexin multiprotein family of gap junction proteins.* Chem Biol, 2005. **12**(5): p. 515-26.

39.	Unger, V.M., N.M. Kumar, N.B. Gilula, and M. Yeager, *Electron cryo-crystallography of a recombinant cardiac gap junction channel.* Novartis Found Symp, 1999. **219**: p. 22-30; discussion 31-43.

40.	Iovine, M.K., A.M. Gumpert, M.M. Falk, and T.C. Mendelson, *Cx23, a connexin with only four extracellular-loop cysteines, forms functional gap junction channels and hemichannels.* FEBS Lett, 2008. **582**(2): p. 165-70.

41.	Foote, C.I., L. Zhou, X. Zhu, and B.J. Nicholson, *The pattern of disulfide linkages in the extracellular loop regions of connexin 32 suggests a model for the docking interface of gap junctions.* J Cell Biol, 1998. **140**(5): p. 1187-97.

42.	Herve, J.-C., P. Phelan, R. Bruzzone, and T.W. White, *Connexins, innexins and pannexins: Bridging the communication gap.* Biochimica et Biophysica Acta (BBA) - Biomembranes

The Connexins Part III, 2005. **1719**(1-2): p. 3-5.

43.	Evans, W.H. and P.E. Martin, *Gap junctions: structure and function (Review).* Mol Membr Biol, 2002. **19**(2): p. 121-36.

44.	Giepmans, B.N., I. Verlaan, T. Hengeveld, H. Janssen, J. Calafat, M.M. Falk, and W.H. Moolenaar, *Gap junction protein connexin-43 interacts directly with microtubules.* Curr Biol, 2001. **11**(17): p. 1364-8.

45.	Maass, K., J. Shibayama, S.E. Chase, K. Willecke, and M. Delmar, *C-terminal truncation of connexin43 changes number, size, and localization of cardiac gap junction plaques.* Circ Res, 2007. **101**(12): p. 1283-91.

46.	Moreno, A.P., M. Chanson, S. Elenes, J. Anumonwo, I. Scerri, H. Gu, S.M. Taffet, and M. Delmar, *Role of the carboxyl terminal of connexin43 in transjunctional fast voltage gating.* Circ Res, 2002. **90**(4): p. 450-7.

47.	Boassa, D., C. Ambrosi, F. Qiu, G. Dahl, G. Gaietta, and G. Sosinsky, *Pannexin1 channels contain a glycosylation site that targets the hexamer to the plasma membrane.* J. Biol. Chem., 2007. **282**: p. 31733-43.

48.   Ambrosi, C., O. Gassmann, J.N. Pranskevich, D. Boassa, A. Smock, J. Wang, G. Dahl, C. Steinem, and G.E. Sosinsky, *Pannexin1 and Pannexin2 channels show quaternary similarities to connexons and different oligomerization numbers from each other.* J Biol Chem, 2010. **285**(32): p. 24420-31.

49.   Pelegrin, P. and A. Surprenant, *Pannexin-1 mediates large pore formation and interleukin-1beta release by the ATP-gated P2X7 receptor.* EMBO J., 2006. **25**(21): p. 5071-82.

50.   Dahl, G. and S. Locovei, *Pannexin: to gap or not to gap, is that a question?* IUBMB Life, 2006. **58**(7): p. 409-19.

51.   Bruzzone, R., M.T. Barbe, N.J. Jakob, and H. Monyer, *Pharmacological properties of homomeric and heteromeric pannexin hemichannels expressed in Xenopus oocytes.* J. Neurochem., 2005. **92**(5): p. 1033-43.

52.   Bruzzone, R. and R. Dermietzel, *Structure and function of gap junctions in the developing brain.* Cell Tissue Res., 2006. **26**(2): p. 239-48.

53.   Lai, C.P.K., J.F. Bechberger, R.J. Thompson, B.A. MacVicar, R. Bruzzone, and C.C. Naus, *Tumor-Suppressive Effects of Pannexin 1 in C6 Glioma Cells.* Cancer Res., 2007. **67**(4): p. 1545-1554.

54.   Vanden Abeele, F., G. Bidaux, D. Gordienko, B. Beck, Y.V. Panchin, A.V. Baranova, D.V. Ivanov, R. Skryma, and N. Prevarskaya, *Functional implications of calcium permeability of the channel formed by pannexin 1.* J. Cell Biol., 2006. **174**(4): p. 535-46.

55.   Locovei, S., L. Bao, and G. Dahl, *Pannexin 1 in erythrocytes: function without a gap.* Proc. Natl. Acad. Sci. U S A, 2006. **103**(20): p. 7655-9.

56.   Huang, Y., J.B. Grinspan, C.K. Abrams, and S.S. Scherer, *Pannexin1 is expressed by neurons and glia but does not form functional gap junctions.* Glia, 2007a. **55**(1): p. 46-56.

57.   Bao, L., S. Locovei, and G. Dahl, *Pannexin membrane channels are mechanosensitive conduits for ATP.* FEBS Lett., 2004. **572**(1-3): p. 65-8.

58.   Saez, J.C., M.A. Retamal, D. Basilio, F.F. Bukauskas, and M.V. Bennett, *Connexin-based gap junction hemichannels: gating mechanisms.* Biochim Biophys Acta, 2005. **1711**(2): p. 215-24.

59.   Penuela, S., R. Bhalla, K. Nag, and D.W. Laird, *Glycosylation Regulates Pannexin Intermixing and Cellular Localization.* Mol Biol Cell, 2009. **20**(20): p. 4313-4323.

60. Locovei, S., J. Wang, and G. Dahl, *Activation of pannexin 1 channels by ATP through P2Y receptors and by cytoplasmic calcium.* FEBS Lett., 2006. **580**(1): p. 239-44.

61. Reigada, D., W. Lu, M. Zhang, and C.H. Mitchell, *Elevated pressure triggers a physiological release of ATP from the retina: Possible role for pannexin hemichannels.* Neuroscience, 2008. **157**(2): p. 396-404.

62. Schenk, U., A.M. Westendorf, E. Radaelli, A. Casati, M. Ferro, M. Fumagalli, C. Verderio, J. Buer, E. Scanziani, and F. Grassi, *Purinergic control of T cell activation by ATP released through pannexin-1 hemichannels.* Sci Signal, 2008. **1**(39): p. ra6.

63. Qiu, F. and G. Dahl, *A permeant regulating its permeation pore: inhibition of pannexin 1 channels by ATP.* Am J Physiol Cell Physiol, 2009. **296**(2): p. C250-255.

64. Wang, J., M. Ma, S. Locovei, R.W. Keane, and G. Dahl, *Modulation of membrane channel currents by gap junction protein mimetic peptides: size matters.* Am J Physiol Cell Physiol, 2007. **293**(3): p. C1112-9.

65. Dando, R. and S.D. Roper, *Cell-to-cell communication in intact taste buds through ATP signalling from pannexin 1 gap junction hemichannels.* J Physiol, 2009. **587**(Pt 24): p. 5899-906.

66. Thompson, R.J., M.F. Jackson, M.E. Olah, R.L. Rungta, D.J. Hines, M.A. Beazely, J.F. MacDonald, and B.A. MacVicar, *Activation of pannexin-1 hemichannels augments aberrant bursting in the hippocampus.* Science, 2008. **322**(5907): p. 1555-1559.

67. Celetti, S.J., K.N. Cowan, S. Penuela, Q. Shao, J. Churko, and D.W. Laird, *Implications of pannexin 1 and pannexin 3 for keratinocyte differentiation.* J Cell Sci, 2010. **123**(Pt 8): p. 1363-72.

68. Bennett, M.V. and R.S. Zukin, *Electrical coupling and neuronal synchronization in the Mammalian brain.* Neuron, 2004. **41**(4): p. 495-511.

69. Berridge, M.J., M.D. Bootman, and H.L. Roderick, *Calcium signalling: dynamics, homeostasis and remodelling.* Nat Rev Mol Cell Biol, 2003. **4**(7): p. 517-29.

70. Scemes, E., D.C. Spray, and P. Meda, *Connexins, pannexins, innexins: novel roles of "hemi-channels".* Pflugers Arch, 2009. **457**(6): p. 1207-26.

71. Barbe, M.T., H. Monyer, and R. Bruzzone, *Cell-cell communication beyond connexins: the pannexin channels.* Physiology (Bethesda), 2006. **21**: p. 103-14.

72. Locovei, S., E. Scemes, F. Qiu, D.C. Spray, and G. Dahl, *Pannexin1 is part of the pore forming unit of the P2X7 receptor death complex.* FEBS Lett., 2007. **581**(3): p. 483-488.

73. Bergfeld, G.R. and T. Forrester, *Release of ATP from human erythrocytes in response to a brief period of hypoxia and hypercapnia.* Cardiovasc Res, 1992. **26**(1): p. 40-7.

74. Huang, Y.-J., Y. Maruyama, G. Dvoryanchikov, E. Pereira, N. Chaudhari, and S.D. Roper, *The role of pannexin 1 hemichannels in ATP release and cell-cell communication in mouse taste buds.* Proc. Natl. Acad. Sci. U S A, 2007b. **104**(15): p. 6436-6441.

75. Ransford, G.A., N. Fregien, F. Qiu, G. Dahl, G.E. Conner, and M. Salathe, *Pannexin 1 Contributes to ATP Release in Airway Epithelia.* Am. J. Respir. Cell Mol. Biol., 2009. **41**(5): p. 525-534.

76. Kanneganti, T.D., M. Lamkanfi, Y.G. Kim, G. Chen, J.H. Park, L. Franchi, P. Vandenabeele, and G. Nunez, *Pannexin-1-mediated recognition of bacterial molecules activates the cryopyrin inflammasome independent of Toll-like receptor signaling.* Immunity, 2007. **26**(4): p. 433-43.

77. Silverman, W.R., J.P. De Rivero Vaccari, S. Locovei, F. Qiu, S.K. Carlsson, E. Scemes, R.W. Keane, and G. Dahl, *The pannexin 1 channel activates the inflammasome in neurons and astrocytes.* J. Biol. Chem., 2009. **284**(27): p. 18143-51.

78. Thompson, R.J., N. Zhou, and B.A. MacVicar, *Ischemia opens neuronal gap junction hemichannels.* Science, 2006. **312**(5775): p. 924-927.

79. Chekeni, F.B., M.R. Elliott, J.K. Sandilos, S.F. Walk, J.M. Kinchen, E.R. Lazarowski, A.J. Armstrong, S. Penuela, D.W. Laird, G.S. Salvesen, B.E. Isakson, D.A. Bayliss, and K.S. Ravichandran, *Pannexin 1 channels mediate 'find-me' signal release and membrane permeability during apoptosis.* Nature, 2010. **467**(7317): p. 863-7.

80. Solan, J.L. and P.D. Lampe, *Connexin phosphorylation as a regulatory event linked to gap junction channel assembly.* Biochim. Biophys. Acta, 2005. **1711**(2): p. 154-63.

81. Boassa, D., F. Qiu, G. Dahl, and G. Sosinsky, *Trafficking dynamics of glycosylated Pannexin1 proteins.* Cell. Commun. Adhes., 2008. **15**(1): p. 119 - 132.

82. Laird, D.W., K.L. Puranam, and J.P. Revel, *Turnover and phosphorylation dynamics of connexin43 gap junction protein in cultured cardiac myocytes.* Biochem J, 1991. **273(Pt 1)**: p. 67-72.

83.   Zhang, J.T., M. Chen, C.I. Foote, and B.J. Nicholson, *Membrane integration of in vitro-translated gap junctional proteins: co- and post-translational mechanisms.* Mol Biol Cell, 1996. **7**(3): p. 471-82.

84.   Ahmad, S., J.A. Diez, C.H. George, and W.H. Evans, *Synthesis and assembly of connexins in vitro into homomeric and heteromeric functional gap junction hemichannels.* Biochem J, 1999. **339 (Pt 2)**: p. 247-53.

85.   Das Sarma, J., F. Wang, and M. Koval, *Targeted gap junction protein constructs reveal connexin-specific differences in oligomerization.* J Biol Chem, 2002. **277**(23): p. 20911-8.

86.   Maza, J., J. Das Sarma, and M. Koval, *Defining a minimal motif required to prevent connexin oligomerization in the endoplasmic reticulum.* J Biol Chem, 2005. **280**(22): p. 21115-21.

87.   Musil, L.S. and D.A. Goodenough, *Multisubunit assembly of an integral plasma membrane channel protein, gap junction connexin43, occurs after exit from the ER.* Cell, 1993. **74**(6): p. 1065-77.

88.   Thomas, T., K. Jordan, J. Simek, Q. Shao, C. Jedeszko, P. Walton, and D.W. Laird, *Mechanisms of Cx43 and Cx26 transport to the plasma membrane and gap junction regeneration.* J. Cell Sci., 2005. **118**(Pt 19): p. 4451-62.

89.   Johnson, R.G., R.A. Meyer, X.R. Li, D.M. Preus, L. Tan, H. Grunenwald, A.F. Paulson, D.W. Laird, and J.D. Sheridan, *Gap junctions assemble in the presence of cytoskeletal inhibitors, but enhanced assembly requires microtubules.* Exp Cell Res, 2002. **275**(1): p. 67-80.

90.   Herve, J.C., N. Bourmeyster, and D. Sarrouilhe, *Diversity in protein-protein interactions of connexins: emerging roles.* Biochim Biophys Acta, 2004. **1662**(1-2): p. 22-41.

91.   Wei, C.J., R. Francis, X. Xu, and C.W. Lo, *Connexin43 associated with an N-cadherin-containing multiprotein complex is required for gap junction formation in NIH3T3 cells.* J Biol Chem, 2005. **280**(20): p. 19925-36.

92.   Ebihara, L., *New roles for connexons.* News Physiol Sci, 2003. **18**: p. 100-3.

93.   Goodenough, D.A. and D.L. Paul, *Beyond the gap: functions of unpaired connexon channels.* Nat Rev Mol Cell Biol, 2003. **4**(4): p. 285-94.

94.   Gaietta, G., T.J. Deerinck, S.R. Adams, J. Bouwer, O. Tour, D.W. Laird, G.E. Sosinsky, R.Y. Tsien, and M.H. Ellisman, *Multicolor and electron microscopic imaging of connexin trafficking.* Science, 2002. **296**(5567): p. 503-7.

95. Lauf, U., B.N. Giepmans, P. Lopez, S. Braconnot, S.C. Chen, and M.M. Falk, *Dynamic trafficking and delivery of connexons to the plasma membrane and accretion to gap junctions in living cells.* Proc Natl Acad Sci U S A, 2002. **99**(16): p. 10446-51.

96. Simek, J., J. Churko, Q. Shao, and D.W. Laird, *Cx43 has distinct mobility within plasma-membrane domains, indicative of progressive formation of gap-junction plaques.* J Cell Sci, 2009. **122**(Pt 4): p. 554-62.

97. Larsen, W.J. and N. Hai, *Origin and fate of cytoplasmic gap junctional vesicles in rabbit granulosa cells.* Tissue Cell, 1978. **10**(3): p. 585-98.

98. Marquart, K.H., *So-called annular gap junctions in bone cells of normal mice.* Experientia, 1977. **33**(2): p. 270-2.

99. Sasaki, T. and P.R. Garant, *Fate of annular gap junctions in the papillary cells of the enamel organ in the rat incisor.* Cell Tissue Res, 1986. **246**(3): p. 523-30.

100. White, F.H., D.A. Thompson, and K. Gohari, *Ultrastructural morphometric of gap junctions during differentiation of stratified squamous epithelium.* J Cell Sci, 1984. **69**: p. 67-85.

101. Jordan, K., R. Chodock, A.R. Hand, and D.W. Laird, *The origin of annular junctions: a mechanism of gap junction internalization.* J Cell Sci, 2001. **114**(Pt 4): p. 763-73.

102. Gumpert, A.M., J.S. Varco, S.M. Baker, M. Piehl, and M.M. Falk, *Double-membrane gap junction internalization requires the clathrin-mediated endocytic machinery.* FEBS Lett, 2008. **582**(19): p. 2887-92.

103. Nickel, B.M., B.H. DeFranco, V.L. Gay, and S.A. Murray, *Clathrin and Cx43 gap junction plaque endoexocytosis.* Biochem Biophys Res Commun, 2008. **374**(4): p. 679-82.

104. Piehl, M., C. Lehmann, A. Gumpert, J.P. Denizot, D. Segretain, and M.M. Falk, *Internalization of large double-membrane intercellular vesicles by a clathrin-dependent endocytic process.* Mol Biol Cell, 2007. **18**(2): p. 337-47.

105. Laing, J.G., P.N. Tadros, E.M. Westphale, and E.C. Beyer, *Degradation of connexin43 gap junctions involves both the proteasome and the lysosome.* Exp Cell Res, 1997. **236**(2): p. 482-92.

106. Leithe, E., A. Kjenseth, S. Sirnes, H. Stenmark, A. Brech, and E. Rivedal, *Ubiquitylation of the gap junction protein connexin-43 signals its trafficking from early endosomes to lysosomes in a process mediated by Hrs and Tsg101.* J Cell Sci, 2009. **122**(Pt 21): p. 3883-93.

107. Leithe, E. and E. Rivedal, *Epidermal growth factor regulates ubiquitination, internalization and proteasome-dependent degradation of connexin43.* J Cell Sci, 2004. **117**(Pt 7): p. 1211-20.

108. Panchin, Y.V., *Evolution of gap junction proteins--the pannexin alternative.* J. Exp. Biol., 2005. **208**(Pt 8): p. 1415-9.

109. Laird, D.W., M. Castillo, and L. Kasprzak, *Gap junction turnover, intracellular trafficking, and phosphorylation of connexin43 in brefeldin A-treated rat mammary tumor cells.* J. Cell Biol., 1995. **131**(5): p. 1193-1203.

110. Willecke, K., Eiberger, J., Degen, J., Eckardt, D., Romualdi, A., Guldenagel, M., Deutsch, U. and Sohl, G., *Structural and functional diversity of connexin genes in the mouse and human genome.* Biol. Chem., 2002. **383**: p. 725-737.

111. Iglesias, R., S. Locovei, A. Roque, A.P. Alberto, G. Dahl, D.C. Spray, and E. Scemes, *P2X7 receptor-Pannexin1 complex: pharmacology and signaling.* Am J Physiol Cell Physiol, 2008. **295**(3): p. C752-60.

112. Pelegrin, P. and A. Surprenant, *Pannexin-1 couples to maitotoxin- and nigericin-induced interleukin-1beta release through a dye uptake-independent pathway.* J. Biol. Chem., 2007. **282**(4): p. 2386-2394.

113. Bukauskas, F.F., K. Jordan, A. Bukauskiene, M.V. Bennett, P.D. Lampe, D.W. Laird, and V.K. Verselis, *Clustering of connexin 43-enhanced green fluorescent protein gap junction channels and functional coupling in living cells.* Proc Natl Acad Sci U S A, 2000. **97**(6): p. 2556-61.

114. Ma, W., H. Hui, P. Pelegrin, and A. Surprenant, *Pharmacological characterization of pannexin-1 currents expressed in mammalian cells.* J. Pharmacol. Exp. Ther., 2009. **328**: p. 409-418.

115. Jordan, K., J.L. Solan, M. Dominguez, M. Sia, A. Hand, P.D. Lampe, and D.W. Laird, *Trafficking, assembly, and function of a connexin43-green fluorescent protein chimera in live mammalian cells.* Mol Biol Cell, 1999. **10**(6): p. 2033-50.

116. Hervé, J.C., N. Bourmeyster, D. Sarrouilhe, and H.S. Duffy, *Gap junctional complexes: from partners to functions.* Prog. Biophys. Mol. Biol., 2007. **94**: p. 29-65.

117. Bunse, S., A. Haghika, G. Zoidl, and R. Dermietzel, *Identification of a potential regulator of the gap junction protein pannexin1.* Cell. Commun. Adhes., 2005. **12**(5-6): p. 231-6.

118. Fan, D., A. Liaw, Y.M. Denkins, J.H. Collins, M. Van Arsdall, J.L. Chang, S. Chakrabarty, D. Nguyen, E. Kruzel, and I.J. Fidler, *Type-1 transforming*

growth factor-beta differentially modulates tumoricidal activity of murine peritoneal macrophages against metastatic variants of the B16 murine melanoma. J Exp Ther Oncol, 2002. **2**(5): p. 286-97.

119. Qin, H., Q. Shao, H. Curtis, J. Galipeau, D.J. Belliveau, T. Wang, M.A. Alaoui-Jamali, and D.W. Laird, *Retroviral delivery of connexin genes to human breast tumor cells inhibits in vivo tumor growth by a mechanism that is independent of significant gap junctional intercellular communication.* J Biol Chem, 2002. **277**(32): p. 29132-8.

120. Lippincott-Schwartz, J., E. Snapp, and A. Kenworthy, *Studying protein dynamics in living cells.* Nat Rev Mol Cell Biol, 2001. **2**(6): p. 444-56.

121. Lee, M.C. and E.A. Miller, *Molecular mechanisms of COPII vesicle formation.* Semin Cell Dev Biol, 2007. **18**(4): p. 424-34.

122. Dong, C., F. Zhou, E.K. Fugetta, C.M. Filipeanu, and G. Wu, *Endoplasmic reticulum export of adrenergic and angiotensin II receptors is differentially regulated by Sar1 GTPase.* Cell Signal, 2008. **20**(6): p. 1035-43.

123. Lippincott-Schwartz, J., L.C. Yuan, J.S. Bonifacino, and R.D. Klausner, *Rapid redistribution of Golgi proteins into the ER in cells treated with brefeldin A: evidence for membrane cycling from Golgi to ER.* Cell, 1989. **56**(5): p. 801-13.

124. Scemes, E., S.O. Suadicani, G. Dahl, and D.C. Spray, *Connexin and pannexin mediated cell-cell communication.* Neuron Glia Biol, 2007. **3**(3): p. 199-208.

125. Penuela, S., S.J. Celetti, R. Bhalla, Q. Shao, and D.W. Laird, *Diverse subcellular distribution profiles of Pannexin1 and Pannexin3.* Cell. Commun. Adhes., 2008. **15**(1): p. 133 - 142.

126. Sato, K., *COPII coat assembly and selective export from the endoplasmic reticulum.* J Biochem, 2004. **136**(6): p. 755-60.

127. Taneja, T.K., J. Mankouri, R. Karnik, S. Kannan, A.J. Smith, T. Munsey, H.B. Christesen, D.J. Beech, and A. Sivaprasadarao, *Sar1-GTPase-dependent ER exit of KATP channels revealed by a mutation causing congenital hyperinsulinism.* Hum Mol Genet, 2009. **18**(13): p. 2400-13.

128. Donaldson, J.G., D. Finazzi, and R.D. Klausner, *Brefeldin A inhibits Golgi membrane-catalysed exchange of guanine nucleotide onto ARF protein.* Nature, 1992. **360**(6402): p. 350-2.

129. Shaw, R.M., A.J. Fay, M.A. Puthenveedu, M. von Zastrow, Y.N. Jan, and L.Y. Jan, *Microtubule plus-end-tracking proteins target gap junctions*

directly from the cell interior to adherens junctions. Cell, 2007. **128**(3): p. 547-60.

130. Rorth, P., *Collective Cell Migration.* Annu Rev Cell Dev Biol, 2009. **25**: p. 407-29.

131. Mayo, C., R. Ren, C. Rich, M.A. Stepp, and V. Trinkaus-Randall, *Regulation by P2X7: epithelial migration and stromal organization in the cornea.* Invest Ophthalmol Vis Sci, 2008. **49**(10): p. 4384-91.

132. Saadoun, S., M.C. Papadopoulos, M. Hara-Chikuma, and A.S. Verkman, *Impairment of angiogenesis and cell migration by targeted aquaporin-1 gene disruption.* Nature, 2005. **434**(7034): p. 786-92.

133. Levite, M., L. Cahalon, A. Peretz, R. Hershkoviz, A. Sobko, A. Ariel, R. Desai, B. Attali, and O. Lider, *Extracellular K(+) and opening of voltage-gated potassium channels activate T cell integrin function: physical and functional association between Kv1.3 channels and beta1 integrins.* J Exp Med, 2000. **191**(7): p. 1167-76.

134. Hendriks, R., D.K. Morest, and L.K. Kaczmarek, *Role in neuronal cell migration for high-threshold potassium currents in the chicken hindbrain.* J Neurosci Res, 1999. **58**(6): p. 805-14.

135. Falk, M.M., S.M. Baker, A.M. Gumpert, D. Segretain, and R.W. Buckheit, 3rd, *Gap junction turnover is achieved by the internalization of small endocytic double-membrane vesicles.* Mol Biol Cell, 2009. **20**(14): p. 3342-52.

136. Angelides, K.J., L.W. Elmer, D. Loftus, and E. Elson, *Distribution and lateral mobility of voltage-dependent sodium channels in neurons.* J Cell Biol, 1988. **106**(6): p. 1911-25.

137. Poo, M., *Rapid lateral diffusion of functional A Ch receptors in embryonic muscle cell membrane.* Nature, 1982. **295**(5847): p. 332-4.

138. Srinivasan, Y., A.P. Guzikowski, R.P. Haugland, and K.J. Angelides, *Distribution and lateral mobility of glycine receptors on cultured spinal cord neurons.* J Neurosci, 1990. **10**(3): p. 985-95.

139. Klausner, R.D., A.M. Kleinfeld, R.L. Hoover, and M.J. Karnovsky, *Lipid domains in membranes. Evidence derived from structural perturbations induced by free fatty acids and lifetime heterogeneity analysis.* J Biol Chem, 1980. **255**(4): p. 1286-95.

140. Nigg, E.A. and R.J. Cherry, *Anchorage of a band 3 population at the erythrocyte cytoplasmic membrane surface: protein rotational diffusion measurements.* Proc Natl Acad Sci U S A, 1980. **77**(8): p. 4702-6.

141. Wang, Y. and B. Rose, *Clustering of Cx43 cell-to-cell channels into gap junction plaques: regulation by cAMP and microfilaments.* J Cell Sci, 1995. **108 (Pt 11)**: p. 3501-8.

142. Langhorst, M.F., G.P. Solis, S. Hannbeck, H. Plattner, and C.A. Stuermer, *Linking membrane microdomains to the cytoskeleton: regulation of the lateral mobility of reggie-1/flotillin-2 by interaction with actin.* FEBS Lett, 2007. **581**(24): p. 4697-703.

143. Paller, M.S., *Lateral mobility of Na,K-ATPase and membrane lipids in renal cells. Importance of cytoskeletal integrity.* J Membr Biol, 1994. **142**(1): p. 127-35.

144. Giepmans, B.N. and W.H. Moolenaar, *The gap junction protein connexin43 interacts with the second PDZ domain of the zona occludens-1 protein.* Curr Biol, 1998. **8**(16): p. 931-4.

145. Sridharan, M., S.P. Adderley, E.A. Bowles, T.M. Egan, A.H. Stephenson, M.L. Ellsworth, and R.S. Sprague, *Pannexin 1 is the conduit for low oxygen tension-induced ATP release from human erythrocytes.* Am J Physiol Heart Circ Physiol, 2010. **299**(4): p. H1146-52.

146. Woehrle, T., L. Yip, A. Elkhal, Y. Sumi, Y. Chen, Y. Yao, P.A. Insel, and W.G. Junger, *Pannexin-1 hemichannel-mediated ATP release together with P2X1 and P2X4 receptors regulate T cell activation at the immune synapse.* Blood, 2010. **116**(18): p. 3475-3484.

147. Pelegrin, P. and A. Surprenant, *The P2X(7) receptor-pannexin connection to dye uptake and IL-1beta release.* Purinergic Signal., 2009. **5**(2): p. 129-137.

148. Khanna, R., M.P. Myers, M. Laine, and D.M. Papazian, *Glycosylation increases potassium channel stability and surface expression in mammalian cells.* J Biol Chem, 2001. **276**(36): p. 34028-34.

149. Petrecca, K., R. Atanasiu, A. Akhavan, and A. Shrier, *N-linked glycosylation sites determine HERG channel surface membrane expression.* J Physiol, 1999. **515 (Pt 1)**: p. 41-8.

150. Watanabe, I., J. Zhu, E. Recio-Pinto, and W.B. Thornhill, *Glycosylation affects the protein stability and cell surface expression of Kv1.4 but Not Kv1.1 potassium channels. A pore region determinant dictates the effect of glycosylation on trafficking.* J Biol Chem, 2004. **279**(10): p. 8879-85.

151. Prochnow, N., S. Hoffmann, R. Vroman, J. Klooster, S. Bunse, M. Kamermans, R. Dermietzel, and G. Zoidl, *Pannexin1 in the outer retina of the Zebrafish, Danio rerio.* Neuroscience, 2009. **162**(4): p. 1039-54.

152.   Bunse, S., M. Schmidt, N. Prochnow, G. Zoidl, and R. Dermietzel, *Intracellular cysteine C346 is essentially involved in regulating PANX1 channel activity.* J Biol Chem, 2010. **285**(49): p. 38444-52.

153.   Bhalla-Gehi, R., S. Penuela, J.M. Churko, Q. Shao, and D.W. Laird, *Pannexin1 and pannexin3 delivery, cell surface dynamics, and cytoskeletal interactions.* J Biol Chem, 2010. **285**(12): p. 9147-60.

154.   Langlois, S., K.N. Cowan, Q. Shao, B.J. Cowan, and D.W. Laird, *Caveolin-1 and -2 interact with Connexin43 and regulate gap junctional intercellular communication in keratinocytes.* Mol. Biol. Cell, 2008. **19**: p. 912-928.

155.   Campbell, R.E., O. Tour, A.E. Palmer, P.A. Steinbach, G.S. Baird, D.A. Zacharias, and R.Y. Tsien, *A monomeric red fluorescent protein.* Proc Natl Acad Sci U S A, 2002. **99**(12): p. 7877-82.

156.   Cordat, E., J. Li, and R.A. Reithmeier, *Carboxyl-terminal truncations of human anion exchanger impair its trafficking to the plasma membrane.* Traffic, 2003. **4**(9): p. 642-51.

157.   Subramanian, V.S., J.S. Marchant, M.J. Boulware, and H.M. Said, *A C-terminal region dictates the apical plasma membrane targeting of the human sodium-dependent vitamin C transporter-1 in polarized epithelia.* J Biol Chem, 2004. **279**(26): p. 27719-28.

158.   Pankevych, H., V. Korkhov, M. Freissmuth, and C. Nanoff, *Truncation of the A1 adenosine receptor reveals distinct roles of the membrane-proximal carboxyl terminus in receptor folding and G protein coupling.* J Biol Chem, 2003. **278**(32): p. 30283-93.

159.   Hresko, R.C., H. Murata, B.A. Marshall, and M. Mueckler, *Discrete structural domains determine differential endoplasmic reticulum to Golgi transit times for glucose transporter isoforms.* J Biol Chem, 1994. **269**(51): p. 32110-9.

160.   Ayala Yanez, R. and P.M. Conn, *Protein disulfide isomerase chaperone ERP-57 decreases plasma membrane expression of the human GnRH receptor.* Cell Biochem Funct, 2010. **28**(1): p. 66-73.

161.   Lobito, A.A., F.C. Kimberley, J.R. Muppidi, H. Komarow, A.J. Jackson, K.M. Hull, D.L. Kastner, G.R. Screaton, and R.M. Siegel, *Abnormal disulfide-linked oligomerization results in ER retention and altered signaling by TNFR1 mutants in TNFR1-associated periodic fever syndrome (TRAPS).* Blood, 2006. **108**(4): p. 1320-7.

162.   Sato, M., K. Sato, and A. Nakano, *Endoplasmic reticulum quality control of unassembled iron transporter depends on Rer1p-mediated retrieval from the golgi.* Mol Biol Cell, 2004. **15**(3): p. 1417-24.

163.   Lukacs, G.L., A. Mohamed, N. Kartner, X.B. Chang, J.R. Riordan, and S. Grinstein, *Conformational maturation of CFTR but not its mutant counterpart (delta F508) occurs in the endoplasmic reticulum and requires ATP.* EMBO J, 1994. **13**(24): p. 6076-86.

164.   Kaykas, A., J. Yang-Snyder, M. Heroux, K.V. Shah, M. Bouvier, and R.T. Moon, *Mutant Frizzled 4 associated with vitreoretinopathy traps wild-type Frizzled in the endoplasmic reticulum by oligomerization.* Nat Cell Biol, 2004. **6**(1): p. 52-8.

165.   Winchester, B., *Lysosomal metabolism of glycoproteins.* Glycobiology, 2005. **15**(6): p. 1R-15R.

166.   Ashok, A. and R.S. Hegde, *Selective processing and metabolism of disease-causing mutant prion proteins.* PLoS Pathog, 2009. **5**(6): p. e1000479.

167.   Maass, K., A. Ghanem, J.S. Kim, M. Saathoff, S. Urschel, G. Kirfel, R. Grummer, M. Kretz, T. Lewalter, K. Tiemann, E. Winterhager, V. Herzog, and K. Willecke, *Defective epidermal barrier in neonatal mice lacking the C-terminal region of connexin43.* Mol Biol Cell, 2004. **15**(10): p. 4597-608.

168.   Schubert, A.L., W. Schubert, D.C. Spray, and M.P. Lisanti, *Connexin family members target to lipid raft domains and interact with caveolin-1.* Biochemistry, 2002. **41**(18): p. 5754-64.

169.   Geimonen, E., E. Boylston, A. Royek, and J. Andersen, *Elevated connexin-43 expression in term human myometrium correlates with elevated c-Jun expression and is independent of myometrial estrogen receptors.* J Clin Endocrinol Metab, 1998. **83**(4): p. 1177-85.

170.   Hendrix, E.M., S.J. Mao, W. Everson, and W.J. Larsen, *Myometrial connexin 43 trafficking and gap junction assembly at term and in preterm labor.* Mol Reprod Dev, 1992. **33**(1): p. 27-38.

171.   Laing, J.G. and E.C. Beyer, *The gap junction protein connexin43 is degraded via the ubiquitin proteasome pathway.* J Biol Chem, 1995. **270**(44): p. 26399-403.

172.   Leithe, E. and E. Rivedal, *Ubiquitination and down-regulation of gap junction protein connexin-43 in response to 12-O-tetradecanoylphorbol 13-acetate treatment.* J Biol Chem, 2004. **279**(48): p. 50089-96.

173. Ungewickell, E.J. and L. Hinrichsen, *Endocytosis: clathrin-mediated membrane budding.* Curr Opin Cell Biol, 2007. **19**(4): p. 417-25.

174. Brazer, S.C., B.B. Singh, X. Liu, W. Swaim, and I.S. Ambudkar, *Caveolin-1 contributes to assembly of store-operated Ca2+ influx channels by regulating plasma membrane localization of TRPC1.* J Biol Chem, 2003. **278**(29): p. 27208-15.

175. Cohen, A.W., B. Razani, X.B. Wang, T.P. Combs, T.M. Williams, P.E. Scherer, and M.P. Lisanti, *Caveolin-1-deficient mice show insulin resistance and defective insulin receptor protein expression in adipose tissue.* Am J Physiol Cell Physiol, 2003. **285**(1): p. C222-35.

176. Wyse, B.D., I.A. Prior, H. Qian, I.C. Morrow, S. Nixon, C. Muncke, T.V. Kurzchalia, W.G. Thomas, R.G. Parton, and J.F. Hancock, *Caveolin interacts with the angiotensin II type 1 receptor during exocytic transport but not at the plasma membrane.* J Biol Chem, 2003. **278**(26): p. 23738-46.

177. Parton, R.G., M. Hanzal-Bayer, and J.F. Hancock, *Biogenesis of caveolae: a structural model for caveolin-induced domain formation.* J Cell Sci, 2006. **119**(Pt 5): p. 787-96.

178. Williams, T.M. and M.P. Lisanti, *The caveolin proteins.* Genome Biol, 2004. **5**(3): p. 214.

179. Lajoie, P. and I.R. Nabi, *Regulation of raft-dependent endocytosis.* J Cell Mol Med, 2007. **11**(4): p. 644-53.

180. Gray, N.W., L. Fourgeaud, B. Huang, J. Chen, H. Cao, B.J. Oswald, A. Hemar, and M.A. McNiven, *Dynamin 3 is a component of the postsynapse, where it interacts with mGluR5 and Homer.* Curr Biol, 2003. **13**(6): p. 510-5.

181. Nakata, T., R. Takemura, and N. Hirokawa, *A novel member of the dynamin family of GTP-binding proteins is expressed specifically in the testis.* J Cell Sci, 1993. **105 (Pt 1)**: p. 1-5.

182. Praefcke, G.J. and H.T. McMahon, *The dynamin superfamily: universal membrane tubulation and fission molecules?* Nat Rev Mol Cell Biol, 2004. **5**(2): p. 133-47.

183. Sontag, J.M., E.M. Fykse, Y. Ushkaryov, J.P. Liu, P.J. Robinson, and T.C. Sudhof, *Differential expression and regulation of multiple dynamins.* J Biol Chem, 1994. **269**(6): p. 4547-54.
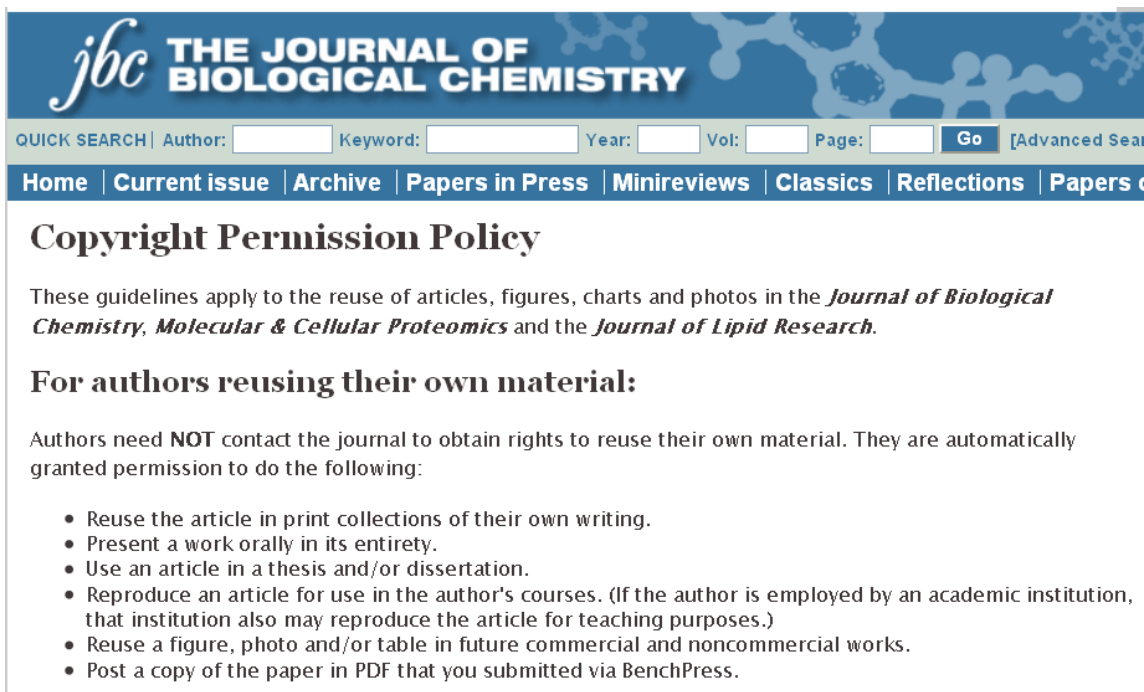
184. Damke, H., T. Baba, D.E. Warnock, and S.L. Schmid, *Induction of mutant dynamin specifically blocks endocytic coated vesicle formation.* J Cell Biol, 1994. **127**(4): p. 915-34.

185. Zhao, Z., X. Li, J. Hao, J.H. Winston, and S.A. Weinman, *The ClC-3 chloride transport protein traffics through the plasma membrane via interaction of an N-terminal dileucine cluster with clathrin.* J Biol Chem, 2007. **282**(39): p. 29022-31.

186. Zeng, W.Z., V. Babich, B. Ortega, R. Quigley, S.J. White, P.A. Welling, and C.L. Huang, *Evidence for endocytosis of ROMK potassium channel via clathrin-coated vesicles.* Am J Physiol Renal Physiol, 2002. **283**(4): p. F630-9.

187. Nabi, I.R. and P.U. Le, *Caveolae/raft-dependent endocytosis.* J Cell Biol, 2003. **161**(4): p. 673-7.

188. Martens, J.R., R. Navarro-Polanco, E.A. Coppock, A. Nishiyama, L. Parshley, T.D. Grobaski, and M.M. Tamkun, *Differential targeting of Shaker-like potassium channels to lipid rafts.* J Biol Chem, 2000. **275**(11): p. 7443-6.

189. Darby, P.J., C.Y. Kwan, and E.E. Daniel, *Caveolae from canine airway smooth muscle contain the necessary components for a role in Ca(2+) handling.* Am J Physiol Lung Cell Mol Physiol, 2000. **279**(6): p. L1226-35.

190. Trouet, D., B. Nilius, A. Jacobs, C. Remacle, G. Droogmans, and J. Eggermont, *Caveolin-1 modulates the activity of the volume-regulated chloride channel.* J Physiol, 1999. **520 Pt 1**: p. 113-9.

191. Benlimame, N., P.U. Le, and I.R. Nabi, *Localization of autocrine motility factor receptor to caveolae and clathrin-independent internalization of its ligand to smooth endoplasmic reticulum.* Mol Biol Cell, 1998. **9**(7): p. 1773-86.

192. Conrad, P.A., E.J. Smart, Y.S. Ying, R.G. Anderson, and G.S. Bloom, *Caveolin cycles between plasma membrane caveolae and the Golgi complex by microtubule-dependent and microtubule-independent steps.* J Cell Biol, 1995. **131**(6 Pt 1): p. 1421-33.

193. Giocondi, M.C., P.E. Milhiet, P. Dosset, and C. Le Grimellec, *Use of cyclodextrin for AFM monitoring of model raft formation.* Biophys J, 2004. **86**(2): p. 861-9.

194. Pawlowski, N., *Dynamin self-assembly and the vesicle scission mechanism: how dynamin oligomers cleave the membrane neck of clathrin-coated pits during endocytosis.* Bioessays, 2010. **32**(12): p. 1033-9.

195. Nichols, B., *Caveosomes and endocytosis of lipid rafts.* J Cell Sci, 2003. **116**(Pt 23): p. 4707-14.

196. Sharma, D.K., J.C. Brown, Z. Cheng, E.L. Holicky, D.L. Marks, and R.E. Pagano, *The glycosphingolipid, lactosylceramide, regulates beta1-integrin clustering and endocytosis.* Cancer Res, 2005. **65**(18): p. 8233-41.

197. Kumari, S., S. Mg, and S. Mayor, *Endocytosis unplugged: multiple ways to enter the cell.* Cell Res, 2010. **20**(3): p. 256-75.

198. Chadda, R., M.T. Howes, S.J. Plowman, J.F. Hancock, R.G. Parton, and S. Mayor, *Cholesterol-sensitive Cdc42 activation regulates actin polymerization for endocytosis via the GEEC pathway.* Traffic, 2007. **8**(6): p. 702-17.

199. Geli, M.I. and H. Riezman, *Role of type I myosins in receptor-mediated endocytosis in yeast.* Science, 1996. **272**(5261): p. 533-5.

200. Liu, J., M. Kaksonen, D.G. Drubin, and G. Oster, *Endocytic vesicle scission by lipid phase boundary forces.* Proc Natl Acad Sci U S A, 2006. **103**(27): p. 10277-82.

201. Murray, S.A., S.Y. Williams, C.Y. Dillard, S.K. Narayanan, and J. McCauley, *Relationship of cytoskeletal filaments to annular gap junction expression in human adrenal cortical tumor cells in culture.* Exp Cell Res, 1997. **234**(2): p. 398-404.

202. D'Souza-Schorey, C. and P. Chavrier, *ARF proteins: roles in membrane traffic and beyond.* Nat Rev Mol Cell Biol, 2006. **7**(5): p. 347-58.

203. Welch, A.Y., K.N. Riley, C. D'Souza-Schorey, and I.M. Herman, *Arf6 modulates the beta-actin specific capping protein, betacap73.* Methods Enzymol, 2005. **404**: p. 377-87.

204. Donaldson, J.G., N. Porat-Shliom, and L.A. Cohen, *Clathrin-independent endocytosis: a unique platform for cell signaling and PM remodeling.* Cell Signal, 2009. **21**(1): p. 1-6.

205. Gong, Q., M. Weide, C. Huntsman, Z. Xu, L.Y. Jan, and D. Ma, *Identification and characterization of a new class of trafficking motifs for controlling clathrin-independent internalization and recycling.* J Biol Chem, 2007. **282**(17): p. 13087-97.

206. Caplan, S., N. Naslavsky, L.M. Hartnell, R. Lodge, R.S. Polishchuk, J.G. Donaldson, and J.S. Bonifacino, *A tubular EHD1-containing compartment involved in the recycling of major histocompatibility complex class I molecules to the plasma membrane.* EMBO J, 2002. **21**(11): p. 2557-67.

207. Banerjee, J. and P.B. Wedegaertner, *Identification of a novel sequence in PDZ-RhoGEF that mediates interaction with the actin cytoskeleton.* Mol Biol Cell, 2004. **15**(4): p. 1760-75.

208. Dominguez, R., *Actin-binding proteins--a unifying hypothesis.* Trends Biochem Sci, 2004. **29**(11): p. 572-8.

APPENDIX 1

COPYRIGHT PERMISSION POLICY

CURRICULUM VITAE

RUCHI GEHI
The Department of Anatomy and Cell Biology
Dental Sciences Building Addition, Rm. 00076
London, ON, NCA 5C1

EDUCATION

Doctor of Philosophy *(Candidate)* in
Anatomy and Cell Biology   2006-Current
University of Western Ontario, London ON
Title of Dissertation: The Dynamic Life of Pannexins: Delivery,
                                Cell Surface Dynamics, Internalization and Degradation

Master of Science in Anatomy and Cell Biology   2004-2006
University of Western Ontario, London ON
Title of Dissertation: Nerve Growth Factor Mediates GJIC through Cx43
Channels
*Recognized by Robert Buck Award
(recognized for special merit and achievement during M.Sc)

Bachelors of Science in Biology   1999-2004
Honors Specialization in Cell Biology
University of Western Ontario, London ON
Title of Research: Growth regulation of gap junctions in Connexin-43 expressing
*   PC12 cells via Epidermal Growth Factor (EGF)*

FELLOWSHIPS and AWARDS *(University of Western Ontario, London ON)*

Western Graduate Research Scholarship	2007-Current
Natural Sciences and Engineering Research	
Council of Canada Scholarship	2008-2010
Travel Award-International Gap	
Junctional Conference	2009
Margaret Moffatt Research Day	
Best Poster Award in Physiology Category	2008
Ontario Graduate Scholarship- *declined*	2008-2009
Ontario Graduate Scholarship- *accepted*	2007-2008
Robert Buck Award-	
recognized for special merit and achievement during M.Sc.	2007
Schulich Graduate Scholarship	2007
Travel Award-International Gap Junctional Conference	2005
Special University Scholarship	2004

Deans Honor List Award   2004
Admission Bursary Award   1999
Ontario Scholar Award   1999

RESEARCH

Manuscript- *in Submission Process*

R. Gehi, Q. Shao and D.W. Laird
The Carboxyl Terminal Tail of Panx1 Regulates Trafficking and homomeric Interactions

R. Gehi, Q. Shao and D.W. Laird
Panx1 Exhibits a Distinct Internalization Pattern from the Connexin Family of Gap Junction Proteins

Manuscript-*Published*

R. Bhalla-Gehi, S. Penuela, J.M. Churko, Q. Shao and D. W. Laird (2010) Panx1 and Panx3 Cell surface Dynamics and Cytoskeletal Interactions. *Journal of Biological Chemistry* (Ph.D. program).

Silvia Penuela, Ruchi Bhalla, Kakon Nag and Dale W. Laird (2009). Glycosylation Regulates Pannexin Family Member Interactions. *Molecular Biology of the Cell* 20(20):4313-23 (Ph.D. program).

Silvia Penuela, Steven J. Celetti, Ruchi Bhalla, Qing Shao and Dale W. Laird (2008). Diverse Sub-cellular Distribution Profiles of the Glycoproteins, Pannexin1 and Pannexin3. *Cell Communication and Adhesion* 15:1-10 (Ph.D. program). (Invited Submission)

Silvia Penuela, Ruchi Bhalla, Xiang-Qun Gong, Kyle N. Cowan, Steven J. Celleti, Bryce J. Cowan Donglin Bai, Qing Shao and Dale W. Laird (2007). Pannexin1 and Pannexin3 are glycoproteins that exhibit many distinct characteristics from the connexin family of gap junction proteins. *The Journal of Cell Science* 120: 3772-3782 (Ph.D. program).
Cushing P, Bhalla R, Johnson AM, Rushlow WJ, Meakin SO and Belliveau DJ (December 2005). Nerve growth factor increases connexin43 phosphorylation and gap junctional intercellular communication.The *Journal of Neuroscience Research* 82(6):788-801 (M.Sc. program).

Platform Presentation at International and Institutional Conferences

Ruchi Bhalla, Jamie Simek, Silvia Penuela, Qing Shao and Dale W. Laird (July 2009). Pannexin1 and Pannexin3 traffic in Sar1-dependent COPII vesicles and Exhibit Cell Surface Mobility Dynamics and Cytoskeletal Interactions that are Distinct from Connexin43. Sedona, USA (Ph.D. program).

Ruchi Bhalla (January 2009). Trafficking and Cell Surface Dynamics of Pannexins. Annual Gap Junction Research Day, London ON, Canada (Ph.D. program).

Poster Presentation at International and Institutional Conferences

Ruchi Bhalla, Silvia Penuela, Jamie Simek, Qing Shao and Dale W. Laird (December 2008). Characterization of Panx1 and Panx3 trafficking and cell surface dynamics. San Francisco, USA (Ph.D. program).

Silvia Penuela, Ruchi Bhalla, Xiang-Qun Gong, Donglin Bai, Qing Shao and Dale W. Laird (August 2007). Pannexin1 and Pannexin3 are glycoproteins that exhibit many distinct characteristics from the connexin family of gap junction proteins. Elsinore, Denmark; and *Margaret P. Moffat Graduate Research Day in London, ON, Canada (Ph.D. program).
*Recognized for the Best Poster Award in Physiology Category

Ruchi Bhalla, Paul Cushing, Dale W. Laird, and Daniel J. Belliveau (September 2006). Nerve Growth Factor Mediates Gap Junctional Intercellular Communication via Cx43 Channels. Anatomy and Cell Biology Graduate Research Day in London, ON, Canada (Ph.D. program).

Ruchi Bhalla, Paul Cushing Dale W. Laird, Walter J. Rushlow, Susan O. Meakin and Daniel J. Belliveau (May 2006). The role of the mitogen-activated protein kinase signaling pathway on Trk-activated up regulation of Cx43. Margaret P. Moffat Graduate Research Day in London, ON, Canada (M.Sc. program).

Ruchi Bhalla, Paul Cushing, Dale W. Laird, Walter J. Rushlow, Susan O. Meakin and Daniel J. Belliveau (August 2005). The role of the mitogen-activated protein kinase signaling pathway on Trk-activated up regulation of Cx43. Whistler, BC, Canada (M.Sc. program).

SCIENTIFIC MEETINGS ATTENDED

Gap Junction International Conference, Sedona, AZ	2009
American Society for Cell Biology, San Francisco, CA	2008
Gap Junction International Conference, Copenhagen, Denmark	2007
Gap Junction International Conference, Whistler, BC	2005